UNIVERSITY OF AGDER

Fault Diagnosis of an Electrical Winch based on Structural Analysis

Torbjørn Farmen
Mina Zarchi

Supervisor
Martin Choux

This master's thesis is carried out as a part of the education at the University of Agder and is therefore approved as a part of this education. However, this does not imply that the University answers for the methods that are used or the conclusions that are drawn.

University of Agder, Spring 2018
Faculty of Engineering and Science
Department of Engineering Sciences

Preface

This report is written as part of the Master's program in Mechatronics at the University of Agder. The project is given by the issue of associate professor Martin Marie Hubert Choux at the University of Agder. It has been an interesting task and has given the group members valuable learning in the complexity of dynamic system.

We would like to thank our supervisor for his guidance and support during this process. We also wish to thank all of the respondents, without whose cooperation we would not have been able to conduct this analysis.

The group consists of the following two members:

Torbjørn Farmen

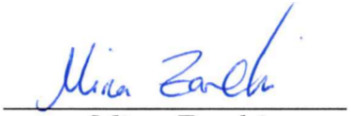

Mina Zarchi

May 25, 2018

Abstract

This report covers development and implementation of a model-based fault-detection and fault diagnosis algorithm based on structural analysis, providing deeper knowledge of predictive maintenance, which offers the industry increased uptime and reduced spending. Failure mode and effect analysis are carried out at component level for an electrical winch. Construction of a Simulink model, used to verify the algorithms, are described in detail including governing equations and implementation. The basis of a structural analysis is outlined and tested on the electrical winch system. Results from the simulation model covers faults in permanent magnet motor, bearings, gearbox and sensors. The structural analysis is able to detect and isolate several types of typical faults that can occur in electrical winch systems.

Contents

Abbreviations

Table 1: Abbreviations

Symbol	**Explanation**
AC	Alternating current
AE	Acoustic Emission
ARRs	Analytical Redundancy Relations
CUSUM	Cumulative Sum Algorithm
DAE	Differential Algebraic Equation
DFT	Discrete Fourier Transform
DM	Dependency Matrix
DOF	Degree of Freedom
D-Q	Direct Quadrature
FDI	Fault Diagnosis and Isolation
FFT	Fast Fourier Transform
FMEA	Failure Mode and Effect Analysis
IATA	International Air Transport Association
IM	Induction Motor
MCSA	Motor Current Signature Analysis
MRO	Maintenance, Repair & Overhaul Market
PMSM	Permanent Magnet Synchronous Motors

1 Introduction

Electrical winches are making an entry in the Norwegian ship and lifting industry, replacing traditional hydraulic actuated systems. They require less space, as there is no need for hydraulic pumps and reservoirs. The maritime supplier, Rolls-Royce, has developed winch technology actuated with a permanent magnet motor that can drive the drum without a gearbox. Using electric motor, the dynamic behaviour is claimed to minimise tension peaks in the wire and reduce the vessels fuel consumption, additionally power can be regenerated.

1.1 Background and Motivation

Maritime winches are often placed on locations that are inaccessible during operation time of a vessel, increasing the need for development of a remote fault diagnosis system to keep productivity continuous and avoid downtime of physical assets. Proper maintenance ensures that machines and equipment will perform as expected whenever they are needed. Maintenance also plays a part in eliminating hazards and accidents that can occur off shore.

Maintenance can be divided in several categories [1, 2]

- Failure based maintenance - Do maintenance once there's a problem or a breakdown. This is the simplest form of maintenance, and obviously, the most expensive as a breakdown most likely will lead to downtime.
- Calendar-based maintenance - Do preventive maintenance at a periodic interval without considering the health status of a physical asset. As products become more complex with higher demands to quality, unnecessary maintenance can be wasteful. In addition, it may not eliminate all failures.
- Condition-based maintenance - "a maintenance program that recommends maintenance actions based on the information collected through condition monitoring." [2] Condition-based and predictive maintenance falls under the same category. It can be said to consist of three steps [3] ; data acquisition, data processing and maintenance decision-making.

In times when technology is rapidly developing, and automated systems are becoming more available, it is important for mechatronic engineers to have knowledge about both monitoring techniques and electrical drives. The motivation for writing this thesis is to learn more about the opportunities that predictive maintenance offer to the industry. This thesis incorporates several of the disciplines covered in the mechatronics master program in addition to providing valuable knowledge regarding electric actuated systems. Implementation of predictive maintenance are relevant for several applications. Furthermore, the thesis is based on modelling and simulation, two subjects that appealed to both group members.

1.2 Problem Statement

This report will investigate further into predictive maintenance, which provides several benefits. Increased up-time and safety in addition to reduction of maintenance cost should be mentioned. The International Air Transport Association (IATA) [4] states this about predictive maintenance: "Predictive maintenance is estimated to increase aircraft availability by up to 35%" and "These innovations are estimated to decrease MRO (Maintenance, Repair & Overhaul Market) spending by 15 to 20% but first, the market needs to innovate with a clear vision and strategy."

The goal of this project is to develop and assess suitable algorithms for fault detection and identification, for an electric winch. The main project goal is divided into the following primary objectives:

- Identify failure modes for an electric winch and its respective components.
- Establish a simulation model for detection and identification of simulated faults.
- Derive diagnosis method based on structural analysis for detection and identification of faults at incipient stage.
- Verify the proposed methods by running simulations that includes generation of faults derived in the Failure Mode and Effect Analysis-chapter.

1.3 Analysis Methods Review

An important aspect during winch operation is to have a safe and efficient system with rapid detection and removal of faults. During literature study it was found that several analyse techniques are in use today, like vibration analysis, acoustic analysis and current analysis. Each of the methods have distinctive characteristics different advantages and disadvantages. This section gives an outline of the most common techniques and their respective applications, and a brief description of sensor fusion that can be used to combine methods, improving detection accuracy.

Vibration Spectrum Analyses

This section is based on various literature and research from [5–7]. Vibration analyses is a beneficial trouble-shooting tool to detect the causes of fault conditions at an early stage but can also be used for quality control of new components that are to work in a harsh environment. All components in a winch produces vibration, sound and heat during operation, which can be measured by utilizing sensors. Raw data from sensors is usually in discrete-time waveform, which is the sum of several sine waves. A single component motion generates a single sine wave with an amplitude and frequency, thus, vibration from additional components adds additional frequencies and amplitudes.

As each component generate distinctive frequencies, the spectral analyses is applied to distinguish the components. Spectrum is generated from the waveform using a Fast Fourier Transform

(FFT). The transformation makes each vibration source easier to see, highlighting the different frequencies as spikes. When the spectra of a healthy system are known, the challenge is to identify changes in this spectrum, which can be caused by e.g. a faulty component.

Acoustic Analyses

This section is a short summation from [2, 8, 9]. An acoustic signature analysis is another method used for condition monitoring that is applicable for induction motors (IM). Recent studies, mentioned in [9], have also considered the use of acoustic emission to detect bearing failures. When a solid substance is under stress, the defects in it produce high-frequency sound waves, acoustic emission (AE). These waves are released in the material and can be received by certain sensors. By analysing these waves, one can determine the type of defect, its location and its severity.

The process to obtain AE-signals is relatively easy, as the sensor is a microphone that is placed near the machine. However, a microphone is sensitive to external noise, increasing the need for good signal filtering. Analysis of AE signal can provide valuable information in relation to the initiation and growth of a discontinuity in a metal, as cracks. As well as detect dislocation movement, testing for leaks, detecting flaws, and generally can used extensively as a research tool.

There are two benefits of acoustic emission compared to most other non-destructive testing. The first is about the origin of a signal. that is, instead of transforming energy to the object under testing, AE test, listens to the energy released by objects, second is that AE test deals with dynamic process, or changes in a material.

Current Signature Analyses

This summary is based on various literature and research from [6, 10–13]. Motor current signature analysis (MCSA) is a tool that can be used to monitor electric motors during normal operation and is well-established in industry. MCSA is performed by attaching a clamp probe to the supplied current. This allows for monitoring of motors that are operating in inaccessible areas by simply attaching a current sensor to the power supply. Data from the sensor can be processed via a spectral analysis or specialized MCSA software. MCSA is also considered a powerful tool for detecting faulty bearings and gears. Dubravko, MILJKOVIĆ, 2018 [14] lists the applications for MCSA as:

- Static and/or dynamic air-gap irregularities
- Broken rotor bar or cracked rotor end-rings
- Stator faults (opening or shorting of one coil or more of a stator phase winding)
- Abnormal connection of the stator windings.
- Bent shaft (akin to dynamic eccentricity) which can result in a rub between the rotor and stator, causing severe damage to stator core and windings.

- Bearing and gearbox failures

Signals obtained by the current sensors can be processed in several ways, where the spectrum analyses (described in section 1.3) is frequently used. The spectra analysis can utilize a Discrete Fourier Transform (DFT) or, in the simpler form, a Fast Fourier Transform (FFT). The data is also filtered using a technique called demodulation, which removes the carrier frequency of the signal (50 Hz in Europe, 60 Hz in USA), making the interesting frequencies more visible [14]. Other processing methods includes wavelet analysis and Park's vector approach, latter requiring current sensors on the three current phases i_a, i_b and i_c.

Structural Analysis

Structural analysis is based on [15–19]. The structural analysis requires a good mathematical model of a system and are used to analyse redundancies. Behaviour of the model are described by considering links between constraints (equations used to model a system) and parameters. The method requires manually composition of a systems bipartite graph, which forms the basis for fault-diagnosis.

The composition of system parameters and constraints has the ability to identify if a failure in a component occurs, in addition to highlight the specific component. Structural analysis utilizes the fact that all components are described by constraints computing the expected behaviour, real time, identifying any deviation from the actual behaviour. Divergence between expected and measured value can indicate that a fault has occurred. Structural analysis is considered effective as it does not require additional hardware and can be performed in real time. However, unlike the other methods, there are not much published material regarding the method of structural analysis.

Sensor Fusion

The brief summary of sensor fusion is based on [2]. Every sensor has its own characteristics, and to achieve accurate condition monitoring readings and measurements of a complex system, a trend is to fusion data from multiple sources. An increase in the number of sensors will collect more data from the system, proportionally increasing the measurement accuracy, easing the process of locating faults. Fusion and processing of the gathered data can be grouped in three methods as listed, and discussed, in [2].

1. Data-level fusion
2. Feature-level fusion
3. Decision-level fusion

Chosen Method

The different analysis methods are not always suitable to detect any kind of fault. Some methods works well at detecting that a fault has occurred but may struggle to isolate in which

component it is, like vibration and current analysis [12, 20]. Spectral analyses can be hard to perform real time, as this method is dependent on data sets from sensors and can require extensive training for feature extractions. The structural analysis is able to provide real-time diagnosis of dynamic systems, isolation of faults are also possible. It was desirable to choose a versatile method that was able to both detect and isolate faults at an acceptable level and operate in real-time.

The literature study revealed that most of the condition monitoring studies are done for single components, like a bearing or electric motor. This motivated the group to investigate condition monitoring of a complex system (electrical winch, with the associated components). Structural analysis was chosen as the preferred method for this thesis.

1.4 Report Structure

This section gives a brief description of each chapter in this master thesis. A summary of each chapter is listed below.

- **Chapter 1 - Introduction**
  Problem statement and motivation are presented along with the objectives for this thesis. Then, a literature review covering a variety of fault diagnosis methods follows. Last, the report structure is explained.
- **Chapter 2 - Failure Mode and Effects Analysis**
  A Failure Mode and Effect Analysis (FMEA) is carried out in this chapter, and relevant literature are presented. The main components of a winch are reviewed to identify the most common failure modes.
- **Chapter 3 - Modelling**
  This chapter covers the theory behind- and implementation of the governing dynamic equations used to model the permanent magnet motor, bearings, gearbox, winch and payload. The chapter is structured as a mixture of theory and implementation.
- **Chapter 4 - Diagnosis using Structural Analysis**
  The theory covering structural analysis and implementation on the modelled winch are presented. Terminologies regarding the method are explained, then the specific implementation is described. Last part of the chapter presents how faults are induced to the simulation model.
- **Chapter 5 - Results**
  In this chapter the achieved results are presented. First, results verifying that the simulation model runs as expected, then the addition of sensor noise are presented. The main part of this chapter shows how the algorithm identifies induced faults.
- **Chapter 6 - Discussion and Conclusion**
  The discussion chapter elaborates the results and methods used. Last the main conclusions are drawn.

2 Failure Mode and Effects Analysis

In this project, Failure Mode and Effect Analysis (FMEA) will be used to identify potential failure and errors that can occur within an electric winch. FMEA was introduced in 1949 by the US Army to study malfunctions of military system. The method has been modified and improved over the years, leading to a well-established analysis method [21]. FMEA is used to determine in which a part or system can malfunction. It can also be used to identify the consequence of failures and prioritize them in order to make the correct actions to prevent them [21–23].

2.1 Main Components

This section introduces the main components of an electrical winch and investigate the most common fault for each component.

2.1.1 Gearbox

A gearbox consists of several moving parts, that are difficult to monitor using vibration analyses. Induced vibrations from a gearbox can be very complicated, since there can be several pairs of gears in contact at the same time [24]. Usually, there is also mounted two or more bearings on each shaft. A gearbox has multiple shafts turning at different speeds that produces both high and low frequencies.

Gearboxes generally operate under a tough working environment, which can lead to several failure modes on the main components [25]. One of the most common failure mode is simply wear, but other failure modes can also occur like broken or damaged teeth, misalignment of the shafts, bent shafts, backlash and tooth load [3, 26].

Tooth damage and wear can cause metal particles in the lubricant. Therefore, an important condition regarding gearboxes design is that the number gear teeth is a prime number. A damaged tooth is likely to cause slightly damage to all meshing teeth in a gear connection. Prime numbered gears lead the wear to spread slow and even across all teeth, in contrast to even numbered gears, where the damage will spread within a limited number of teeth

Gear eccentricity can occur if gear centres move relative to each other, If one of the shafts has a circular trajectory it can result in a varying mesh force (high mesh force during part of the rotation and a lower mesh force in the other part of the rotation). Eccentricity can be caused by poor installation, poor misalignment, a bent shaft or if the gear hole is not in centre.

Table 2.1: Gear failure mode

Component	Failure Mode
Tooth	Physical damage
	Broken
	Wear
	Load shearing
Gear	Misalignment
	Eccentricity
	Backlash
	Wear
Shaft	Fatigue
	Bent shaft
	Overload

2.1.2 Bearing

Failing of bearings can roughly be sorted in to three main sources. Fatigue, lubrication-contamination and handling-installation. This subsection presents a small overview of the respective failure modes [20, 27–30].

Excessive loading can cause premature fatigue of bearings and can be caused by the use of wrong bearings for a given application. Indentations or dents in balls or raceways are referred to as brinell marks and are indicators that loading has been excessive.

Brinelling is a localized surface corrosion and occurs in two forms; true brinelling points to a load that has exceeded the elastic limit of the bearing material. Typically leaving indentations in the raceway of both outer and inner ring which can cause vibration in the bearings. False brinelling marks usually take the form of a depression around the race due to vibration or swaying between the rolling elements and the raceways. False brinelling is usually seen in non-rotating applications.

Spalling failure can occur at contact points, between rolling elements and the raceway, subjected to high stress just below the surface, shearing the spall of. This leads to metal adhesion where small parts of metal are acting between the moving parts of the bearing and can weld themselves together during service.

Proper lubrication will reduce friction, prevent metal to metal adhesion, dissipation of heat, corrosion protection and removal of solid debris. However, improper lubrication may account for most of bearing failures since bearings are designed to operate in a state where they are correctly lubricated.

Incorrect lubrication for the work environment can lead to premature wear and failure. Examples can be wrong lubrication viscosity, or simply the wrong operating temperature for a given lubricant. Too long maintenance intervals between renewal of lubrication or the lack of lubrication is also considered a failure mode. Another failure mode is over lubrication.

A contaminated lubricant can cause several failures, like abrasive wear to races and balls, micro-cracks in races due to solid wear particulate in grease, micro-adhesion between balls and races and seizure of the bearing due to overheating. Contamination of lubricant may originate from seal failure or other external sources like lubricant storage, machine wash-down and location of the device. Corrosion can occur due to chemical or moisture exposures leading to both pitting and rusting which again can lead to the mentioned brinelling.

Fits and tolerances are critical, correct personnel training and tools is important. A bearing mounted with to loose fit leads to unbalanced load, where the load will move around in the bearing causing the bearing to vibrate. On the other hand, tight fits from improper interference can lead to excess loading which again can lead to heat generation and seizure of the bearing due to overheating. Misalignment of both shaft or bearing can cause edge loading and brinelling.

Table 2.2: Bearing failure mode

Component	**Failure Mode**
Bearing	Incorrect lubrication
	Inadequate maintenance
	Overlubrication
	Contamination
	Corrosion
	Excessive loading
	Misalignment
	Brinelling

2.1.3 Permanent-Magnet Synchronous Motor

Permanent Magnet Synchronous Motors (PMSMs) are widely used in industry as the PM-motor can deliver high torque and has a simple construction that is easy to maintain [10]. Thus, the PM-motor can be exposed to adverse conditions, increasing the need for condition monitoring. A PMSMs failure mode is defined as the specific failure of a component to perform its function and can occur in different components on a motor. Faults of PMSMs can be sorted in to several categories, discussed in [31]. Figure 2.1 states that the most common faults is related to bearings, stator windings or external factors, like overloading.

Faults	IEEE-IAS (%) Electrical Safety Workshop	EPRI (%) Electric Power Research Institute
Bearing	44	41
Winding	26	36
Rotor	8	9
Other	22	14

Figure 2.1: Percentage of failures [31]

Eccentricity-related faults occurs frequently due to mechanical reasons, like bearing failures, bent shaft and overload [11]. Eccentric faults is defined as the relative displacement between both rotor and stator centre axis, and is divided in to two types: dynamic and static eccentricity [20, 32]. Optimally, the axes should be perfectly aligned.

Table 2.3: PMSM failure mode

Component	Failure Mode
Housing	Improper installation
	Physical damage
	Corrosion
	Material build up
Stator	Physical damage
	Contamination
	Corrosion
	High temperature
	Voltage imbalance
	Broken supports
	Rewind burnout procedures
Rotor	Thermal stress
	Contamination
	Physical damage
	Imbalance
	Broken rotor bar
	Improper installation
Fan	Physical damage
	Ice build up
	Foreign material
	Corrosion
Insulation/Windings	Contamination
	Over heating
	Improper storage
	Moisture
	Insulation breakdown
	Cycling/Flexing
	AC drive stress
Shaft	Physical damage
	Improper manufacturing
	Improper installation
	Corrosion
Bearings	Improper handling/storage
	Improper installation
	Misalignment
	Improper lubricant
	Lack of/Over/Under lubrication
	Start/stop loss of lube film
	Contamination
	Overhung load
	Motor fan imbalance

2.1.4 Winch Related Faults

There is limited open research regarding failure modes for a winch, but some common failures are known based on hands-on experience. Actuator and bearing faults are considered as external in this case, and are already covered in sections 2.1.2 and 2.1.3. Other faults are often related to the wire. The innermost layers of wires tend to be spooled more rear than the outer. If the winch operates in seawater, then salt water can gather near the drum core and increase corrosion in the innermost wire layers. Therefore, it can be beneficial to unroll all wire at a certain interval and lubricate the wire.

Reduction in the wire area can occur over time due to usage, especially in outer wire sections that are often rolled on and off the drum. At times, the wire can spool close to the drum housing, causing metal to metal contact that can wear out the wire faster than under normal conditions. Wind-ups can also occur in situations where the wire are rolled in with high velocity, leading to additional wear and tear.

2.2 Component Faults

After investigating the main components of a winch, it was decided to focus on the most frequent faults for each of the components. It was also desirable to include possible misreading from sensors, i.e. faulty sensors. The selected faults are listed in table 2.4, which presents the chosen component and sensor failures, categorized as "Parametric" and "Additive" - respectively.

Table 2.4: The selected failure modes for the winch system

Item	Failure mode	Component	Failure effect	Type	Variable
f_1	Stator windings	Internal resistance	Heat dissipation	Parametric	R_s
f_2	Contamination	Rotor	Increased friction	Parametric	$b_{friction}$
f_3	Sensor fault	Current sensor	Incorrect readings	Additive	i_{am}
f_4	Sensor fault	Rotor encoder	Incorrect readings	Additive	θ_r
f_5	Brinelling	Bearing	Increased vibration	Parametric	Db_{out}
f_6	Misalignment	Bearing	Heat generation and seizure	Parametric	F_u
f_7	Sensor fault	Displacement sensor	Incorrect readings	Additive	X_{inn}
f_8	Tooth damage	Gearbox	Stiffness change	Parametric	C_k
f_9	Lubrication	Gearbox	Increased friction	Parametric	μ_{wh}
f_{10}	Sensor fault	Drum encoder	Incorrect readings	Additive	θ_d
f_{11}	Wear and tear	Wire	Decreased stiffness	Parametric	A_w
f_{12}	Sensor fault	Pressure sensor	Incorrect readings	Additive	Z_{pl}
f_{13}	Sensor fault	Displacement sensor	Incorrect readings	Additive	Y_{inn2}
f_{14}	Brinelling	Bearing 2	Increased vibration	Parametric	Db_{out2}
f_{15}	Misalignment	Bearing 2	Heat generation and seizure	Parametric	F_{u2}

3 | Modelling

This chapter describes layout of the Simulink model and derives the mathematical equations implemented to run the simulation. MATLAB/Simulink provides libraries of various component models. The model consists of different subsystems and MATLAB function blocks which represents components of a winch. A more detailed description of the subsystems are given in the following sections.

3.1 Permanent-Magnet Synchronous Motor

The PMSM-model uses dynamic equations from the book "Control of Voltage-Source Converters and Variable-Speed Drives " [33] and are based on a PMSM motor that are installed at a winch set-up at the university. It was considered important to base the PMSM-model on an existing motor to achieve a good model. Needed electric parameters was provided on the motors nameplate, figure 3.1, and listed in table 3.1.

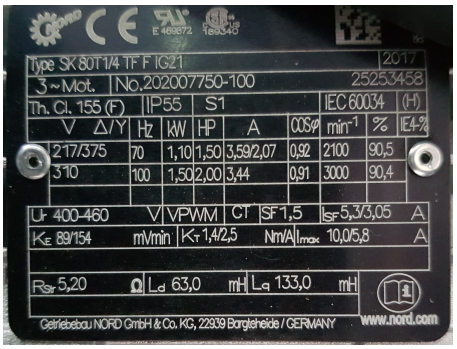

Figure 3.1: Photo of nameplate for SK80T1/4 TF, where electrical parameters are listed

Table 3.1: Motor parameters SK80T1/4 TF

Description	Parameter	Value	Unit
Number of poles	p	4	$[-]$
Number of pole pairs	n_p	2	$[-]$
Torque constant	K_t	2.5	$[Nm/A]$
Rated current	I_{rated}	2.07	$[A]$
Rated torque	T_{rated}	5.175	$[Nm]$
Revolutions per minute	n_N	2 000	$[rpm]$
Motor inertia	J	0.0011	$[kgm^2]$
Stator resistance	R_s	5.2	$[\Omega]$
Stator inductance	L_s	98	$[mH]$

Electric parameters are implemented in the model parameter script, seen in appendix A.1. In addition, the following assumptions are made to simplify the dynamic motor model:

- Stator resistance and inductance are constant
- Perfect field orientation is assumed
- Iron loss are neglected
- Sensor dynamics are ignored, and measurements are assumed to be real-time

Figure 3.2 shows the model outline, and a more detailed description of the subsystems follows.

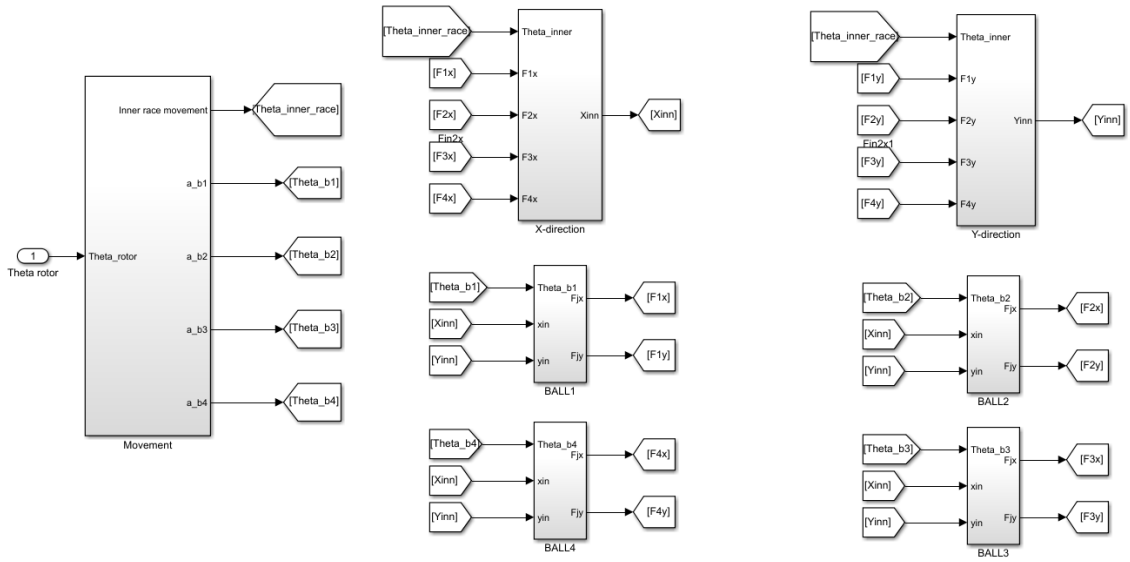

Figure 3.2: Overview PMSM

A Direct Quadrature (d-q) transformation approach is used to model the motor. The transformation simplifies the three-phase circuit in terms of reducing the three AC quantities (v_a, v_b, v_c) to two quantities (v_α, v_β), which reduces the computational power demand. The transformation is invertible, thus, the three phase results is recoverable [34]. The transformation between two and three phases are valid for both voltages and current, thus, the covered equations will only be derived using voltages as current transformations are identical.

Utilizing the property of a symmetric system, equation 3.1 allows for reduction to a two degree of freedom system, as one component always can be expressed in the remaining two.

$$v_a(t) + v_b(t) + v_c(t) = 0 \tag{3.1}$$

Reducing the degrees of freedom gives the opportunity to express the three phase system as an equivalent two-phase system denoted v_α and v_β, where α and β are perpendicular to each other.

$$\vec{v_s} = v_\alpha + jv_\beta = v_a + \exp^{j\frac{2\pi}{3}} v_b + \exp^{j\frac{2\pi}{3}} v_c \tag{3.2}$$

Equation 3.2 is the basis for deriving the transformation matrices T_{32} and T_{23} that are used for the transition between two- and three-phase.

$$\underbrace{\begin{bmatrix} v_\alpha(t) \\ v_\beta(t) \end{bmatrix}}_{\vec{v_s}} = \underbrace{\begin{bmatrix} 1 & -\frac{1}{2} & -\frac{1}{2} \\ 0 & \frac{\sqrt{3}}{2} & -\frac{\sqrt{3}}{2} \end{bmatrix}}_{T_{32}} \cdot \underbrace{\begin{bmatrix} v_a(t) \\ v_b(t) \\ v_c(t) \end{bmatrix}}_{v_s} \tag{3.3}$$

$$\underbrace{\begin{bmatrix} v_a(t) \\ v_b(t) \\ v_c(t) \end{bmatrix}}_{v_s} = \underbrace{\begin{bmatrix} \frac{2}{3} & 0 \\ -\frac{1}{3} & \frac{1}{\sqrt{3}} \\ -\frac{1}{3} & -\frac{1}{\sqrt{3}} \end{bmatrix}}_{T_{23}} \cdot \underbrace{\begin{bmatrix} v_\alpha(t) \\ v_\beta(t) \end{bmatrix}}_{\vec{v_s}} \tag{3.4}$$

Transformation between the fixed stator coordinate system and synchronous coordinates, $\vec{v}$ (a coordinate system rotating with the stator frequency ω) is given by

$$\vec{v} = exp^{-j\theta_e}\vec{v_s} \quad (3.5)$$
$$\vec{v_s} = exp^{j\theta_e}\vec{v} \quad (3.6)$$

$\vec{v}$	-	Space vector in synchronous coordinates	$[d, q]$
$\vec{v_s}$	-	Space vector in stator coordinates	$[\alpha, \beta]$
θ_r	-	Electrical rotational angle	$[rad]$

Figure 3.3 represents the dynamics of a PMSM motor and consists of several equations that will be described. The PMSM model has four inputs, whereas three of them are the three-phased voltages v_a, v_b, v_c and the forth is load torque. Block outputs are the induced electromagnetic torque, T_{em}, the electrical rotational speed and angle, ω_m and θ_r, then the three phase currents i_a, i_b and i_c.

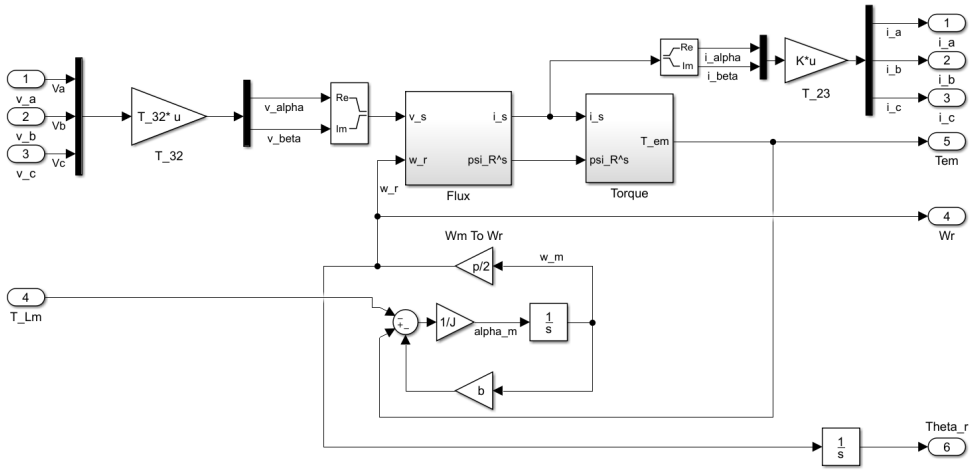

Figure 3.3: Inside PMSM model block

The PMSM block calculates the mechanical rotational speed, equation 3.7, then converts it to electrical rotational speed with equation 3.8. θ_r is obtained from integrating ω_r.

$$\frac{d\omega_m}{dt} = \frac{1}{J}(T_{em} - b \cdot \omega_m - T_{Lm}) \quad (3.7)$$

$$\omega_r = \frac{p}{2}\omega_m \quad (3.8)$$

$$\theta_r = \int \omega_r dt \quad (3.9)$$

p	-	Number of poles	$[-]$
ω_m	-	Fixed mechanical rotor speed	$[rad/s]$
J	-	Moment of inertia	$[kgm^2]$
T_{Lm}	-	Load torque on motor side	$[Nm]$
T_{em}	-	Electromagnetic torque	$[Nm]$

The block called Flux are expanded in figure 3.4 and bases on equations 3.10 and 3.11. The complex integrator subsystem simply divides a complex signal into a real and imaginary part, then the integration is done separately for each part before they are combined into a complex signal. There are two inputs to the flux block. First is the two-phased vector v_s which is calculated using the transformation matrix derived in equation 3.3, next is electrical rotor speed, ω_r. The block computes stator current, i_s and the flux linkage ψ_R^s.

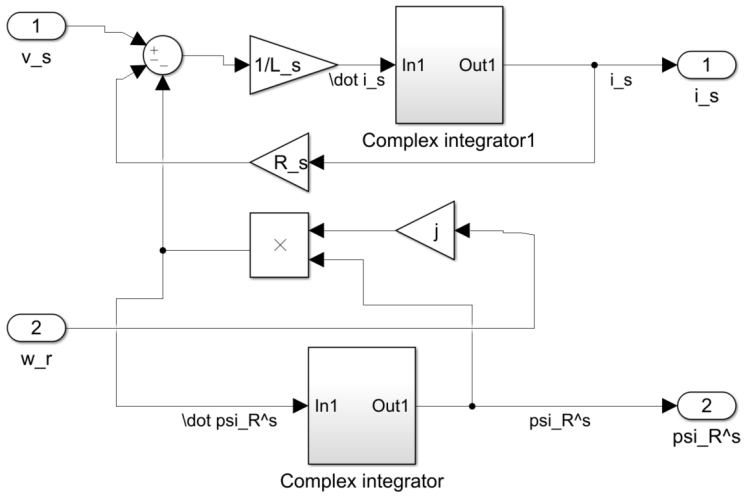

Figure 3.4: Inside the Flux block

$$L_s \frac{d\, i_s}{dt} = v_s - R_S i_s + \omega_r \psi_R^s \quad (3.10)$$

$$\frac{d\, \vec{\psi}_R^s}{dt} = j\omega_r \vec{\psi}_R^s \quad (3.11)$$

L_s	-	Stator inductance	$[H]$
$\vec{v_s}$	-	Space vector	$[H]$
ψ_R^s	-	Rotor flux linkage	$[-]$
$\vec{i_s}$	-	Stator current	$[A]$
R_s	-	Stator resistance	$[\Omega]$
ω_r	-	Electrical rotor speed	$[rad/s]$

The electromagnetic torque, equation 3.13, is calculated in the "Torque" block. Dependent on inputs computed in the flux block, expanded in figure 3.5.

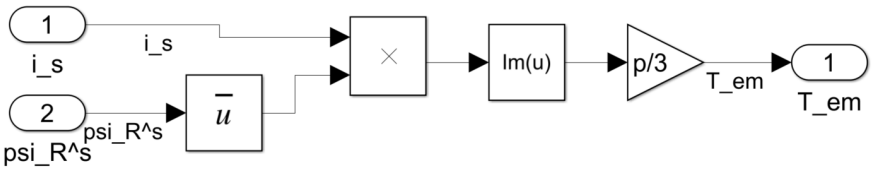

Figure 3.5: Inside the torque block

$$T_{em} = \frac{3n_p}{2K^2} \cdot \Im\left\{\left(\vec{\psi}_R^s\right)^* \vec{i_s}\right\} \quad (3.12)$$

T_{em}	-	Electromagnetic torque	$[Nm]$
n_p	-	Number of pole pairs	$[-]$
K	-	Constant coefficient	$[-]$

By choosing $K = \frac{3}{2}$ and substitute number of pole pairs by the number of poles , p, the electromagnetic torque equation can be written as

$$T_{em} = \frac{p}{3} \cdot \Im\left\{\left(\vec{\psi}_R^s\right)^* \vec{i_s}\right\} \quad (3.13)$$

3.2 Bearing

Ball bearings are used to support rotating shafts and to reduce friction and absorb external stress. A schematic model of a ball bearing can be seen in figure 3.6, pointing to the outer- and inner raceway, the cage and balls (four balls for this case). Ball diameter are given as D_b while cage diameter is given as D_c. The bearings are modelled with two degrees of freedom, bases on literature from [35]. The parameters are based on the SKF Deep Groove Ball Bearing 6204-2Z, which are mounted in the chosen motor.

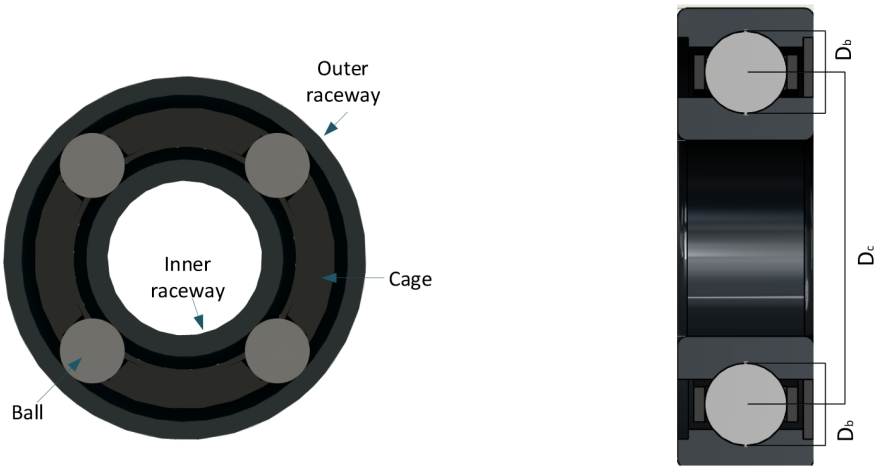

Figure 3.6: A schematic model of the bearing

Figure 3.7 illustrates the kinematic relations inside a bearing. Outer raceway are stationary, while rotation of the input shaft ,ω_{inn}, is directly transferred to inner raceway with a tangential velocity of the point P given by equation 3.14. The balls will rotate in the opposite direction of inner raceway, with a tangential velocity of ball centre O that are half of the velocity of point P.

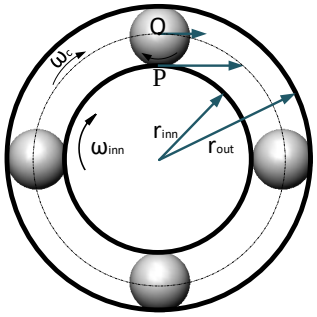

Figure 3.7: Kinematic model of the bearing

$$v_p = r_{inn} \cdot w_{inn} \tag{3.14}$$

The cage angular velocity, ω_c is given by:

$$w_c = w_{inn} \cdot \frac{r_{inn}}{2 \cdot (r_{inn} + r_b)} \tag{3.15}$$

The bearings are simplified to a mass-spring-damper system seen in figure 3.8. Each ball is indexed with a number j, ranging from one to n_b (number of balls).

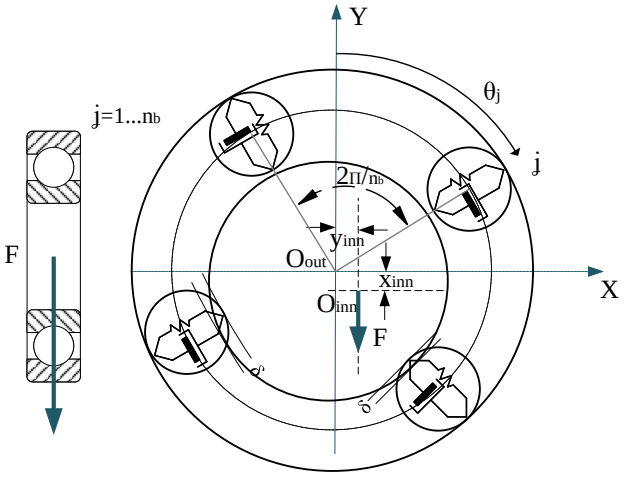

Figure 3.8: Diagram of a rolling-element load distribution

Where

x_{inn}	-	Displacement of the inner ring movement in x-direction	$[mm]$
y_{inn}	-	Displacement of the inner ring movement in y-direction	$[mm]$
θ_j	-	Angular position of the j-th ball	$[rad]$
F	-	Total elastic force	$[N]$
O_{inn}	-	Centre of inner race	$[-]$
O_{out}	-	Centre of outer race	$[-]$
δ	-	Elastic deformation	$[mm]$
n_b	-	Number of balls	$[-]$

The elastic deformation, δ, between the raceways and a ball has a non-linear force-deformation relationship which is obtained by applying the Hertz theory (page 291. [36]). Hertzian forces are only valid if the ball is in contact with either inner- or outer-raceway. Spring force is modelled so that it will only be greater than zero when the spring is compressed, else zero. The elastic deformation can be expressed analytically by:

$$\begin{cases} \delta & = x_{inn} \cdot \cos(\theta_j) + y_{inn} \cdot \sin(\theta_j) \quad if \quad \delta \geq 0 \\ \delta & = 0 \quad if \quad \delta < 0 \end{cases} \tag{3.16}$$

The elastic force, F_j, are calculated for every j-th ball using equation 3.17. The total elastic force, F are then computed using 3.18.

$$F_j = C(\delta_j)^{\frac{3}{2}} \tag{3.17}$$

$$F = \Sigma F_j \quad j = 0 \dots n_b \tag{3.18}$$

Values of the spring constants between inner- and outer raceway and the balls (C_{inn} and C_{out} respectively) are calculated by equation 3.19 - 3.24. Contact stiffness are dependent on the curvature sum $\Sigma\rho$ and curvature difference, F_ρ that are expressed in the equations 3.19 and 3.20 [36].

$$\Sigma\rho = \rho_{11} + \rho_{12} + \rho_{21} + \rho_{22} = \frac{1}{r_{11}} + \frac{1}{r_{12}} + \frac{1}{r_{21}} + \frac{1}{r_{22}} \tag{3.19}$$

$$F_\rho = \frac{(\frac{1}{r_{11}} - \frac{1}{r_{12}})(\frac{1}{r_{21}} - \frac{1}{r_{22}})}{\Sigma\rho} \tag{3.20}$$

Where

ρ_{ij}	-	Curvature according to the two planes i and j	$[1/mm]$
r_{ij}	-	Radii of curvature of the contact surfaces according to the two planes i and j	$[mm]$

The equations are separated for the inner- and outer- race ball contact. When the surface is concave at the contact point, curvature radius is negative. Kinematic model of inner- and outer-race derived for XZ- and YZ-plane as seen below.

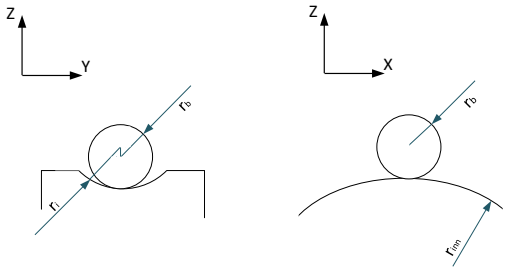

Figure 3.9: Inner race

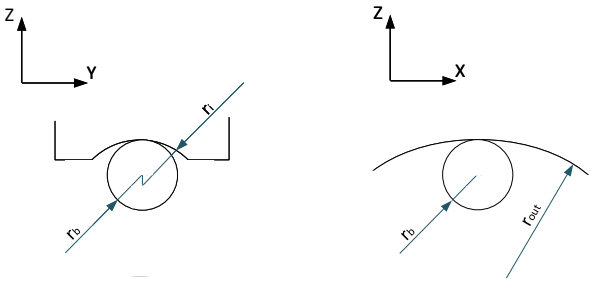

Figure 3.10: Outer race

The contact surface between balls and the raceways will form an ellipse, with semi-major axis, a, and semi-minor axis, b. Values for a^*, b^* and δ^* are obtained from figure 3.11 using the calculated curvature difference, F_ρ. Values for a^*, b^* and δ^* are used to calculate the deformation values and maximum normal tension for a given load.

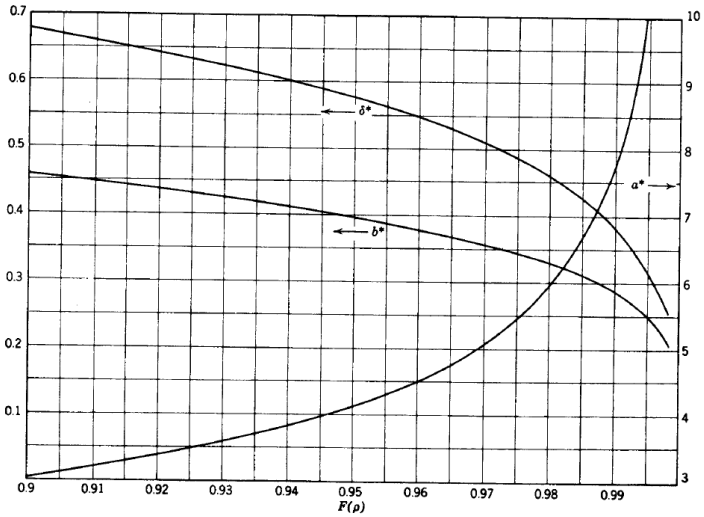

Figure 3.11: a^* ,b^* and δ^* Vs $F(\rho)$ [36]

The load-deformation relation, for steel bearings, is given by the expression:

$$F = \underbrace{\left(\frac{1}{2.79 \cdot 10^{-4} \cdot \delta^*(\sigma\rho)^{\frac{1}{3}}}\right)^{\frac{3}{2}}}_{C} \cdot \delta^{\frac{3}{2}} \tag{3.21}$$

Equation 3.21 must be calculated for both inner- and outer raceway contact. The load of elasticity deformation is the same for both inner- and outer raceway as shown in equation 3.22.

$$F = C_{inn} \cdot \delta_{in}^{\frac{3}{2}} = C_{out} \cdot \delta_{out}^{\frac{3}{2}} \tag{3.22}$$

Total deformation is the sum of the deformation between the ball and the inner race and the outer race. Allowing the equivalent stiffness constant, C_{eq}, to be determined for two springs in series, figure 3.12 by combining equations 3.22 and 3.23.

$$\delta = \delta_{in} + \delta_{out} \tag{3.23}$$

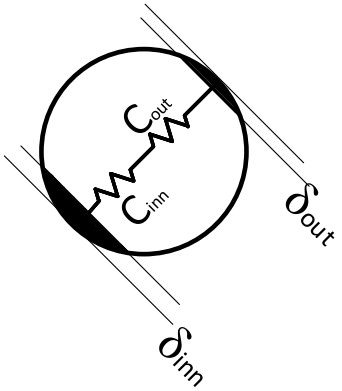

Figure 3.12: The total deformation inner/outer race

$$C_{eq} = \frac{C_{in} \cdot C_{out}}{(C_{in}^{\frac{2}{3}} + C_{out}^{\frac{2}{3}})^{\frac{3}{2}}} \tag{3.24}$$

The dynamic study assumes that the bearing only support radial load. Movement equations are obtained by Newtons second law. Figure 3.13 shows the forces that act on the ball, F_j and the inner race, F, G, F_{ey}, F_{ex} and F_u. The angle β is close to zero and hereby neglected.

$$m_s \cdot \ddot{x} = F_{ex} + F_u \cdot \cos(\alpha_j) - D\dot{x} - \Sigma F_j \cdot \cos(\alpha_j) \tag{3.25}$$
$$m_s \cdot \ddot{y} = F_{ey} + F_u \cdot \sin(\alpha_j) - D\dot{y} - \Sigma F_j \cdot \sin(\alpha_j) - m_s \cdot g \tag{3.26}$$

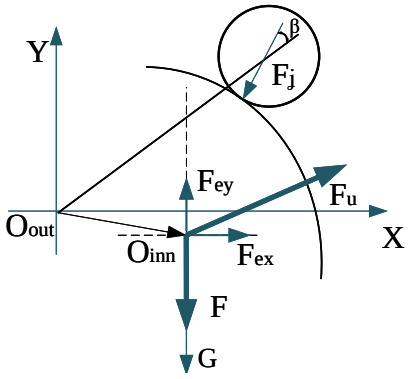

Figure 3.13: Forces in the bearing

F_j	-	Forces due to the elasticity of the contact	$[N]$
$F_{ex,ey}$	-	External force	$[N]$
F_u	-	Radial force due to unbalance in the shaft	$[N]$
G	-	Gravity force of the total weight of the inner race and balls	$[N]$
β	-	Contact angle between ball and raceway	$[rad]$

Figure 3.14 shows the outline of how bearing dynamics are implemented in Simulink. The model consists of multiple subsystems with a more detailed description in the following pages.

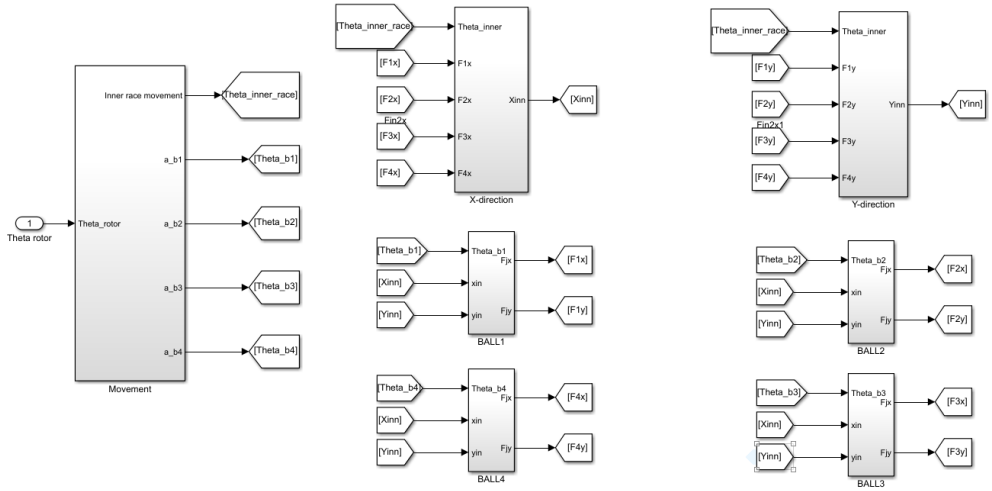

Figure 3.14: Overview of bearing

The block called movement is based on equation 3.15, but has the shaft rotation as input. Outputs are inner raceway angle, with a one-to-one ratio, and rotational angle of each ball (phase shifted with $2\pi/n_b$).

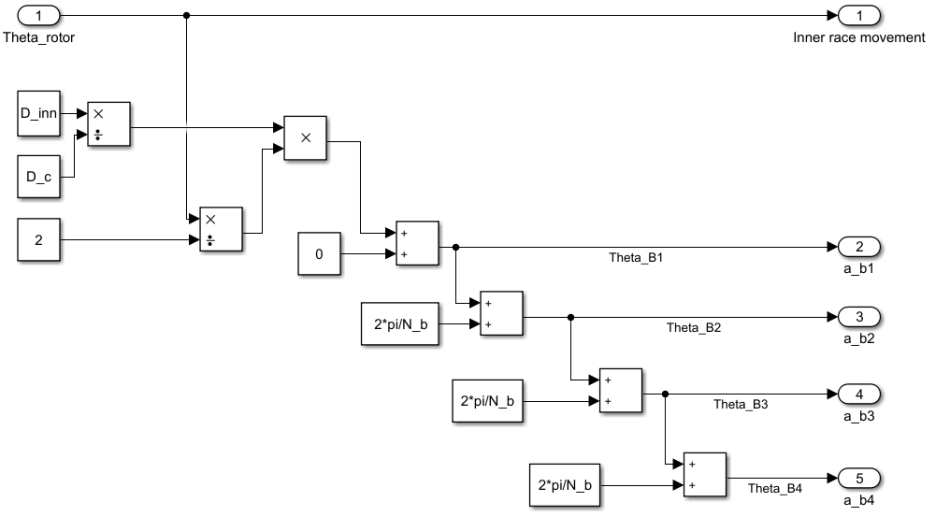

Figure 3.15: Inside the movement block

Figure 3.16 is an expansion of the block called "BALL1", which bases on equation 3.17. The block computes F_x and F_y, which are the two components of the total elastic force, F. The inputs are x_{inn} and y_{inn}, both are corrected from meter to millimetre through a gain of 1000, and the rotational angle of the ball (from figure 3.15).

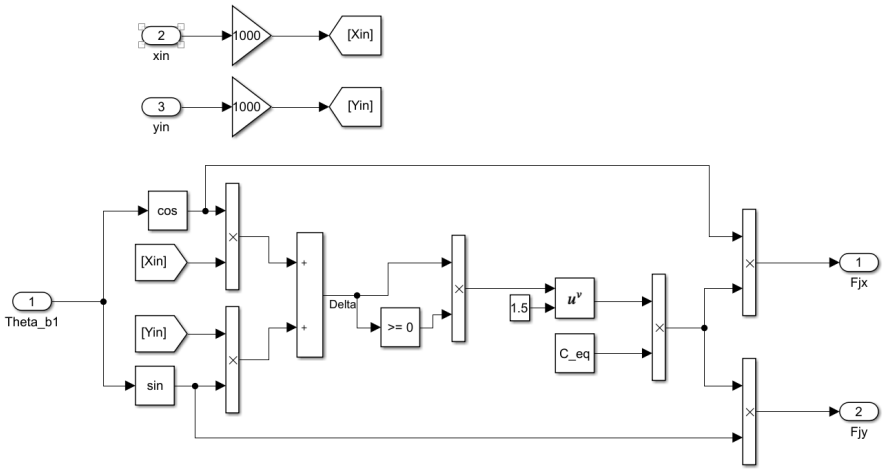

Figure 3.16: Inside the ball block

The X- and Y-direction blocks are based on equations 3.25 and 3.26, respectively. The only difference between the structure of the block are that the gravity force is subtracted in the Y-direction block. Inputs for the direction blocks are the inner raceway angle and the components of total elastic force, F, from each ball. Output are the displacement of inner race.

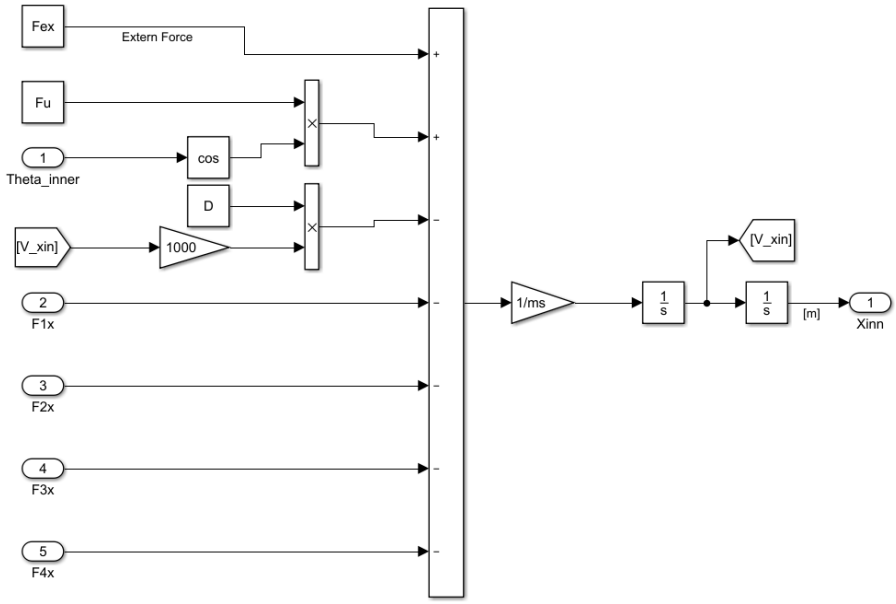

Figure 3.17: Overview over Inner race X direction

3.3 Gearbox

Gears of different kind have been used for centuries to control needed rotational speed and load torque. A gearbox can be used to increase delivered motor torque at the cost of reduced rotational speed, which allows to select a motor that produces smaller torque. The gear model used in the system is assumed as a one-step gearbox consisting of one pair involute spur gears with straight cut teeth. The two gears are called pinion and wheel, subscripted with p and wh, respectively. Equation 3.27 is used to calculate the dimensions of the pinion and gear.

$$D_p = m \cdot Z \qquad (3.27)$$

D_p	-	Pitch diameter	$[mm]$
Z	-	Number of teeth	$[-]$
m	-	Module	$[mm]$

The gearbox is modelled as two stiff disks connected via a spring and damper in parallel. The inputs to the dynamic model are torque and rotational speed produced by the motor (T_{em} and ω_p), and the counteracting torque from the load side (T_{DL}).

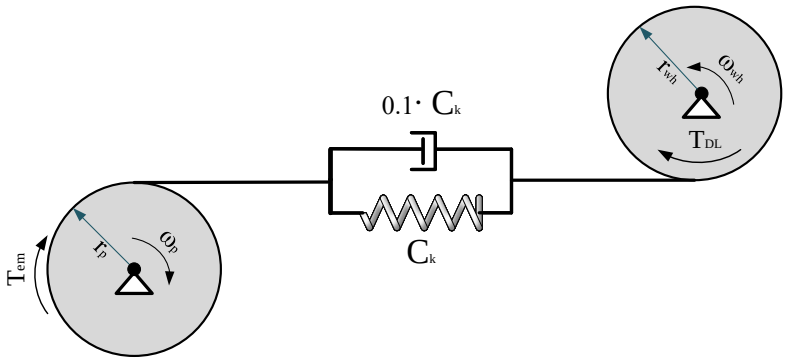

Figure 3.18: Gearbox Model

Equation 3.28 is used to calculate output speed and torque from the gearbox.

$$J_{wh} \cdot \ddot{\theta}_d = F_{sd} \cdot r_{wh} - \mu_f \cdot \dot{\theta}_d + T_{DL} \qquad (3.28)$$

Where

J_{wh}	-	Moment of inertia for the wheel	$[kgm^2]$
$\ddot{\theta}_d$	-	Angular acceleration of the wheel	$[rad/s^2]$
F_{sd}	-	Tooth coupling torque between gears	$[N]$
r	-	Pitch radius	$[m]$
μ_f	-	Friction coefficient	$[-]$
$\dot{\theta}_d$	-	Angular velocity of the wheel	$[rad/s]$
T_{DL}	-	Load torque	$[Nm]$

The feedback load torque, from gearbox to motor, is described by

$$T_{Lm} = \frac{J_{wh} \cdot \ddot{\theta}_d}{n} \qquad (3.29)$$

Figure 3.19 shows implementation of the gearbox model in Simulink.

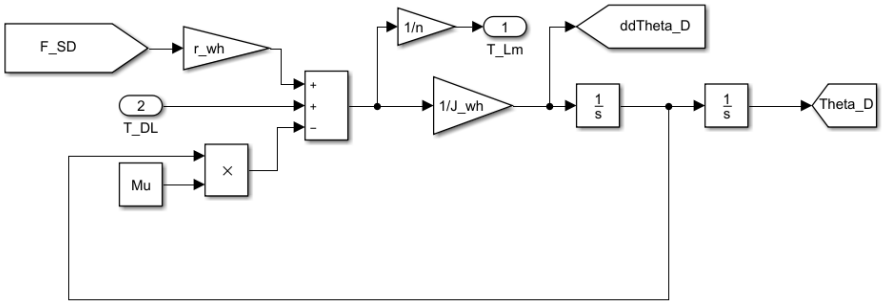

Figure 3.19: Gearbox model in Simulink

The tooth coupling force, which is the reaction force from the modelled spring-damper between the cogwheels is described with the following equation.

$$F_{sd} = C_k \left(\theta_p \cdot r_p - \theta_{wh} \cdot r_{wh}\right) + 0.1 C_k \left(\omega_p \cdot r_p - \omega_{wh} \cdot r_{wh}\right) \tag{3.30}$$

Where

C_k	-	Spring stiffness coefficient for gears	$[\frac{N}{mm}]$
F_{sd}	-	Tooth coupling torque between gears	$[N]$

Figure 3.20 shows how equation 3.30 is implemented in Simulink.

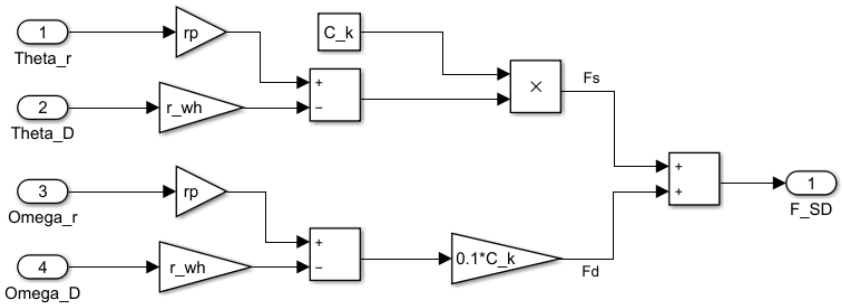

Figure 3.20: Implementation of F_{sd} in Simulink

3.4 Winch

The following section presents the mechanical modelling of the winch drawwork. The model was created using traditional mechanics theory for the drum and payload, where the steel wire was modelled as a massless spring-damper in parallel.

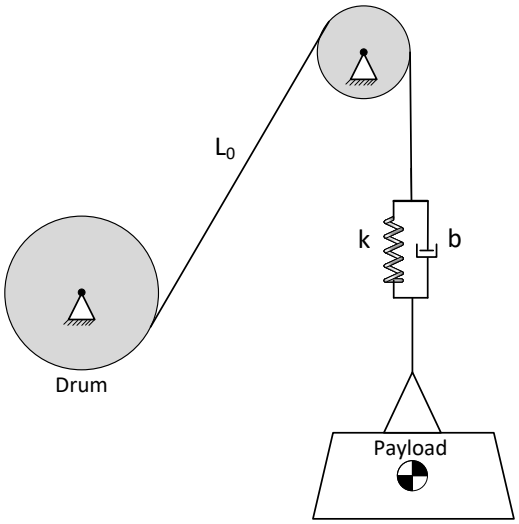

Figure 3.21: Winch overview

The winch is based on the PMSM output torque as an input, and this torque is used to rotate the drum, hence, hoist or lower the payload.

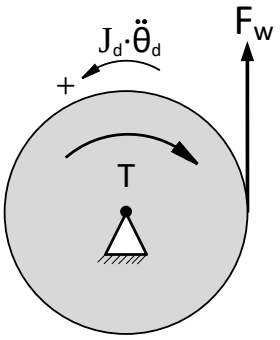

Figure 3.22: Kinetic diagram for the drum

Figure 3.22 shows the kinetic diagram for the drum, which combined with Newton's second law (3.31), forms the basis of the motion eqation 3.32

$$\overset{\curvearrowleft}{\Sigma M} = J_d \cdot \ddot{\theta}_d \tag{3.31}$$

$$J_d \cdot \ddot{\theta}_d = F_w \cdot r_d - T_{DL} \tag{3.32}$$

Where

J_d	-	Drum inertia	$[kgm^2]$
F_w	-	Wire force	$[N]$
r_d	-	Drum radius	$[m]$

Figure 3.23 shows how equation 3.32 is implemented in Simulink, using drum angular acceleration as input.

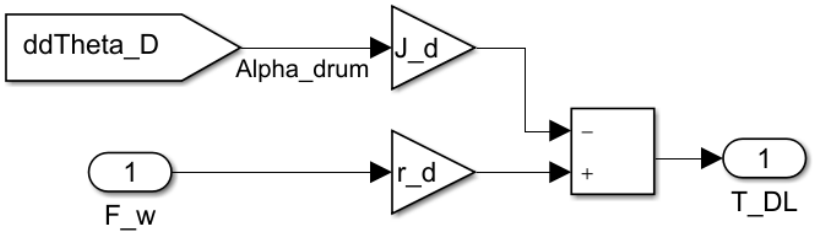

Figure 3.23: Implementation of drum kinematics

As the wire is modelled as a spring and damper in parallel, the wire force, F_w will vary as a function of the wire elongation, δ, and will be used to express the payload position.

$$F_w(\delta, \dot{\delta}) = \delta_w \cdot k_w + \dot{\delta}_w \cdot b_w \tag{3.33}$$

Figure 3.24 shows how equation 3.33 is implemented in Simulink, using real time wire elongation as input.

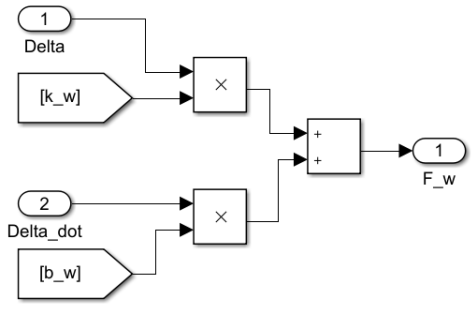

δ_w	-	Elongation of the wire	$[m]$
$\dot{\delta}_w$	-	Elongation rate of the wire	$[m/s]$
k_w	-	Wire stiffness	$[N/m]$
b_w	-	Damping coefficient of wire	$[Ns/m]$

Figure 3.24: Implementation of wire force

Elongation of the wire is dynamically dependent on both drum and payload movement, and is derived in equation 3.34. Equation 3.35 is the time derivative of $\delta(t)$, needed to model damping in the wire.

$$\delta_w(t) = -\theta_d \cdot r_d + x_{pl} + \delta_0 \qquad (3.34)$$

$$\dot{\delta}_w(t) = -\dot{\theta}_d \cdot r_d + v_{pl} \qquad (3.35)$$

θ_d	-	Angle of rotation	$[rad]$
x_{pl}	-	Payload displacement	$[m]$
v_{pl}	-	Payload velocity	$[m/s]$
δ_0	-	Static deflection of wire	$[m]$

Figure 3.25 shows how equations 3.34 and 3.35 is implemented in Simulink.

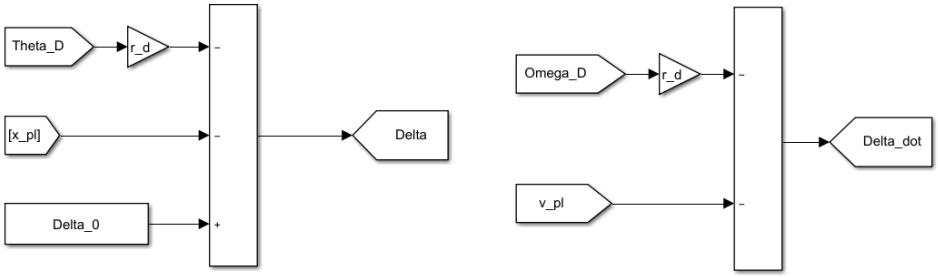

Figure 3.25: Implementation of wire elongation

The wire must be assumed flexible during operation, as a wire will stretch under the impact of an external load. Wire stiffness will wary as a function of the length of unrolled wire, L_{wire}, which again is a function of the drum rotation angle, θ_d.

$$k_w = \frac{E_w \cdot A_w}{\theta_d \cdot r_d + L_0} \qquad (3.36)$$

k_w	-	Wire stiffness	$[N/m]$
E_w	-	E-modulus of steel	$[Pa]$
A_w	-	Cross-sectional area of wire	$[m^2]$
L_0	-	Initial length of wire	$[m]$

Figure 3.26 shows how equation 3.36 is implemented in Simulink. Note that the length of unrolled wire, L_{wire} is dependent on θ_d.

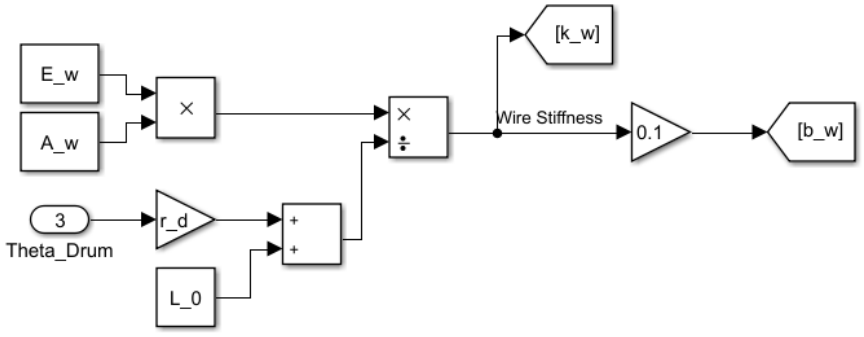

Figure 3.26: Implementation of wire stiffness and damping

Knowing the wire stiffness, the initial static deflection of the wire can be calculated to avoid transients at the simulation initialization. The static deflection term, δ_0 will be valid for any initial position, L_0, of the payload.

$$\delta_0 = \frac{m_{pl} \cdot g \cdot L_0}{E_w \cdot A_w} \qquad (3.37)$$

δ_0 - Static deflection of wire $[m]$
m_{pl} - Payload mass $[kg]$

Deriving the wire force allows us to obtain the payload acceleration, velocity and position (a, v, z) at any time, by simply applying Newton's second law to the payload, 3.27.

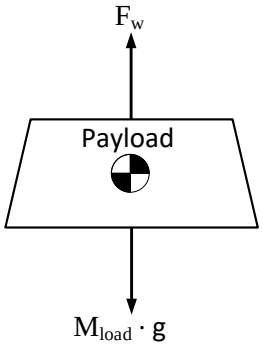

Figure 3.27: Free body diagram of payload

$$m_{pl} \cdot a = F_w - m_{pl} \cdot g \qquad (3.38)$$

$$a = \frac{F_w - m_{pl} \cdot g}{m_{pl}} \qquad (3.39)$$

Figure 3.28 shows how equations 3.39 - 3.39 are implemented in Simulink.

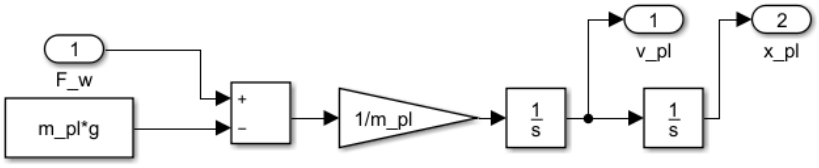

Figure 3.28: Payload block

3.5 Full Model

Figure 3.29 presents the full version of the mechanical model composed of the main components, in addition to a cascaded PID-controller setup. The model input are a velocity profile, seen in the lower plot in figure 3.30, that lowers and elevates the payload.

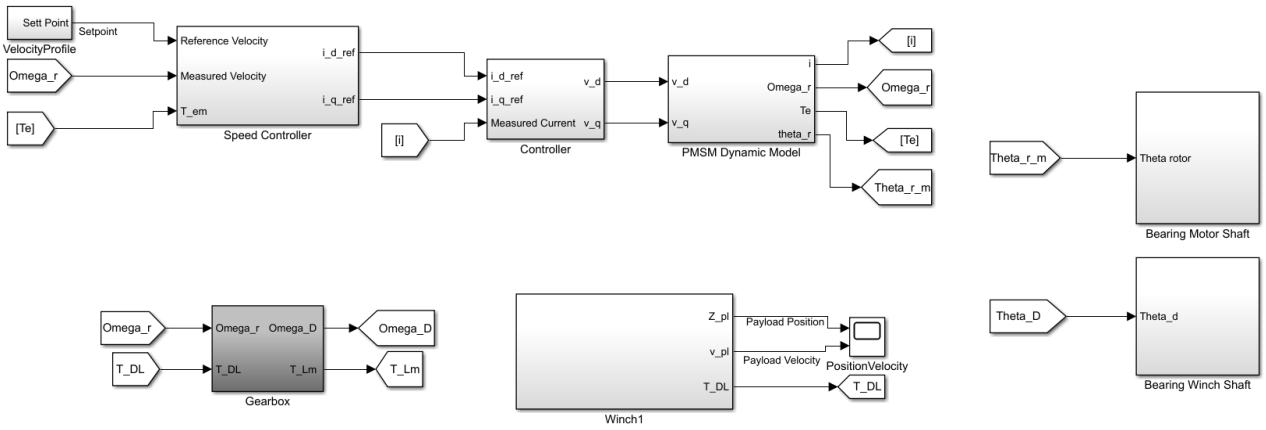

Figure 3.29

Figure 3.30 shows the output values for the payload position and velocity after the simulation is run for thirty seconds. The upper plot shows that the payload has an initial position at five meters below the surface and is lowered to ten meters below, then hoisted back up to five meters.

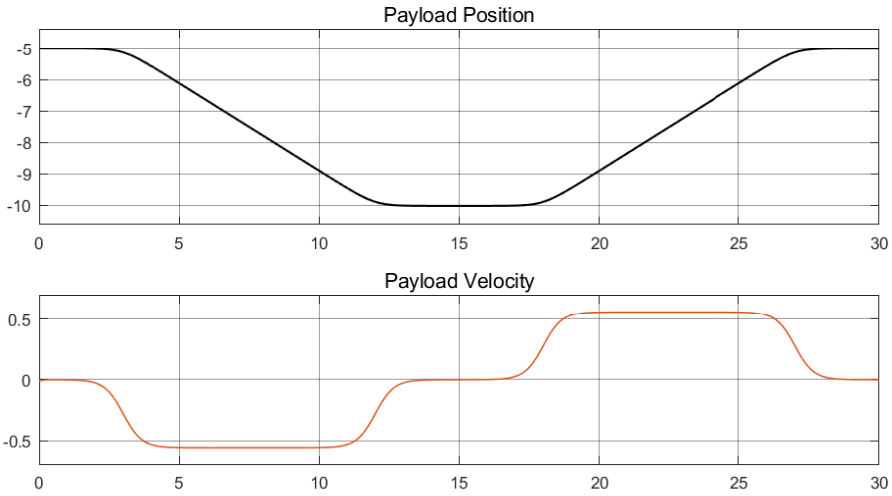

Figure 3.30: The upper plot shows the payload position during a 30 second simulation, while the corresponding velocity is shown in the lower plot

Dynamic behaviour of the model is considered sufficient to proceed to introduce faults and implement the diagnosis method.

4 Diagnosis using Structural Analysis

This chapter presents the structural analysis approach that forms the basis of creating a Fault Diagnosis and Isolation (FDI) algorithm. FDI are considered critical to guarantee safety, reliability and continuous operation for complex systems, but also to detect possible failures in an early stage and provide insight to a systems behaviour. The theory covered in the following section bases, solely, on chapter five in the book "Diagnosis and Fault-Tolerant Control" [16].

4.1 Structural Model

Structural analysis bases on a systems structural model, which according to the introduction to chapter five in [16], is described as:

"The structural model of a system is an abstraction of its behaviour model in the sense that only the structure of the constraints, i.e. the existence of links between variables and parameters is considered and not the constraints themselves"

Structure and constraints can be represented as a bipartite graph, which represents basic features and properties of an independent system. The behaviour model is defined by $[C, Z]$ where Z is a set of variables and parameters, and C is a set of constraints. Constraint can be expressed in several forms, such as algebraic and differential equations.

The set of variables Z consists of known variables, K, and unknown variables, X. Where K are measured variables and known control inputs . X refer to algebraic variables, dynamic states defined in the model, unknown inputs and parameters. The system constraints are a set of algebraic, differential and measurement constraint.

4.2 Canonical Subsystem

Canonical decomposition utilizes the mathematical tool Dulmage-Mendelsohn Decomposition (DMD), where a structural model can be decomposed into three sub graphs with the specific properties [17]:

- Structurally over-constrained subsystem S^+, where there are more constraints than unknowns
- Structurally just-constrained subsystem S^0, where there are equally number of constraints than unknowns
- Structurally under-constrained subsystem S^-, where there are less constraints than unknowns

The over-constrained subsystem has one unique solution and it also can be used to define Analytical Redundancy Relations (ARRs) for FDI. The just-constrained subsystem has one unique solution, and the under-constrained subsystem has no unique solution, i.e. the unknown variables can't be uniquely defined [16, 17].

The three subsystems play a key role in analysing the systems structural properties such as observability, controllability, monitorability and reconfigurability [15]. The over- and just-constrained subsystem is called casual if there exists a complete matching with respect to variables which does not contain any differential loop.

4.2.1 Redundancy of a Structural Model

Fault diagnosis based on residuals has high performance without the need for additional hardware. Residuals are generated by calculating the difference between parameters estimated by a mathematical model of the system and measurements from sensors and actuators. A residual is a generated signal that is zero when a system is healthy and non-zero when faults occurs.

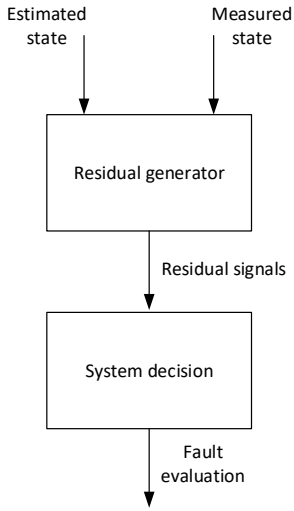

Figure 4.1: Fault diagnosis system

In order to find a system residual, all unknown variables, X, must be computed using the known variables, K. The incidence matrix and the bipartite graph defines the interrelationship between constrains and variables, but does not provide information about the unknown variables. A technique called matching is used to determine unknown variables of the structural model. Matching of the structural graph gives an orientated bipartite graph, where the unknown variable can be determined by combining constraints with unknown variables.

4.3 Application on Electrical Winch

Figure 4.2 is an overview of the electrical winch structure. The system consists of a PMSM with associated controllers, a one-stage gearbox, two bearings and the drum. In addition, there are mounted a variety of sensors that are used to give the measurable states and output of the system. (equation 4.1).

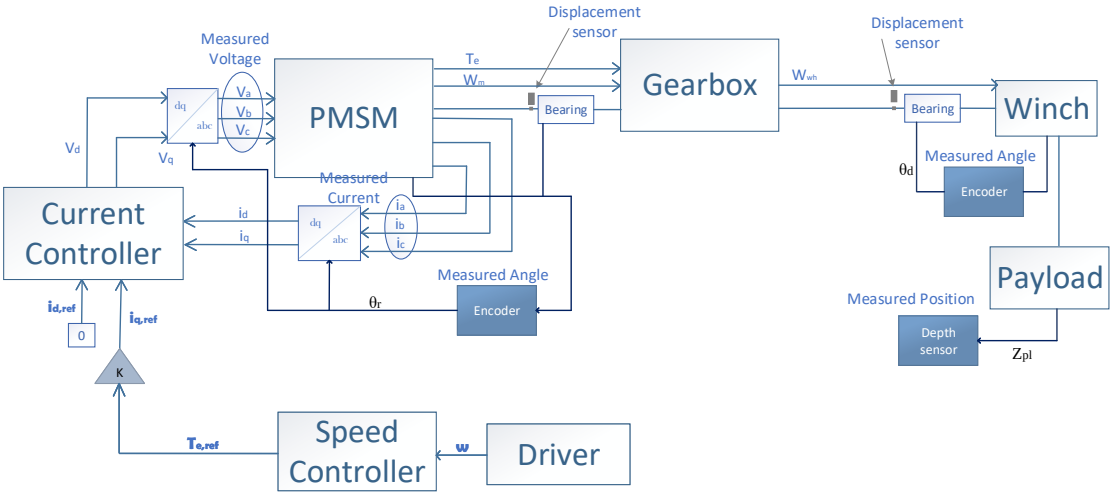

Figure 4.2: Drive system of electrical winch

The electrical winch is assumed to be fitted with a variety of sensors to detect irregularities. The three phase currents i_a, i_b and i_c are measured by using a current sensor, a simple device that can be clamped to a cord. In addition, the three phase input voltages v_a, v_b and v_c are measured using a voltage sensor. Knowing the input voltage at any time allows for excluding internal faults if it should be obvious that there is a problem with the power supply.

Angular position of both rotor and drum are measured with two optical quadratic encoders that are used to measure rotation of the motor shaft, θ_r, and the shaft connected to the drum, θ_d. Use of encoders allows identifying the direction of rotation, number of rotations and rotational speed. Optical encoders are virtually immune to noise due to the digital signal transmission.

Eddy current sensors are used to measure the relative shaft displacement, x_{inn} and y_{inn}, to detect misalignment. The sensors work by generating magnetic fields in metal surfaces and measure eddy currents in the target material.

Last, a pressure sensor is used to measure the payload underwater depth, and to establish the relative payload position, Z_{pl}.

The modelled electrical winch is used as a reference source for information about the system being diagnosed in the form of differential equations and measured system output. The relation of variables is linked by a set of constraints using the system parameters derived in chapter 3.

$$\zeta = \{C_1, \ldots, C_{41}, d_1, \ldots, d_{16}, m_1, \ldots, m_{13}\}$$

Where constraints C_1 - C_{11} and C_{13} - C_{16} represents the PMSM. Constraints C_{18} - C_{23} represents the internal motor bearing. Constraints C_{24} - C_{34} represents the mechanical system, including the gearbox. Constraints C_{36} to C_{41} represents the bearing connected to the drum. All the applied constraints are written in the following eqautions, included differential constraints, indexed d_x, and measured constraints, indexed m_x.

C_1 : $V_\alpha = V_a - \frac{1}{2}V_b - \frac{1}{2}V_c$

C_2 : $V_\beta = \frac{\sqrt{3}}{2}V_b - \frac{\sqrt{3}}{2}V_c$

C_3 : $V_s = V_\alpha + jV_\beta$

C_4 : $i_s = i_\alpha + ji_\beta$

C_5 : $i_a = \frac{2}{3}i_\alpha$

C_6 : $i_b = \frac{-1}{3}i_\alpha + \frac{1}{\sqrt{3}}i_\beta$

C_7 : $i_c = \frac{-1}{3}i_\alpha - \frac{1}{\sqrt{3}}i_\beta$

C_8 : $L_s\dot{i}_\alpha = V_\alpha - R_s i_\alpha + \psi^s_{R\beta}\omega_r$

C_9 : $L_s\dot{i}_\beta = V_\beta - R_s i_\beta - \psi^s_{R\alpha}\omega_r$

C_{10} : $T_{em} = \frac{p}{3}(i_\beta\psi^s_{R\alpha} - i_\alpha\psi^s_{R\beta})$

C_{11} : $\dot{\omega}_m = \frac{1}{J}(T_{em} - b\omega_m - T_{Lm})$

C_{12} : $\omega_d = \frac{\omega_r}{n}$

C_{13} : $\psi^s_R = \psi_R \cdot (\cos(\theta_r) + j\sin(\theta_r))$

C_{14} : $\psi^s_{R\alpha} = j\psi_R\cos(\theta_r)$

C_{15} : $\psi^s_{R\beta} = \psi_R\sin(\theta_r)$

C_{16} : $\omega_r = \frac{p}{2}\omega_m$

C_{17} : $\theta_{inn} = \theta_r$

C_{18} : $\theta_{cage} = \frac{D_{inn}}{D_c}\cdot\frac{\theta_r}{2}$

C_{19} : $\theta_i = \theta_{cage} + \frac{2\pi}{n_b}\cdot k \qquad k = 0, ..., (n_b - 1)$

C_{20} : $m\ddot{x}_{inn} = F_{ex} + F_u\cos(\theta_{inn}) - D\dot{x}_{inn} - \Sigma F(i)\cos(\theta_i)$

C_{21} : $m\ddot{y}_{inn} = F_{ey} + F_u\sin(\theta_{inn}) - D\dot{y}_{inn} - \Sigma F(i)\sin(\theta_i)$

C_{22} : $\delta_i = x_{inn}\cos(\theta_i) + y_{inn}\sin(\theta_i)$

C_{23} : $F(i) = C_{eq}\delta_i^{\frac{3}{2}}$

C_{24} : $T_{DL} = F_w \cdot r_d - J_d \cdot \ddot{\theta}_d$

C_{25} : $F_w = \delta_w \cdot k_w + \dot{\delta}_w \cdot b_w$

C_{26} : $\delta_w = -x_{pl} - \theta_d \cdot r_d + \delta_0$

C_{27} : $\dot{\delta}_w = -v_{pl} - \omega_d \cdot r_d$

C_{28} : $T_{Lm} = (T_{DL} + F_{SD} \cdot r_{wh})/n$

C_{29} : $F_{SD} = C_k\left(\theta_r \cdot r_p - \theta_d \cdot r_{wh}\right) + 0.1 \cdot C_k\left(\omega_r \cdot r_p - \omega_d \cdot r_{wh}\right)$

C_{30} : $J_{wh}\ddot{\theta}_d = F_{SD} \cdot r_{wh} - \mu_{friction}\omega_d + T_{DL}$

C_{31} : $k_w = \frac{E_w \cdot A_w}{\theta_d \cdot r_d + L_0}$

C_{32} : $b_w = 0.1 \cdot k_w$

C_{33} : $m_{pl} \cdot a_{pl} = F_w - m_{pl} \cdot g$

C_{34} : $x_{pl} - x_{pl_{init}} = Z_{pl}$

C_{35} : $\theta_{inn2} = \theta_d$

C_{36} : $\theta_{d_{cage}} = \frac{D_{inn}}{D_c}\frac{\theta_d}{2}$

C_{37} : $\theta_{i2} = \theta_{d_{cage}} + \frac{2\pi}{n_b}\cdot k$

C_{38} : $m\ddot{x}_{inn2} = F_{ex} + F_u\cos(\theta_{inn2}) - D\dot{x}_{inn2} - \Sigma F(i2)\cos(\theta_{i2})$

C_{39} : $m\ddot{y}_{inn2} = F_{ey} + F_u\sin(\theta_{inn2}) - D\dot{y}_{inn2} - \Sigma F(i2)\sin(\theta_{i2})$

C_{40} : $\delta_{i2} = x_{inn2}\cos(\theta_{i2}) + y_{inn2}\sin(\theta_{i2})$

C_{41} : $F_{i2} = C_{eq}\delta_{i2}^{\frac{3}{2}}$

d_1 : $\frac{di_\alpha}{dt} = \dot{i}_\alpha$

d_2 : $\frac{di_\beta}{dt} = \dot{i}_\beta$

d_3 : $\frac{d\theta_r}{dt} = \omega_r$

d_4 : $\frac{d\omega_m}{dt} = \dot{\omega}_m$

d_5 : $\frac{dx_{inn}}{dt} = \dot{x}_{inn}$

d_6 : $\frac{d\dot{x}_{inn}}{dt} = \ddot{x}_{inn}$

d_7 : $\frac{dy_{inn}}{dt} = \dot{y}_{inn}$

d_8 : $\frac{d\dot{y}_{inn}}{dt} = \ddot{y}_{inn}$

d_9 : $\frac{d\theta_d}{dt} = \omega_d$

d_{10} : $\frac{d\omega_d}{dt} = \alpha_d$

d_{11} : $\frac{dx_{pl}}{dt} = v_{pl}$

d_{12} : $\frac{dv_{pl}}{dt} = a_{pl}$

d_{13} : $\frac{dx_{inn2}}{dt} = \dot{x}_{inn2}$

d_{14} : $\frac{d\dot{x}_{inn2}}{dt} = \ddot{x}_{inn2}$

d_{15} : $\frac{dy_{inn2}}{dt} = \dot{y}_{inn2}$

d_{16} : $\frac{d\dot{y}_{inn2}}{dt} = \ddot{y}_{inn2}$

m_1 : $y_{v_a} = V_a$

m_2 : $y_{v_b} = V_b$

m_3 : $y_{v_c} = V_c$

m_4 : $y_{i_a} = i_a$

m_5 : $y_{i_b} = i_b$

m_6 : $y_{i_c} = i_c$

m_7 : $y_{\theta_d} = \theta_d$

m_8 : $y_{\theta_r} = \theta_r$

m_9 : $y_{x_{inn}} = x_{inn}$

m_{10} : $y_{y_{inn}} = y_{inn}$

m_{11} : $y_{Z_{pl}} = Z_{pl}$

m_{12} : $y_{x_{inn1}} = x_{inn1}$

m_{13} : $y_{y_{inn1}} = y_{inn1}$

The system parameters can be categorized as known and unknown . Where
R_s, J, p, D_{inn}, D_c, n_b, D, m, C_{eq}, r_d, J_d, d_w, r_{wh}, r_p are known constant parameters.
And b, F_u, F_{ex}, F_{ey}, $F(i)$, $\mu_{friction}$ are unknown parameters that are related to system faults. The unknown parameters are zero for a healthy system.

Additionally, there are known and unknown system variables.
The set of known variables (listed in 4.1) are available in real time, through sensor readings, and applied directly in the fault detection algorithm.

$$K_m = \{v_{am}, v_{bm}, v_{cm}, i_{am}, i_{bm}, i_{cm}, \theta_{dm}, \theta_{rm}, z_{plm}, x_{innm}, y_{innm}, x_{inn2m}, y_{inn2m}\} \tag{4.1}$$

Using the listed constraints and all known parameters and variables allows for calculation of the unknown variables. The set of unknown variables are listed in 4.2.

$$\begin{aligned} X_m = \{&v_a, v_b, v_c, v_\alpha, v_\beta, i_a, i_b, i_c, i_\alpha, i_\beta, v_s, i_s, \psi^s_R, \psi^s_{R\alpha}, \psi^s_{R\beta}, \theta_r, T_{em}, T_{Lm}, \dot{i}_\alpha, \dot{i}_\beta \\ &\omega_r, \omega_m, \dot{\omega}_m, \theta_{cage}, \theta_{inn}, \theta_i, x_{inn}, y_{inn}, \dot{x}_{inn}, \dot{y}_{inn}, \ddot{x}_{inn}, \ddot{y}_{inn}, F_i, \delta_i \\ &\theta_d, \omega_d, \theta_{dcage}, \theta_{inn2}, \theta_{i2}, x_{inn2}, y_{inn2}, \dot{x}_{inn2}, \dot{y}_{inn2}, \ddot{x}_{inn2}, \ddot{y}_{inn2}, F_{i2}, \delta_{i2} \\ &\ddot{\theta}_d, F_w, F_{SD}, F_{DL}, x_{pl}, v_{pl}, a_{pl}, \delta_w, \dot{\delta}_w, K_w, b_w, Z_{pl}\} \end{aligned} \tag{4.2}$$

The constraints are graphically presented in figure 4.5 and grouped dependent to which component they are valid. Variables are highlighted in the circles, while the constraints are portrayed as a black rectangle. All constraints are connected to their respective variables using simple lines that initially, has no direction. All variables have the same status and each constraint can be used to calculate any unknown variable.

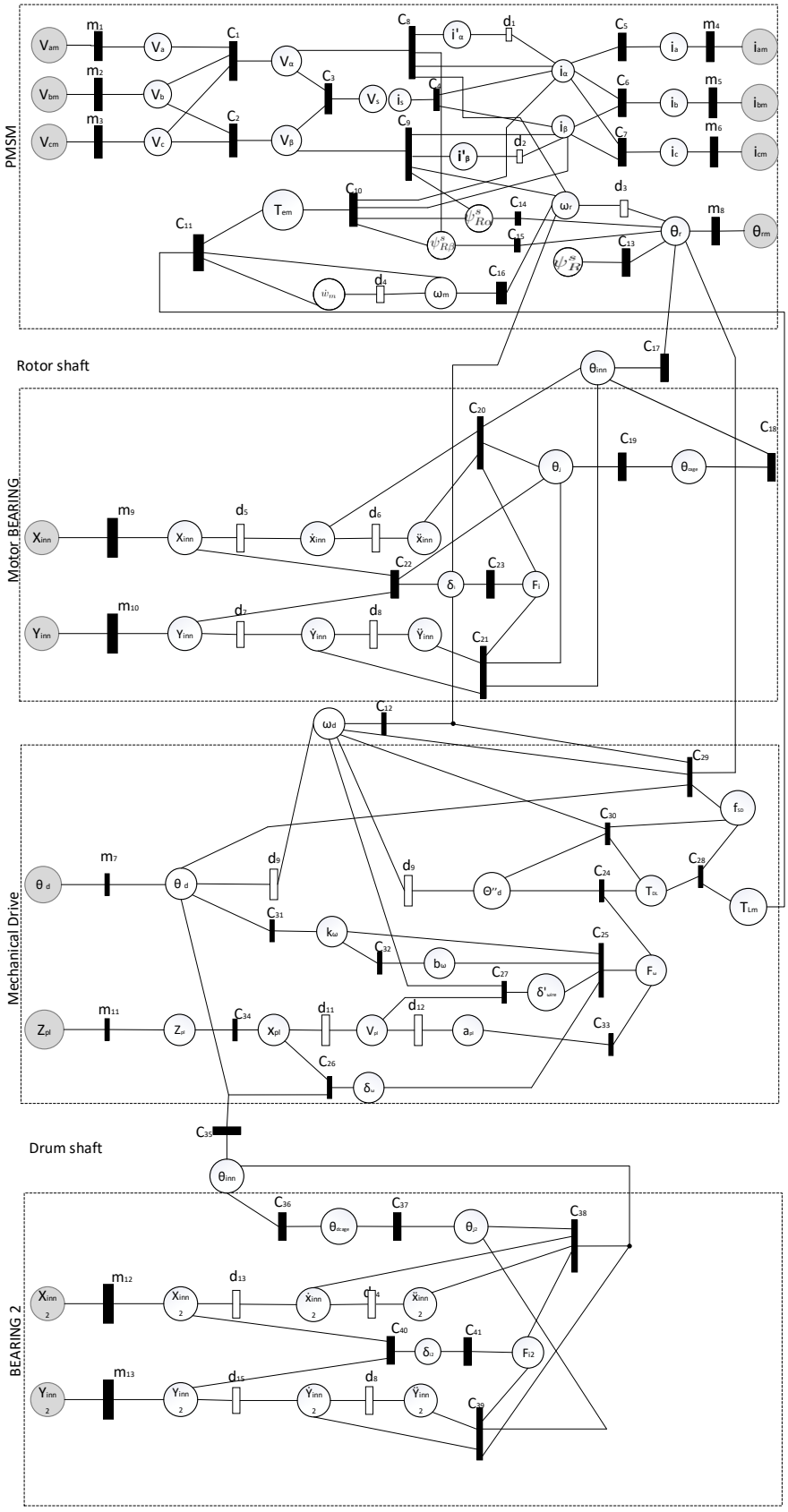

Figure 4.3: Structural graph of the electrical winch

The structural graph are then matched, and the result can be seen in figure 4.4. The constraints are divided into two groups; non-matched or matched. A matched constraint has arrows leading both in and out, while a non-matched constraint has arrows leading only in, therefore non-matched constraints has zero as output.

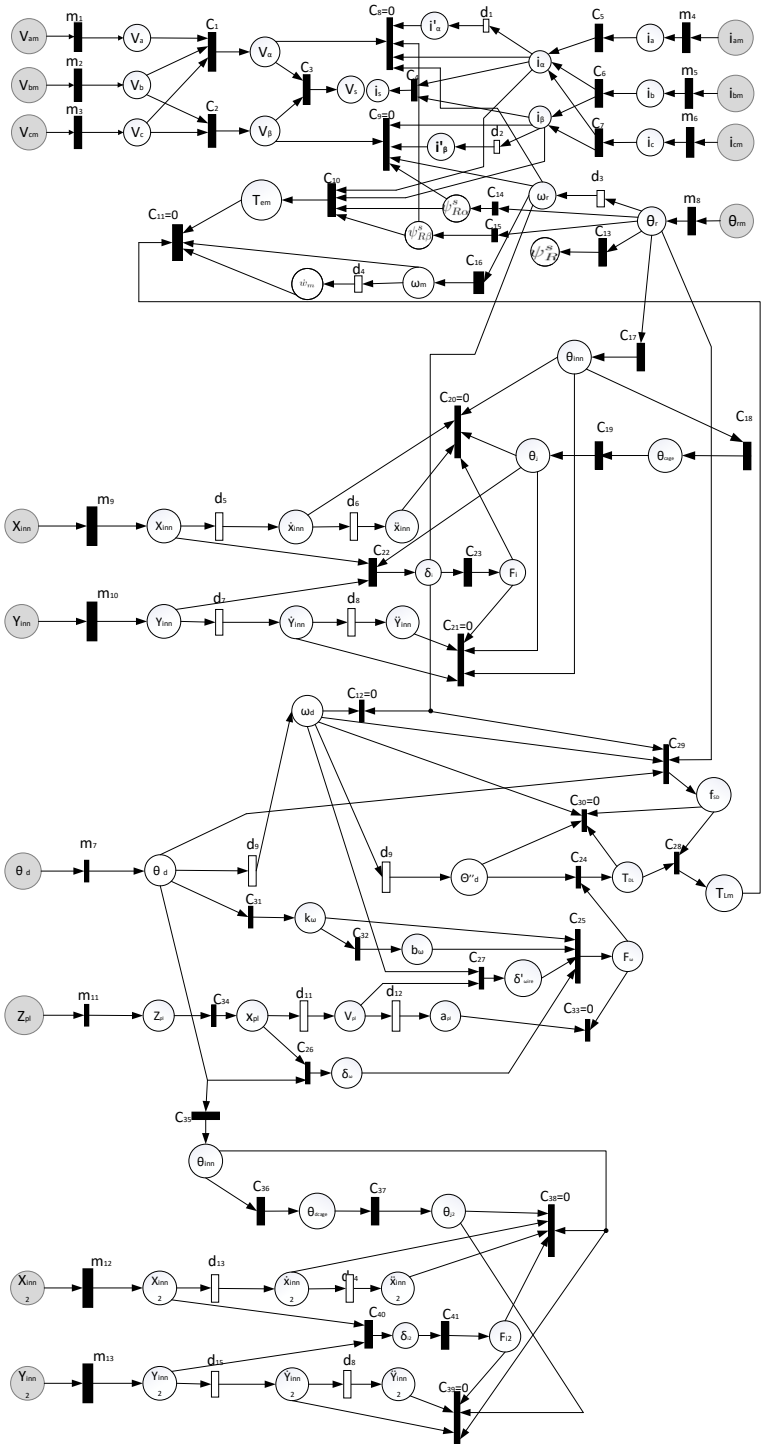

Figure 4.4: Oriented bipartite graph

The bipartite graph can also be expressed in the form of an incidence matrix (chapter five in [16]). The matrix rows represent the constraints while the columns represent variables in two categories; known and unknown. For a given constraint the matched variables are identified by a circle, while the non-matched variables are identified by a line.

Differential constraints can only be matched in one way. A known variable can always be differentiated but cannot be integrated due to the lack of initial conditions. Therefore, differential constraints are marked with an x, which forbids integral matching in the incidence matrix.

The incidence matrix show that this system has seventy constraints, $|\zeta|$, and fifty-nine unknown variables, $|X_m|$. This gives a maximum of eleven residuals, resulting in a structurally over-constrained subsystem.

$$|\zeta| - |X_m| = 70 - 59 = 11$$

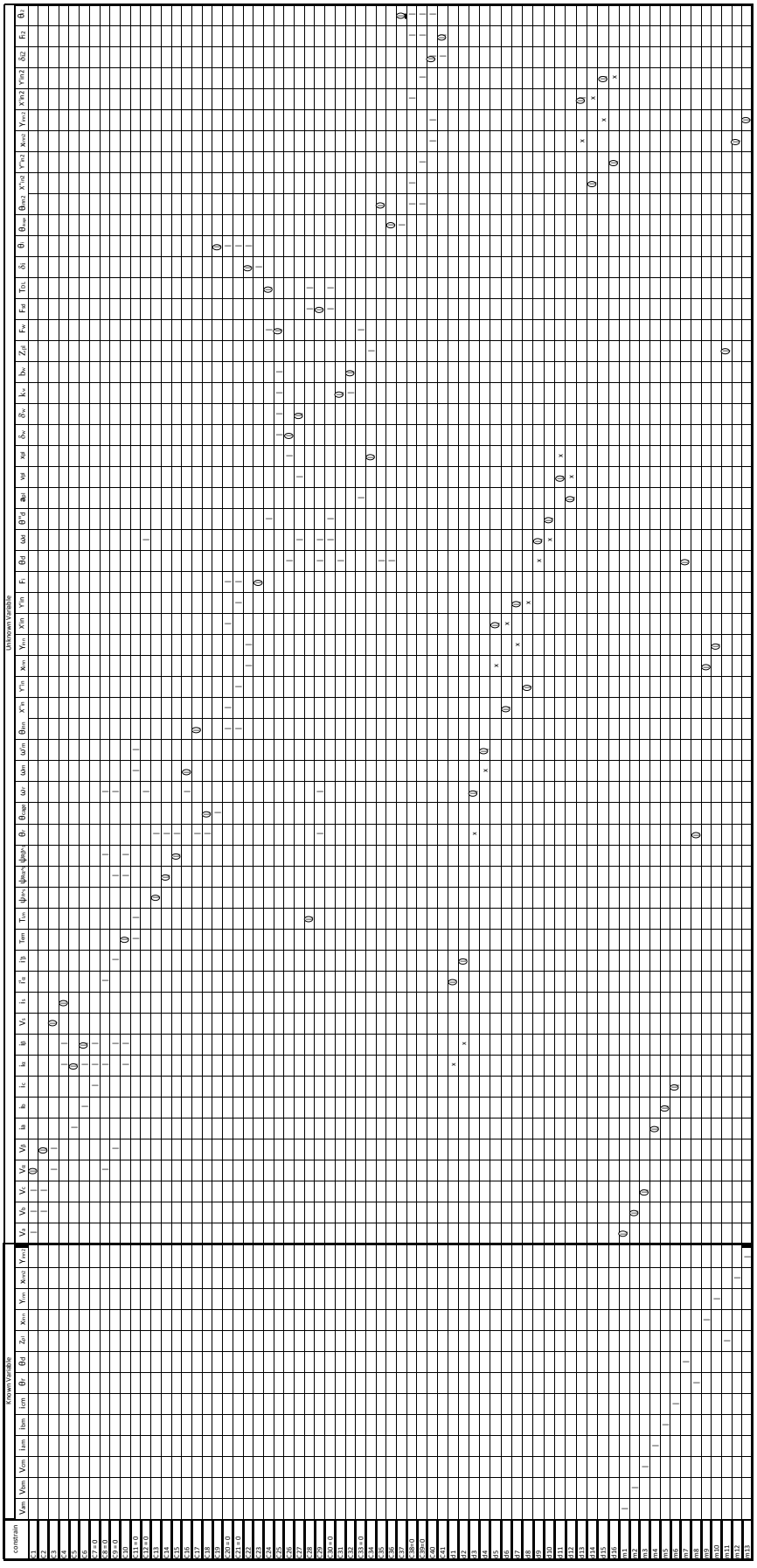

Figure 4.5: Structural graph of the electrical winch

The parity relations of the system is listed below, where backtracking to known variables gives a suggestion for relations that can be used as residual generators.

$$\boldsymbol{C_7}\big(m_6(i_c),\quad C_5(m_4(i_a)),\quad C_6(C_5(m_4(i_a)),m_5(i_b))\big)$$

$$\begin{aligned}&\boldsymbol{C_8}\big(C_1(m_1(V_{am}),m_2(V_{bm}),m_3(V_{cm})),\\&\quad C_5(m_4(i_{am})),\quad d_1(C_5(m_4(i_{am}))),\quad C_{15}(m_8(\theta_r)),\quad d_3(m_8(\theta_r))\big)\end{aligned}$$

$$\begin{aligned}&\boldsymbol{C_9}\big(C_2(m_2(V_{bm}),m_3(V_{cm})),\quad C_6(C_5(m_4(i_{am})),m_5(i_{am})),\\&\quad d_2(C_6(C_5(m_4(i_{am})),m_5(i_{am})),\quad C_{14}(m_8(\theta_r)),\quad d_3(m_8(\theta_r))\big)\end{aligned}$$

$$\begin{aligned}&\boldsymbol{C_{11}}\big(C_{10}(C_6(C_5(m_4(i_{am})),m_5(i_{bm})),C_5(m_4(i_{am})),C_{14}(m_8(\theta_r)),C_{15}(m_8(\theta_r)))\\&\quad C_{28}(C_{29}(d_9(m_7(\theta_d),m_7(\theta_d),d_3(m_8(\theta_r)),m_8(\theta_r)),\\&\qquad C_{24}(C_{25}(C_{32}(C_{31}(m_7(\theta_d))),C_{31}(m_7(\theta_d)),C_{27}(d_{11}(C_{34}(m_{11}(Z_{PL}))),\\&\qquad d_9(m_7(\theta_d))),C_{26}(C_{34}(m_{11}(Z_{PL})),m_7(\theta_d)))),d_{10}(d_9(m_7(\theta_d))))\\&\quad d_4(C_{16}(d_3(m_8(\theta_r)))))\big)\end{aligned}$$

$$\boldsymbol{C_{12}}\big(d_3(m_8(\theta_r)),\quad d_9(m_7(\theta_d))\big)$$

$$\begin{aligned}&\boldsymbol{C_{20}}\big(C_{17}(m_8(\theta_{rm})),\quad d_6(d_5(m_9(X_{inn}))),\quad d_5(m_9(X_{inn})),\\&\quad C_{23}(C_{22}(C_{19}(C_{18}(m_8(\theta_{rm}))),m_{10}(Y_{inn}),m_9(X_{inn})),\\&\quad C_{19}(C_{18}(m_8(\theta_{rm})))\big)\end{aligned}$$

$$\begin{aligned}&\boldsymbol{C_{21}}\big(C_{17}(m_8(\theta_{rm})),\quad d_8(d7(m_{10}(Y_{inn}))),\quad d_7(m_{10}(Y_{inn})),\\&\quad C_{23}(C_{22}(C_{19}(C_{18}(C_{17}(m_8(\theta_{rm})))),m_{10}(Y_{inn}),m_9(X_{inn})),\\&\quad C_{19}(C_{18}(m_8(\theta_{rm})))\big)\end{aligned}$$

$$\begin{aligned}&\boldsymbol{C_{30}}\big(d_{10}(d_9(m_7(\theta_d))),\\&\quad C_{29}(d_9(m_7(\theta_d)),(m_7(\theta_d)),d_3(m_8(\theta_r)),m_8(\theta_r)),\\&\quad C_{24}(C_{25}(C_{32}(C_{31}(m_7(\theta_d))),C_{31}(m_7(\theta_d)),C_{27}(d_{11}(C_{34}(m_{11}(Z_{PL}))),\\&\qquad d_9(m_7(\theta_d))),C_{26}(C_{34}(m_{11}(Z_{PL})),m_7(\theta_d))),d_{10}(d_9(m_7(\theta_d))))\big)\end{aligned}$$

$$\begin{aligned}&\boldsymbol{C_{33}}\big(d_{12}(C_{34}(m_{11}(Z_{PL}))),\\&\quad C_{25}(C_{32}(C_{31}(m_7(\theta_d))),C_{31}(m_7(\theta_d)),C_{27}(d_{11}(C_{34}(m_{11}(Z_{PL}))),\\&\qquad d_9(m_7(\theta_d))),C_{26}(C_{34}(m_{11}(Z_{PL})),m_7(\theta_d)))\big)\end{aligned}$$

$$\begin{aligned}&\boldsymbol{C_{38}}\big(C_{35}(m_7(\theta_{dm})),\quad d_{14}(d_{13}(m_{12}(X_{inn2}))),\quad d_{13}(m_{12}(X_{inn2})),\\&\quad C_{41}(C_{40}(C_{37}(C_{36}(m_7(\theta_{dm}))),m_{12}(X_{inn2}),m_{13}(Y_{inn2})),\\&\quad C_{37}(C_{36}(m_7(\theta_{dm}))))\big)\end{aligned}$$

$$\begin{aligned}&\boldsymbol{C_{39}}\big(C_{35}(m_7(\theta_{dm})),\quad d_{16}(d_{15}(m_{13}(Y_{inn2}))),\quad d_{15}(m_{13}(Y_{inn2})),\\&\quad C_{41}(C_{40}(C_{37}(C_{36}(m_7(\theta_{dm}))),m_{12}(X_{inn2}),m_{13}(Y_{inn2})),\\&\quad C_{37}(C_{36}(m_7(\theta_{dm}))))\big)\end{aligned}$$

The analytical form of the parity relations are obtained from the symbolic expressions, which gives the following equations. Residuals are indexed with the same number as the corresponding constraint.

$$
\begin{cases}
r_7: & i_{am} + i_{bm} + i_{cm} = 0 \\[2ex]
r_8: & \frac{3 \cdot L_s}{2} \cdot \frac{di_{am}}{dt} - (V_{am} - \frac{V_{bm}}{2} - \frac{V_{cm}}{2}) + \frac{R_s \cdot i_{am}}{2} - j\Psi_R \sin(\theta_{rm}) \frac{d\theta_r}{dt} = 0 \\[2ex]
r_9: & L_s \frac{d((i_{bm} + \frac{i_{am}}{2})\sqrt{3})}{dt} - (\frac{\sqrt{3}V_{bm}}{2} - \frac{\sqrt{3}V_{bm}}{2}) + \sqrt{3}R_s(i_{bm} + \frac{i_{am}}{2}) + \Psi_R \cos(\theta_{rm}) \frac{d\theta_r}{dt} = 0 \\[2ex]
r_{11}: & \frac{2}{p}\frac{d^2\theta_{rm}}{dt^2} - \frac{1}{j}\Big(\frac{p}{3}\big((i_{bm} + \frac{i_{am}}{2})\Psi_R \cos(\theta_{rm}) - \frac{3}{2} i_{am} \Psi_R \sin(\theta_{rm})\big) + b_f \frac{d\theta_{rm}}{dt} - \big(F_w r_d - J_d \ddot{\theta}_d + F_{SD} r_{wh}\big)\Big) = 0 \\[2ex]
r_{12}: & \frac{d\theta_{dm}}{dt} - \frac{1}{n} \cdot \frac{d\theta_{rm}}{dt} = 0 \\[2ex]
r_{20}: & m_s \frac{d^2 x_{inn,m}}{dt^2} - F_u \cdot \cos(\theta_{rm})) + D \frac{dx_{inn,m}}{dt} + ... \\
& \Sigma C_{eq}\Big(\big(x_{inn,m} \cos(\frac{D_{inn}}{2 \cdot D_c}(\theta_{rm}) + \frac{2\pi}{n_b} \cdot k)\big) + ... \\
& \big(y_{inn,m} \sin(\frac{D_{inn}}{2 \cdot D_c}(\theta_{rm}) + \frac{2\pi}{n_b} \cdot k)\big)\Big)^{\frac{3}{2}} \cos(\frac{D_{inn}}{2 \cdot D_c}(\theta_{rm}) + \frac{2\pi}{n_b} \cdot k) = 0 \\[2ex]
r_{21}: & m_s \frac{d^2 y_{inn,m}}{dt^2} - F_u \cdot \sin(\theta_{rm}) + D \frac{dy_{inn,m}}{dt} + m_s g + ... \\
& \Sigma C_{eq}\Big(\big(x_{inn,m} \cos(\frac{D_{inn}}{2 \cdot D_c}(\theta_{rm}) + \frac{2\pi}{n_b} \cdot k)\big) + ... \\
& \big(y_{inn,m} \sin(\frac{D_{inn}}{2 \cdot D_c}(\theta_{rm}) + \frac{2\pi}{n_b} \cdot k)\big)\Big)^{\frac{3}{2}} \sin(\frac{D_{inn}}{2 \cdot D_c}(\theta_{rm})) + \frac{2\pi}{n_b} \cdot k) = 0 \\[2ex]
r_{30}: & J_{wh}\frac{d^2\theta_{dm}}{dt^2} - r_{wh}\big(C_k(\theta_{rm} r_p - \theta_{dm} r_{wh}) + 0.1 C_k(\frac{d\theta_{rm}}{dt} r_p - \frac{d\theta_{rm}}{dt} r_{wh})\big) + \mu_f \frac{d\theta_{dm}}{dt} - \big(F_w r_d - J_d \frac{d^2\theta_{dm}}{dt^2}\big) = 0 \\[2ex]
r_{33}: & m_{pl} \frac{d^2(Z_{pl,m} - x_{plinit})}{d^2 t} + m_{pl} g - ... \\
& \Big(\frac{E_w \cdot A_w}{\theta_{dm} \cdot r_d + L_0}\big(-(Z_{pl,m} - x_{plinit}) - \theta_{dm} \cdot r_d + \delta_0\big) + \frac{0.1 \cdot E_w \cdot A_w}{\theta_{dm} \cdot r_d + L_0}\big(\frac{-d(Z_{pl,m} - x_{plinit})}{dt} - \frac{d\theta_{dm}}{dt} \cdot r_d\big)\Big) = 0 \\[2ex]
r_{38}: & m_s \frac{d^2 x_{inn2,m}}{dt^2} - F_u \cdot \cos(\theta_{dm}) + D \frac{dx_{inn2,m}}{dt} + ... \\
& \Sigma C_{eq}\Big(\big(x_{inn2,m} \cos(\frac{D_{inn}}{2 \cdot D_c}(\theta_{dm}) + \frac{2\pi}{n_b} \cdot k)\big) + ... \\
& \big(y_{inn2,m} \sin(\frac{D_{inn}}{2 \cdot D_c}(\theta_{dm}) + \frac{2\pi}{n_b} \cdot k)\big)\Big)^{\frac{3}{2}} \cos(\frac{D_{inn}}{2 \cdot D_c}(\theta_{dm}) + \frac{2\pi}{n_b} \cdot k) = 0 \\[2ex]
r_{39}: & m_s \frac{d^2 y_{inn2,m}}{dt^2} - F_u \cdot \sin(\theta_{dm}) + D \frac{dy_{inn2,m}}{dt} + m_s g + ... \\
& \Sigma C_{eq}\Big(\big(x_{inn2,m} \cos(\frac{D_{inn}}{2 \cdot D_c}(\theta_{dm}) + \frac{2\pi}{n_b} \cdot k)\big) + ... \\
& \big(y_{inn2,m} \sin(\frac{D_{inn}}{2 \cdot D_c}(\theta_{dm}) + \frac{2\pi}{n_b} \cdot k)\big)\Big)^{\frac{3}{2}} \sin(\frac{D_{inn}}{2 \cdot D_c}(\theta_{dm}) + \frac{2\pi}{n_b} \cdot k) = 0
\end{cases}
$$

A dependency matrix (DM) is made to represent dependencies between residual and constraints. The eleven residuals represent each of the rows and all columns are labelled with the constraints. Cells marked by "1" indicates which constraint contributes to information regarding the residuals.

The dependency matrix is used to determine the signature of a faulty condition. To perform diagnosis, each column gives information about faulty situations, which can be distinguished from each other by evaluating the different combinations. Some conditions have the same signature which means it can be a group fault, while a unique combination means that a fault is structurally isolable.

$$
\begin{pmatrix} C_x \\ r_7 \\ r_8 \\ r_9 \\ r_{11} \\ r_{12} \\ r_{20} \\ r_{21} \\ r_{30} \\ r_{33} \\ r_{38} \\ r_{39} \end{pmatrix} =
\begin{pmatrix}
C_1 & C_2 & C_3 & C_4 & C_5 & C_6 & C_7 & C_8 & C_9 & C_{10} & C_{11} & C_{12} & C_{13} & C_{14} & C_{15} & C_{16} & C_{17} & C_{18} \\
0 & 0 & 0 & 0 & 1 & 1 & 1 & 0 & 0 & 0 & 0 & 0 & 0 & 0 & 0 & 0 & 0 & 0 \\
1 & 0 & 0 & 0 & 1 & 0 & 0 & 1 & 0 & 0 & 0 & 0 & 0 & 0 & 1 & 0 & 0 & 0 \\
0 & 1 & 0 & 0 & 1 & 1 & 0 & 0 & 1 & 0 & 0 & 0 & 0 & 1 & 0 & 0 & 0 & 0 \\
0 & 0 & 0 & 0 & 1 & 1 & 0 & 0 & 0 & 1 & 1 & 0 & 0 & 1 & 1 & 1 & 0 & 0 \\
0 & 0 & 0 & 0 & 0 & 0 & 0 & 0 & 0 & 0 & 0 & 1 & 0 & 0 & 0 & 0 & 0 & 0 \\
0 & 0 & 0 & 0 & 0 & 0 & 0 & 0 & 0 & 0 & 0 & 0 & 0 & 0 & 0 & 0 & 1 & 1 \\
0 & 0 & 0 & 0 & 0 & 0 & 0 & 0 & 0 & 0 & 0 & 0 & 0 & 0 & 0 & 0 & 1 & 1 \\
0 & 0 & 0 & 0 & 0 & 0 & 0 & 0 & 0 & 0 & 0 & 0 & 0 & 0 & 0 & 0 & 0 & 0 \\
0 & 0 & 0 & 0 & 0 & 0 & 0 & 0 & 0 & 0 & 0 & 0 & 0 & 0 & 0 & 0 & 0 & 0 \\
0 & 0 & 0 & 0 & 0 & 0 & 0 & 0 & 0 & 0 & 0 & 0 & 0 & 0 & 0 & 0 & 0 & 0 \\
0 & 0 & 0 & 0 & 0 & 0 & 0 & 0 & 0 & 0 & 0 & 0 & 0 & 0 & 0 & 0 & 0 & 0
\end{pmatrix}
$$

$$
\begin{pmatrix}
C_{19} & C_{20} & C_{21} & C_{22} & C_{23} & C_{24} & C_{25} & C_{26} & C_{27} & C_{28} & C_{29} & C_{30} & C_{31} & C_{32} & C_{33} & C_{34} & C_{35} \\
0 & 0 & 0 & 0 & 0 & 0 & 0 & 0 & 0 & 0 & 0 & 0 & 0 & 0 & 0 & 0 & 0 \\
0 & 0 & 0 & 0 & 0 & 0 & 0 & 0 & 0 & 0 & 0 & 0 & 0 & 0 & 0 & 0 & 0 \\
0 & 0 & 0 & 0 & 0 & 0 & 0 & 0 & 0 & 0 & 0 & 0 & 0 & 0 & 0 & 0 & 0 \\
0 & 0 & 0 & 0 & 0 & 1 & 1 & 1 & 1 & 1 & 1 & 0 & 1 & 1 & 0 & 1 & 0 \\
0 & 0 & 0 & 0 & 0 & 0 & 0 & 0 & 0 & 0 & 0 & 0 & 0 & 0 & 0 & 0 & 0 \\
1 & 1 & 0 & 1 & 1 & 0 & 0 & 0 & 0 & 0 & 0 & 0 & 0 & 0 & 0 & 0 & 0 \\
1 & 0 & 1 & 1 & 1 & 0 & 0 & 0 & 0 & 0 & 0 & 0 & 0 & 0 & 0 & 0 & 0 \\
0 & 0 & 0 & 0 & 0 & 1 & 1 & 1 & 1 & 0 & 1 & 1 & 1 & 1 & 0 & 1 & 0 \\
0 & 0 & 0 & 0 & 0 & 0 & 0 & 0 & 0 & 1 & 0 & 0 & 0 & 1 & 1 & 1 & 0 \\
0 & 0 & 0 & 0 & 0 & 0 & 1 & 1 & 1 & 0 & 0 & 0 & 1 & 1 & 1 & 1 & 0 \\
0 & 0 & 0 & 0 & 0 & 0 & 0 & 0 & 0 & 0 & 0 & 0 & 0 & 0 & 0 & 0 & 1 \\
0 & 0 & 0 & 0 & 0 & 0 & 0 & 0 & 0 & 0 & 0 & 0 & 0 & 0 & 0 & 0 & 1
\end{pmatrix}
$$

$$
\begin{pmatrix}
C_{36} & C_{37} & C_{38} & C_{39} & C_{40} & C_{41} & m_1 & m_2 & m_3 & m_4 & m_5 & m_6 & m_7 & m_8 & m_9 & m_{10} & m_{11} \\
0 & 0 & 0 & 0 & 0 & 0 & 0 & 0 & 0 & 1 & 1 & 1 & 0 & 0 & 0 & 0 & 0 \\
0 & 0 & 0 & 0 & 0 & 0 & 1 & 1 & 1 & 1 & 0 & 0 & 0 & 1 & 0 & 0 & 0 \\
0 & 0 & 0 & 0 & 0 & 0 & 0 & 1 & 1 & 1 & 1 & 0 & 0 & 1 & 0 & 0 & 0 \\
0 & 0 & 0 & 0 & 0 & 0 & 0 & 0 & 0 & 1 & 1 & 0 & 1 & 1 & 0 & 0 & 1 \\
0 & 0 & 0 & 0 & 0 & 0 & 0 & 0 & 0 & 0 & 0 & 0 & 1 & 1 & 0 & 0 & 0 \\
0 & 0 & 0 & 0 & 0 & 0 & 0 & 0 & 0 & 0 & 0 & 0 & 0 & 1 & 1 & 1 & 0 \\
0 & 0 & 0 & 0 & 0 & 0 & 0 & 0 & 0 & 0 & 0 & 0 & 0 & 1 & 1 & 1 & 0 \\
0 & 0 & 0 & 0 & 0 & 0 & 0 & 0 & 0 & 0 & 0 & 0 & 1 & 1 & 0 & 0 & 1 \\
0 & 0 & 0 & 0 & 0 & 0 & 0 & 0 & 0 & 0 & 0 & 0 & 1 & 0 & 0 & 0 & 1 \\
1 & 1 & 1 & 0 & 1 & 1 & 0 & 0 & 0 & 0 & 0 & 0 & 1 & 0 & 0 & 0 & 0 \\
1 & 1 & 0 & 1 & 1 & 1 & 0 & 0 & 0 & 0 & 0 & 0 & 1 & 0 & 0 & 0 & 0
\end{pmatrix}
$$

$$
\begin{pmatrix}
m_{12} & m_{13} & d_1 & d_2 & d_3 & d_4 & d_5 & d_6 & d_7 & d_8 & d_9 & d_{10} & d_{11} & d_{12} & d_{13} & d_{14} & d_{15} & d_{16} \\
0 & 0 & 0 & 0 & 0 & 0 & 0 & 0 & 0 & 0 & 0 & 0 & 0 & 0 & 0 & 0 & 0 & 0 \\
0 & 0 & 1 & 0 & 1 & 0 & 0 & 0 & 0 & 0 & 0 & 0 & 0 & 0 & 0 & 0 & 0 & 0 \\
0 & 0 & 0 & 1 & 1 & 0 & 0 & 0 & 0 & 0 & 0 & 0 & 0 & 0 & 0 & 0 & 0 & 0 \\
0 & 0 & 0 & 0 & 1 & 1 & 0 & 0 & 0 & 0 & 1 & 1 & 1 & 0 & 0 & 0 & 0 & 0 \\
0 & 0 & 0 & 0 & 1 & 0 & 0 & 0 & 0 & 0 & 1 & 0 & 0 & 0 & 0 & 0 & 0 & 0 \\
0 & 0 & 0 & 0 & 0 & 0 & 1 & 1 & 0 & 0 & 0 & 0 & 0 & 0 & 0 & 0 & 0 & 0 \\
0 & 0 & 0 & 0 & 0 & 0 & 0 & 0 & 1 & 1 & 0 & 0 & 0 & 0 & 0 & 0 & 0 & 0 \\
0 & 0 & 0 & 0 & 1 & 0 & 0 & 0 & 0 & 0 & 1 & 1 & 1 & 0 & 0 & 0 & 0 & 0 \\
0 & 0 & 0 & 0 & 0 & 0 & 0 & 0 & 0 & 0 & 1 & 0 & 1 & 1 & 0 & 0 & 0 & 0 \\
1 & 1 & 0 & 0 & 0 & 0 & 0 & 0 & 0 & 0 & 0 & 0 & 0 & 1 & 1 & 0 & 0 & 0 \\
1 & 1 & 0 & 0 & 0 & 0 & 0 & 0 & 0 & 0 & 0 & 0 & 0 & 0 & 0 & 1 & 1 & 0
\end{pmatrix}
$$

Any constraint is mapped onto the residuals, so all faults are detectable. Once the fault is detected successfully in the system, the next challenge is fault isolation. Fault isolation involves determining location of the error in a faulty component. To detect the fault a single residual signal is sufficient but fault isolation requires a set of residuals. The right-hand side column indicates which faults from table 2.4 corresponds a given combination.

$(0,0,0,0,0,0,0,0,0,0,0)$		Everything OK.	
$(1,0,0,0,0,0,0,0,0,0,0)$	C_7, m_6	Current fault or sensor fault (i_c) .	
$(1,0,1,1,0,0,0,0,0,0,0)$	C_6, m_5	Current fault or sensor fault(i_b).	
$(1,1,1,1,0,0,0,0,0,0,0)$	C_5, m_4	Current fault or sensor fault (i_a)	f_3
$(0,1,0,0,0,0,0,0,0,0,0)$	C_1, C_8, d_1 and m_1	Group fault (L_s, R_s, Current, Voltage).	f_1, f_3 and f_4
$(0,1,1,0,0,0,0,0,0,0,0)$	m_2, m_3	Sensor fault (Voltage sensor)	
$(0,1,1,1,1,0,0,1,0,0,0)$	d_3	Sensor fault (Rotor encoder).	f_4
$(0,1,0,1,0,0,0,0,0,0,0)$	C_{15}	Flux fault(ψ_R^s, θ_r)	f_4
$(0,1,1,1,1,1,1,1,0,0,0)$	m_8	Encoder fault.	f_4
$(0,0,1,0,0,0,0,0,0,0,0)$	C_2, C_9 and d_2	Group fault (L_s, R_s, Current, Voltage).	f_1, f_3 and f_4
$(0,0,1,1,0,0,0,0,0,0,0)$	C_{14}	Fault(ψ_R^s, θ_r)	f_4
$(0,0,0,1,0,0,0,0,0,0,0)$	$C_{10}, C_{11}, C_{16}, C_{28}, d_4$	Group Fault.	
$(0,0,0,1,0,0,0,1,0,0,0)$	C_{24}, C_{29}, d_{10}	Group Fault(F_{SD}, F_{DL}).	
$(0,0,0,1,0,0,0,1,1,0,0)$	$C_{25}, C_{26}, C_{27}, C_{31}, C_{32}, C_{34}, m_{11}, d_{11}$	Group Fault.	
$(0,0,0,1,1,0,0,1,1,1,1)$	m_7	Drum encoder Fault.	f_{10}
$(0,0,0,1,1,0,0,1,1,0,0)$	d_9	Drum Encoder Fault.	f_{10}
$(0,0,0,0,1,0,0,0,0,0,0)$	C_{12}	Fault.	f_4 and f_{10}
$(0,0,0,0,0,1,0,0,0,0,0)$	C_{20}, d_5, d_6	Bearing fault.	f_7
$(0,0,0,0,0,1,1,0,0,0,0)$	$C_{17}, C_{18}, C_{19}, C_{22}, C_{23}, m_9, m_{10}$	Group fault.	f_5, f_6 and f_7
$(0,0,0,0,0,0,1,0,0,0,0)$	C_{21}, d_7, d_8	Bearing fault.	
$(0,0,0,0,0,0,0,1,0,0,0)$	C_{30}	Gearbox fault.	
$(0,0,0,0,0,0,0,0,1,0,0)$	C_{33}, d_{12}	Payload fault.	f_{11} and f_{12}
$(0,0,0,0,0,0,0,0,0,1,0)$	C_{38}, d_{13}, d_{14}	Bearing 2 fault.	
$(0,0,0,0,0,0,0,0,0,1,1)$	$C_{35}, C_{36}, C_{37}, C_{40}, C_{41}, m_{12}, m_{13}$	Group fault.	f_{13}, f_{14} and f_{15}
$(0,0,0,0,0,0,0,0,0,0,1)$	C_{39}, d_{15}, d_{16}	Bearing 2 Fault.	f_{13}

$C_{12}, C_{14}, C_{15}, C_{20}, C_{30}, d_3, d_9, m_7$ and m_8 are structurally isolable because of unique signature.

4.3.1 Implementation in Simulink

The parity relations are implemented in Simulink via subsystems that are calculating the residuals for each time step in the simulation. To illustrate how the residuals are implemented in Simulink residual seven and eight, referred to as C_7, r_7 and C_8, r_8 (dependent on what form it is referred to as), are shown here. All residuals are implemented in the same manner.

Parity relation seven in symbolic and analytical form

$$\boldsymbol{C_7}\Big(m_6(i_c),\quad C_5(m_4(i_a)),\quad C_6\big(C_5(m_4(i_a)),m_5(i_b)\big)\Big)$$

$$r_7:\quad i_{am}+i_{bm}+i_{cm}=0$$

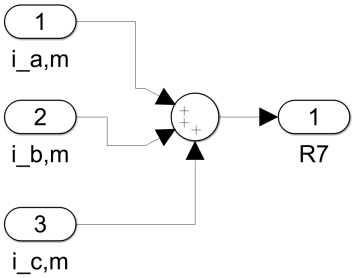

Figure 4.6: Implementation of r_7 in Simulink

Parity relation eight is more complex but implementation is done in the same manner as above.

$$\boldsymbol{C_8}\Big(C_1\big(m_1(V_{am}),m_2(V_{bm}),m_3(V_{cm})\big),$$
$$C_5(m_4(i_{am})),\quad d_1(C_5(m_4(i_{am}))),\quad C_{15}(m_8(\theta_r)),\quad d_3(m_8(\theta_r))\Big)$$

$$r_8:\frac{3\cdot L_s}{2}\cdot\frac{di_{am}}{dt}-(V_{am}-\frac{V_{bm}}{2}-\frac{V_{cm}}{2})+\frac{R_s\cdot i_{am}}{2}-j\Psi_R\sin(\theta_{rm})\frac{d\theta_r}{dt}=0$$

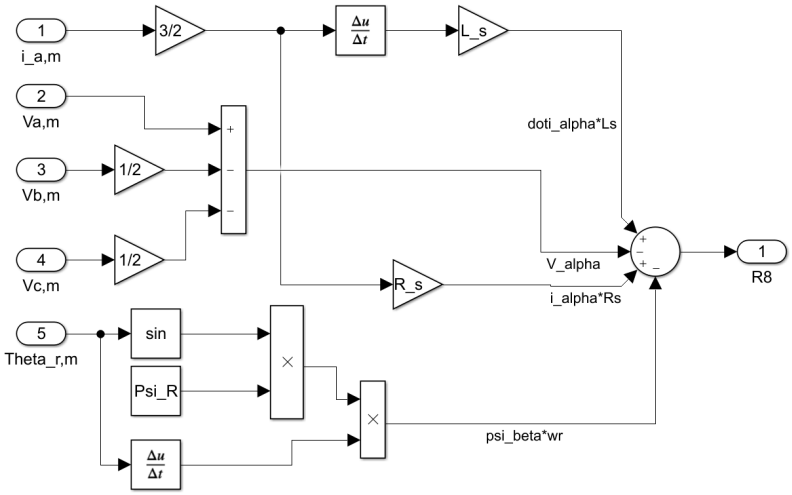

Figure 4.7: Implementation of r_8 in Simulink

4.3.2 Residuals Evaluation

Induced faults from table 2.4 are linked with the derived residuals, listed in table 4.8, in order to draw a correct conclusion about isolability for selected fault from the structural analysis [19]. The faults can result in fifteen different binary combinations of residuals (however, not all combinations are unique) that can be used to identify a fault.

Residual	PMSM				Bearing1			Gearbox			Bearing2			Winch	
	Parametric Faults		Additive Faults		Parametric Faults		Additive Faults	Parametric Faults		Additive Faults	Parametric Faults		Additive Faults	Parametric Faults	Additive Faults
	ΔR_s	$\Delta b_{friction}$	Δi_{am}	$\Delta\theta_r$	Db_{out}	F_u	$X_{inn\ sensor\ fault\ 1}$	ΔC_k	$\Delta\mu_{wh}$	$\Delta\theta_d$	Db_{out2}	F_{u2}	$Y_{inn\ sensor\ fault\ 2}$	ΔA_w	ΔZ_{pl}
r_7			1												
r_8	1	1	1	1				1	1					1	
r_9	1	1	1	1				1	1					1	
r_{11}		1	1	1				1	1	1				1	1
r_{12}		1		1				1	1	1					
r_{20}				1	1	1	1								
r_{21}				1	1	1	1								
r_{30}		1		1				1	1	1				1	1
r_{33}		1						1	1	1				1	1
r_{38}										1	1	1	1		
r_{39}										1	1	1	1		

Figure 4.8: Residual evaluation

Unique combinations that are structurally isolable, can be fault in the stator resistance, ΔR_s, and change in wire section, ΔA_w. While a change in the motor friction, $\Delta b_{friction}$, or stiffness change in the gearbox , ΔC_k, give the same combination and are then classified as not isolable. The bearings have a unique fault situation, but it is not possible to distinguish which part of the bearing that are damaged.

4.4 Fault Generation

This section details the difference between additive and parametric faults. In short, sensor faults are classified as additive while component faults are parametric.

4.4.1 Additive Faults

Faulty sensor measurement is a failure mode applied to the electrical winch. Sensor faults can occur in diverse ways; bias, drift, loss of accuracy, sensor freezing or calibration error [37]. For this application, implementation of bias is considered sufficient to represent faulty sensors. Bias is represented by adding or subtracting a constant value to the sensor signal, using equation 4.4.

$$y = x_i(t) \pm b_i \tag{4.3}$$

Where $x_i(t)$ denotes the measured signal and b_i denotes the constant value.

The modelled sensor measurements are added a percentage of zero mean Gaussian white noise to mirror a real situation. The noise is calculated based on a note ([38]) published by Mogens Blanke, one of the co-writers of "Diagnosis and Fault-Tolerant Control" [16]. The sensor noises are given by the auto correlation function:

$$H(s) = \frac{\sqrt{\beta}}{s+\beta} \cdot \sigma_w \tag{4.4}$$

Where β is a positive real constant and σ_w is the variance. The noise is implemented in Simulink by using a random signal generator as input and $H(s)$ as the transfer function. Figure 4.9 shows how noise is added to the current sensor measurement, i_a, in Simulink. Numerical values for σ and β are tuned iteratively.

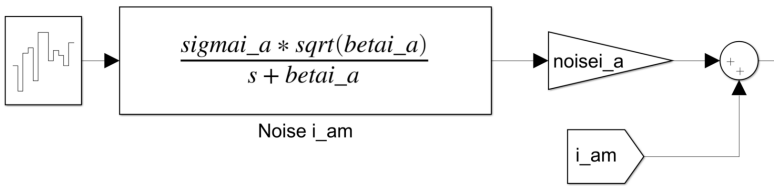

Figure 4.9: Implementation of noise in Simulink

4.4.2 Parametric faults

Fault in components are modelled as a sudden change in a parameter value, by using a Simulink function called pulse. The step is added to a parameters value (the parameters that are subjected to faults are listed in table 2.4) in order to simulate a fault. Figure 4.10 shows a specific example of how a step is added to the motor stator resistance. Figure 4.11 shows the internal block settings, like that the step is activated at $t = 2$ seconds and increases the stator resistance with 50%. R_s is a static motor parameter, while $FaultR_s$ is toggled between one and zero, depending on if the pulse should appear or not.

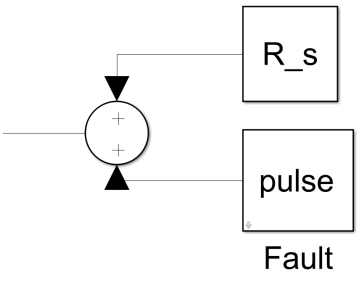

Figure 4.10: Adding a step to the stator resistance value

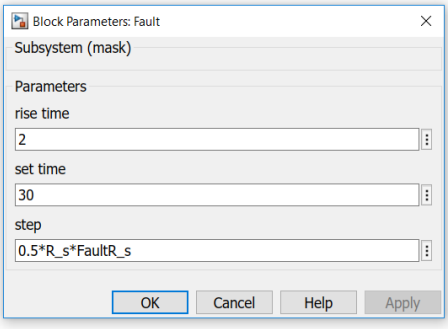

Figure 4.11: Settings of the step block in Simulink

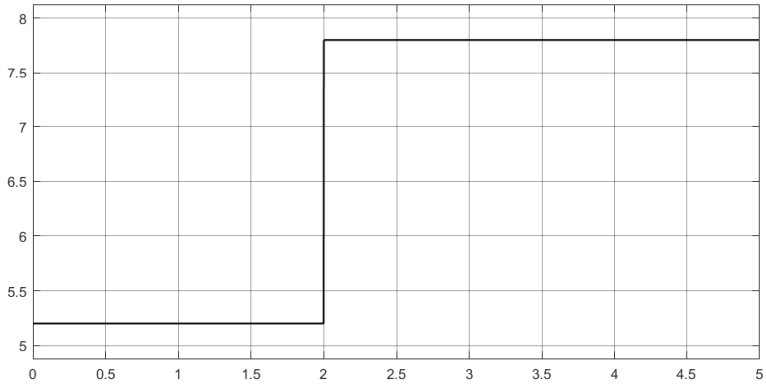

Figure 4.12: Graphic representation of the step at $t = 2$ seconds.

Bearing faults are implemented in a separate way. Figure 4.13 shows how a dent in the outer raceway will affect ball movement. When a ball passes the dent, it will penetrate the outer race with a depth given by δ_h, [39]. The geometric relationships in figure 4.13 are derived in equations 4.6 - 4.8.

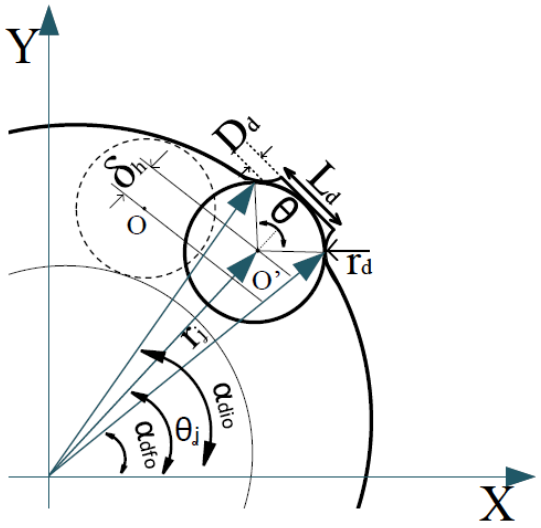

$$\theta = \frac{L_d}{r_b} \tag{4.5}$$

$$L_d = R_{out} \cdot (\alpha_{dio} - \alpha_{dfo}) \tag{4.6}$$

$$\delta_h = r_b(1 - \cos(\frac{\theta}{2})) \tag{4.7}$$

Figure 4.13: Motion of ball around the outer race defect

θ	-	Angle of the arc extended along the defect length	$[rad]$
L_d	-	Length of defect,	$[mm]$
D_d	-	Depth of defect	$[mm]$
r_d	-	Radius of defect	$[rad]$
α_{dio}	-	The initial angle of defect	$[rad]$
α_{dfo}	-	The finite angle of defect	$[rad]$

The elastic deformation between the raceways and the rolling elements increase when the ball

passes through defect, as it adds up to the already existing deformation, δ.

$$\delta_j = \delta + Db_{j,out} \cdot \delta_h \tag{4.8}$$

Where $Db_{j,out}$ is equal one when the j-th ball passes the defect and zero for all other cases.

Implementation of the defect are shown in figure 4.14, with the defect modelled stationary in the first quadrant of the bearing (as in figure 4.13). Angles of the passing balls centre are decomposed to sines and cosines then compared with the angles of the defect (α_{dio} and α_{dfo}). A pulse is emitted when the balls are in the defect region.

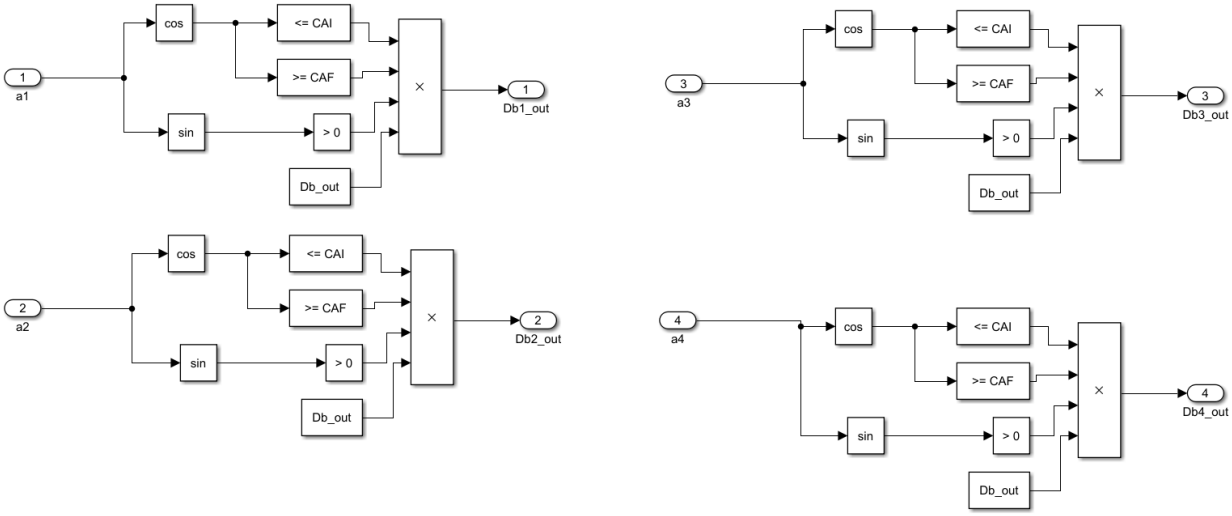

Figure 4.14: Pulse generation at outer race defect contact

The model is structured in a way that three conditions must be met to emit a pulse.

- The sine angle of a given balls centre must be greater than zero
- The cosine angle of the given balls centre must lay in the interval between start and end of the defect angle (4.13)
- Defect, Db_{out} , has to be activated in the associated MATLAB-script

4.5 Cumulative Sum

The CUmulative SUM algorithm (CUSUM) is implemented to process the output values from noisy residuals and to help detect minor faults. CUSUM bases on identifying if there is a change in a residual mean value, which is likely to happen when a fault occurs. CUSUM is given by equation 4.10 and is derived in [16].

$$g(k) = g(k-1) + \frac{\mu_1 - \mu_0}{\sigma^2}\left(z(k) - \frac{\mu_1 + \mu_0}{2}\right) \tag{4.9}$$

Implementation of CUSUM in Simulink (figure 4.15) requires several test runs in order to obtain the necessary parameters, μ_0, μ_1, variance σ and threshold value h. The parameters are tuned iteratively by evaluating the mean of every residual for both healthy and faulty simulations. Threshold values for maximum amplitudes of the residuals are also needed. Then, a threshold value for the calculated CUSUM must be found by tuning the value of h, and make sure that sensor noise do not give false alarms.

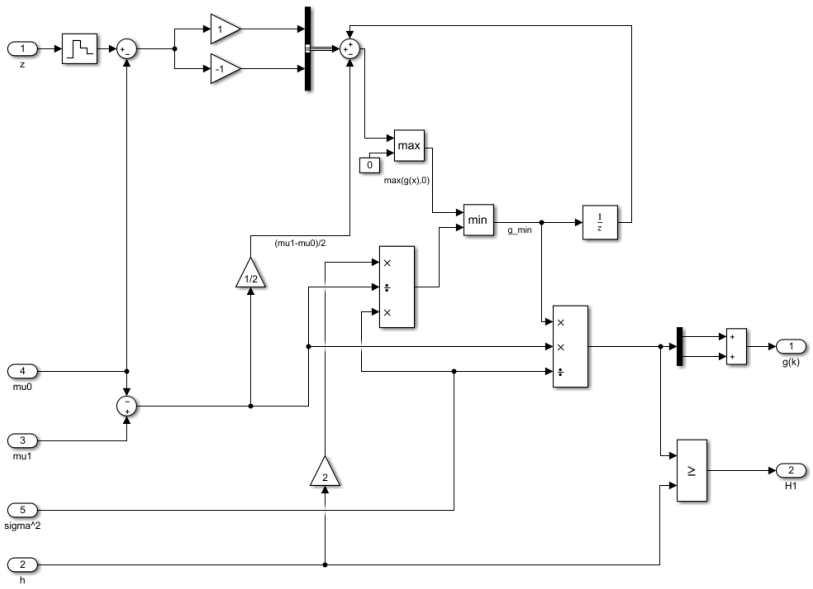

Figure 4.15: Implementation of CUSUM in Simulink

5 Results

This chapter contains different simulation results from implementation of noise to specific faults and how they are detected. Every result section includes a short introduction and which parts of the model used to achieve the results.

5.1 Noise

This section shows how introduction of sensor noise affects the plotted residuals over a thirty second simulation. Figure 5.1 shows the residuals that are generated in simulations without any faults. The left figures are unbiased, while the right figures are biased. Bias parameters were empirically tuned to resemble actual sensor bias. It should be noted that the X-axis is the same at all figures, but the Y-axis resolution may vary.

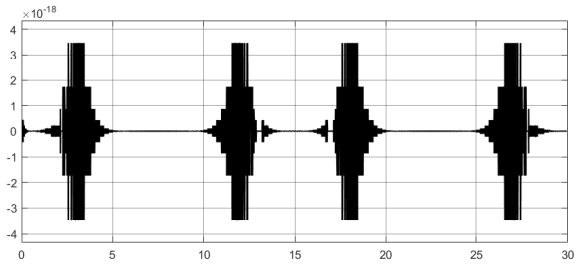

(a) R7 without noise

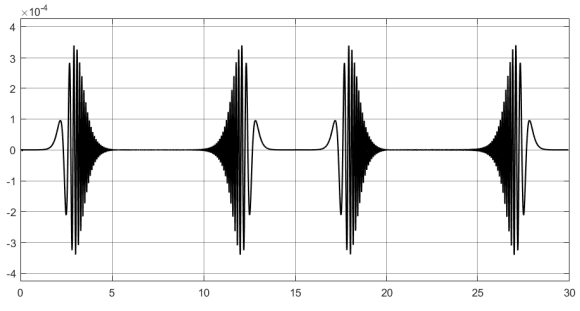

(b) R8 without noise

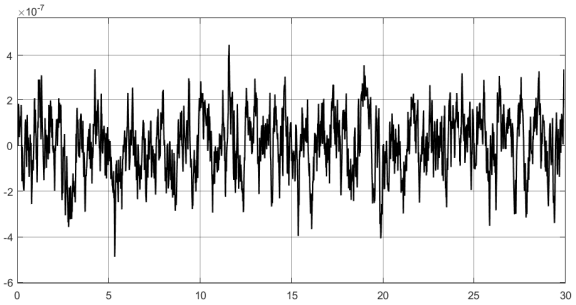

(c) R7 with noise

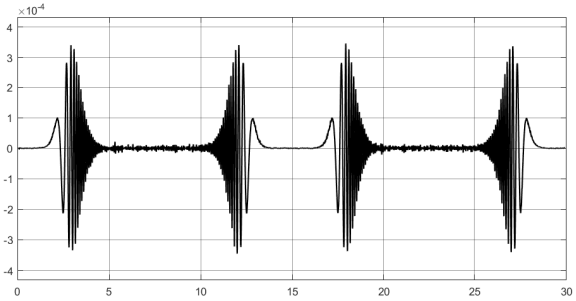

(d) R8 with noise

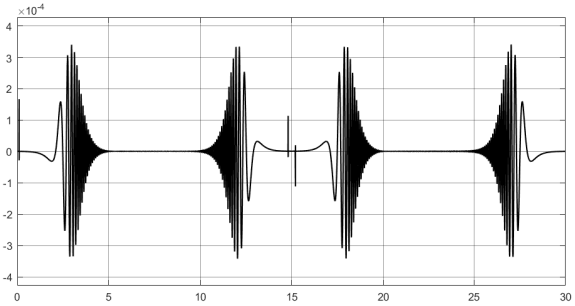

(e) R9 without noise

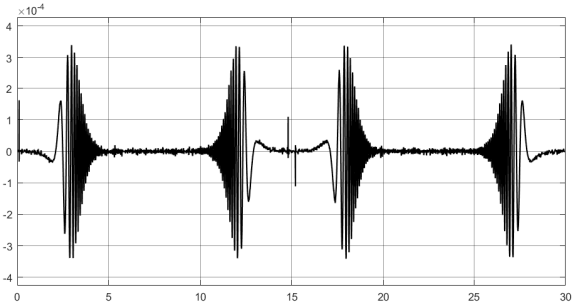

(j) R9 with noise

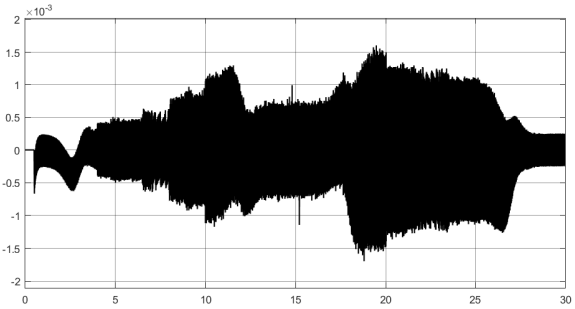

(f) R11 without noise

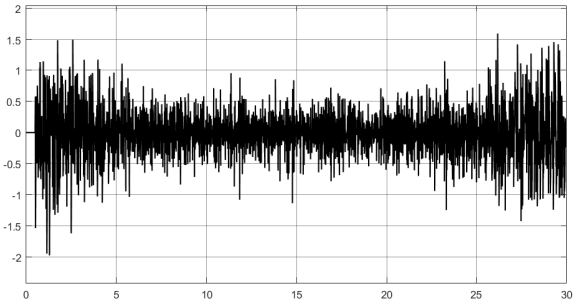

(k) R11 with noise

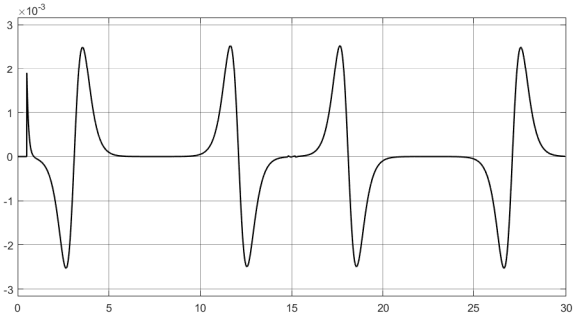

(g) R12 without noise

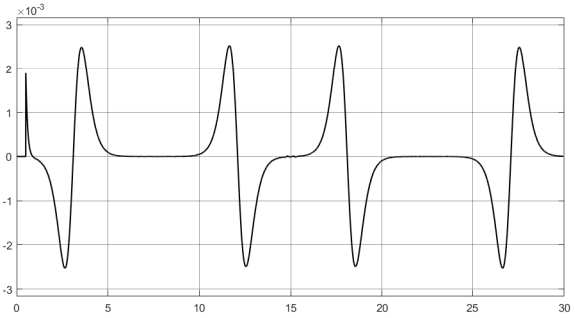

(l) R12 with noise

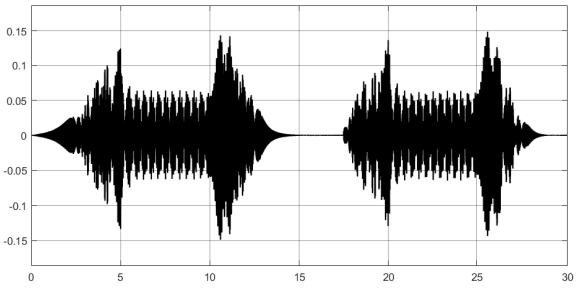

(h) R20 without noise

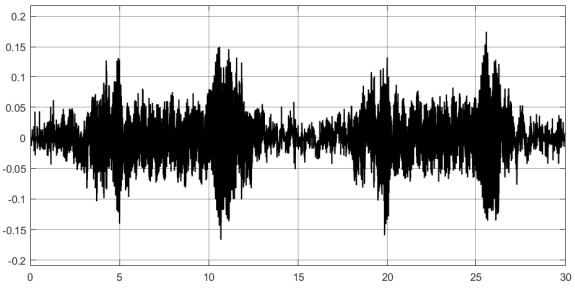

(m) R20 with noise

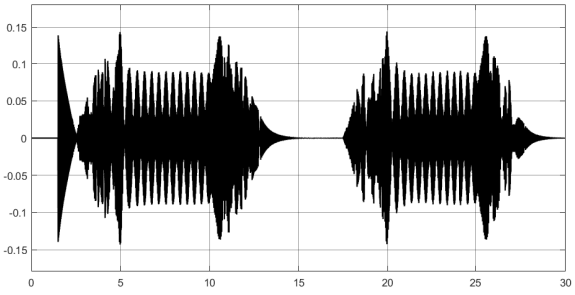

(i) R21 without noise

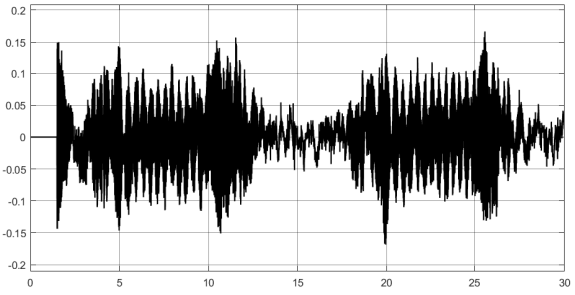

(n) R21 with noise

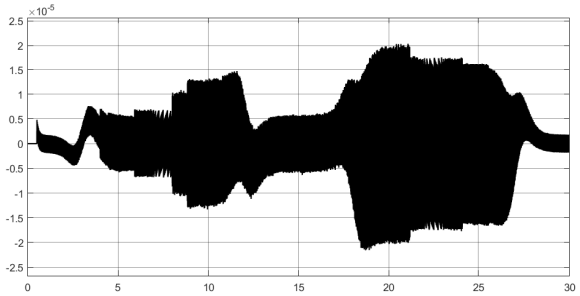

(o) R30 without noise

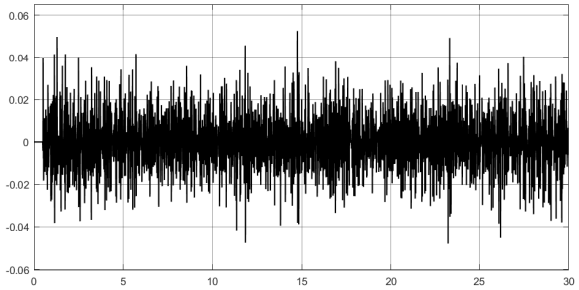

(s) R30 with noise

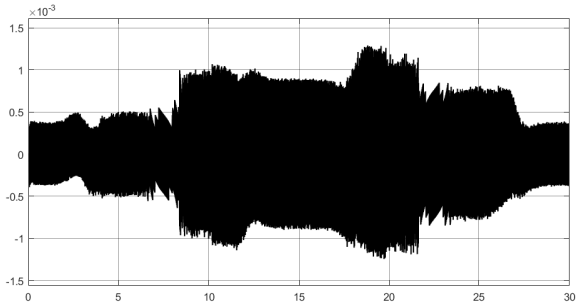

(p) R33 without noise

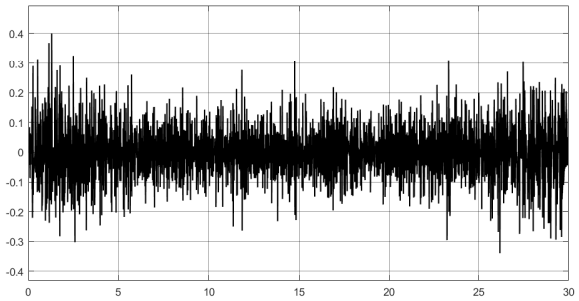

(t) R33 with noise

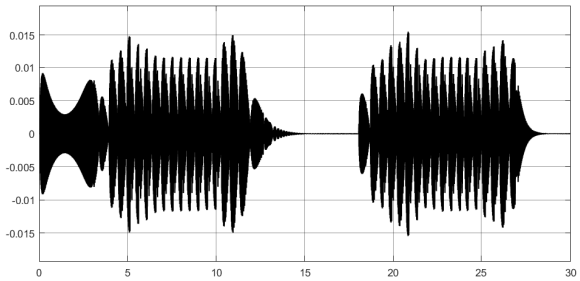

(q) R38 without noise

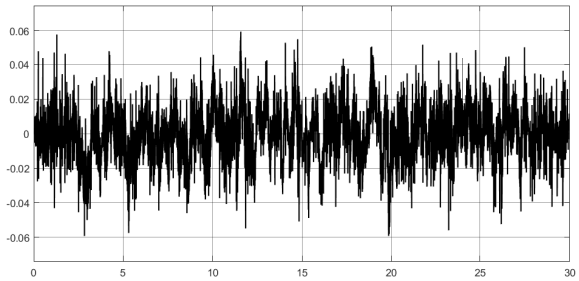

(u) R38 with noise

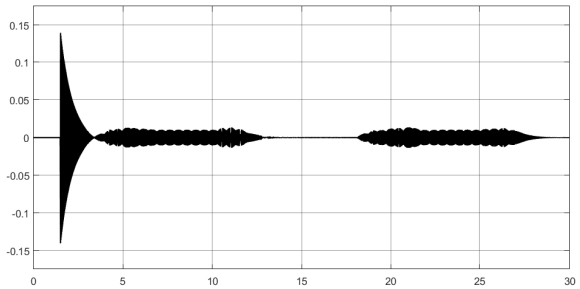

(r) R39 without noise

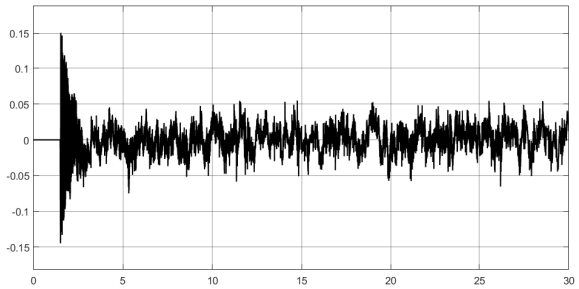

(v) R39 with noise

Figure 5.1: An overview of how the generated residuals (left-hand side) are affected by the random generated noise (right-hand side).

5.2 Threshold Values in Cumulative Sum

The CUSUM plots are supposed to give zero as output during absence of faults. However, addition of bias affected some of the CUSUM calculation and led to false detections. These were solved by introducing threshold values to the relevant CUSUM function, conditioning the peaks to be greater than a certain value [40] , illustrated by a red line, in order to pass through a fault warning.

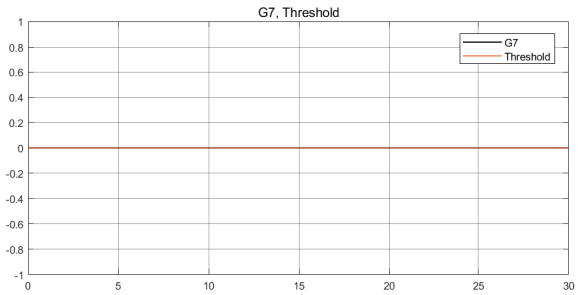

(a) G7

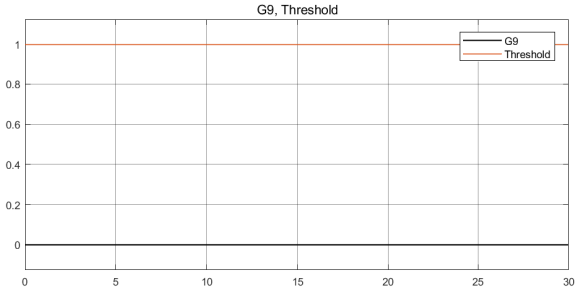

(b) G9

(c) G12

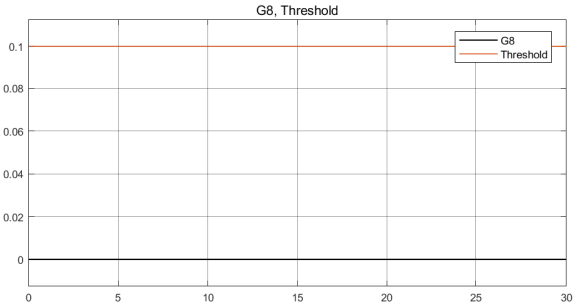

(d) G8

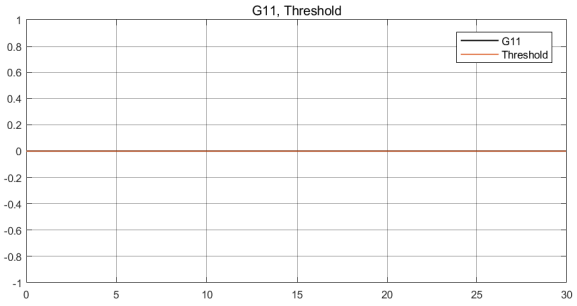

(e) G11

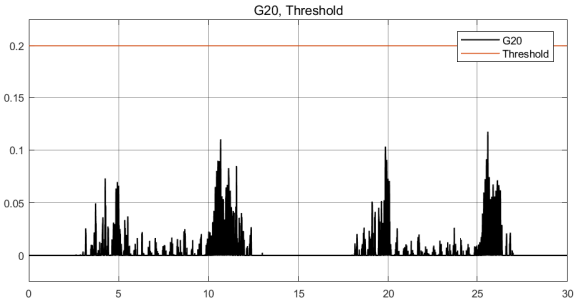

(f) G20

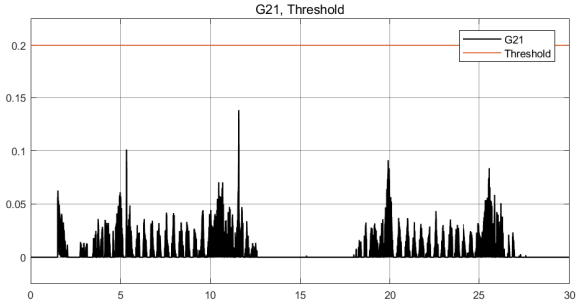

(g) G21

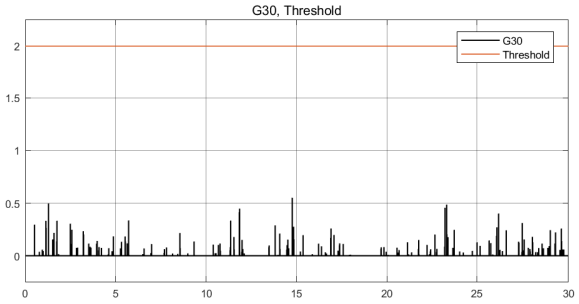

(j) G30

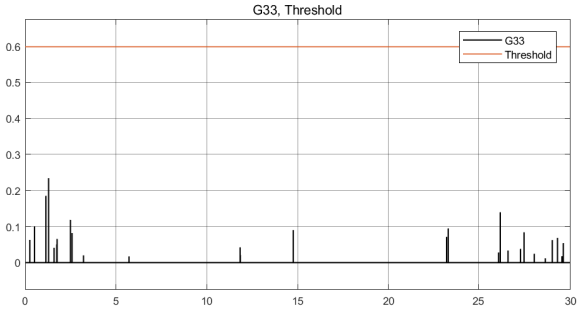

(h) G33

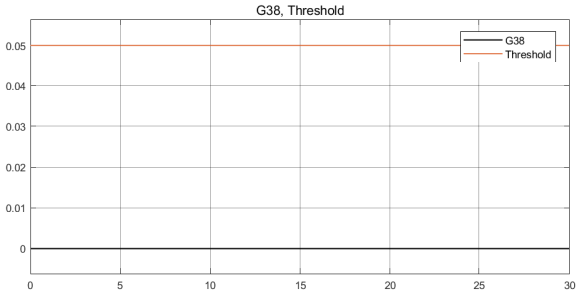

(k) G38

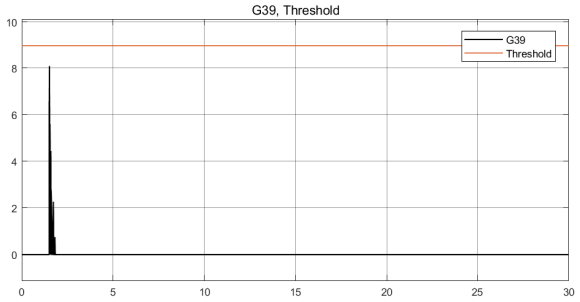

(i) G39

Figure 5.2: Illustration of the threshold values (red line) that must be exceeded in order to give an error signal.

5.3 Fault in Motor Resistance

This section, and the following four, will show the process of identifying five different faults. One from each of the major components; PMSM, gearbox, winch, bearing and current sensor - respectively. The faults are applied as steps, mimicking a sudden change in value. All the residual plots will have two blue lines indicating the maximum and minimum amplitude values for a flawless simulation.

Figure 5.3 shows how the internal stator resistance, R_s, is increased from $5.2\,\Omega$ to $15.6\,\Omega$ at $time = 15$ seconds.

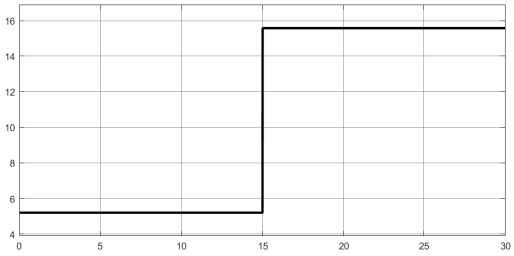

Figure 5.3: The step representing a fault i R_s

Figure 5.4 shows how the change in resistance affects the residual and CUSUM plots.

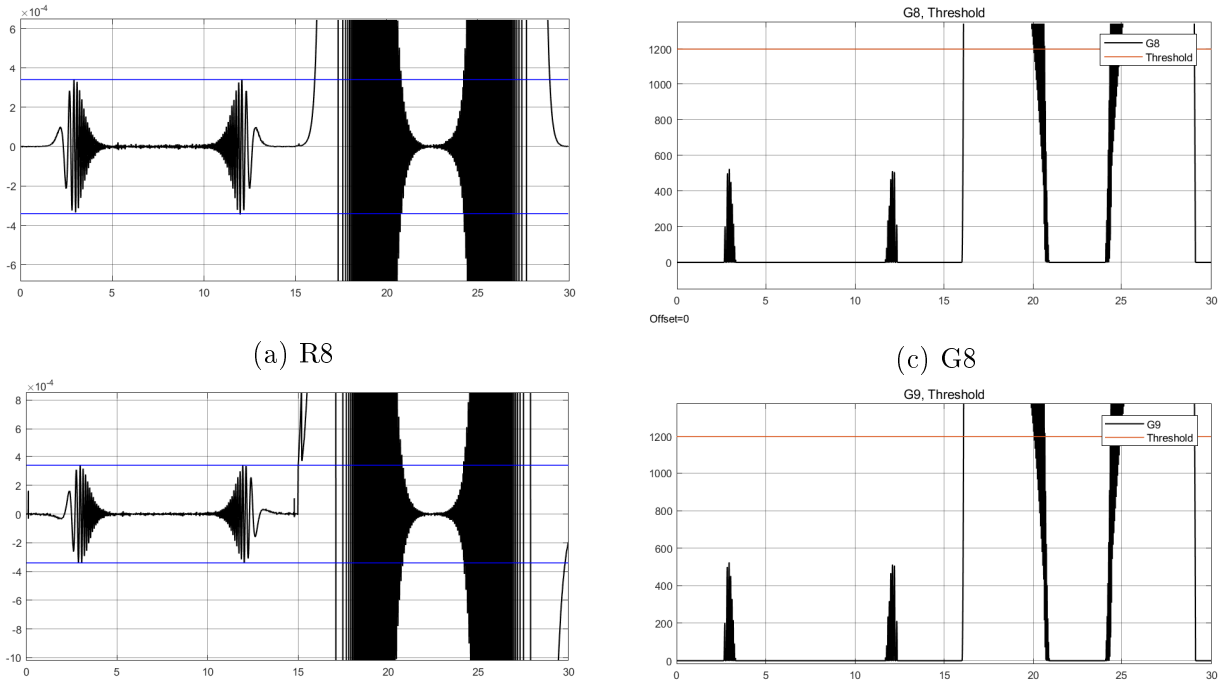

(a) R8

(c) G8

(b) R9

(d) G8

Figure 5.4: Residual plots (left-hand side) and CUSUM plots (right-hand side) with a fault occurring at $time = 15$ seconds. The blue lines in the residual plots indicates the maximum and minimum amplitude values for a flawless simulation.

A series of indicators are programmed to give a red light if the calculated CUSUM exceeds their respective threshold value during simulation. This allows for identification of the faulty region, by comparison of the pattern to known faults, listed in table 4.8.

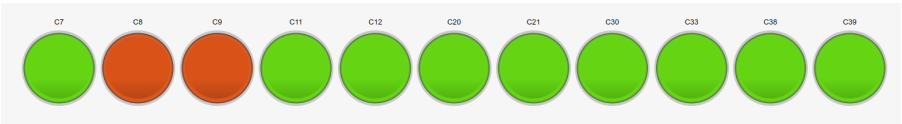

Figure 5.5: Indicators that corresponds to a fault in resistance according to table 4.8

5.4 Fault in Gear Friction

The next test is an increase in the internal friction of the gearbox. Figure 5.6 shows how the internal gear friction, μ_{wh} goes from zero to $0.5Nm$ at $time = 12$ seconds.

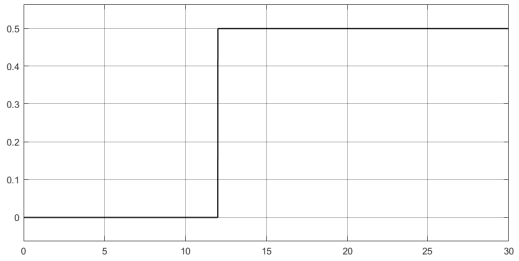

Figure 5.6: The step representing an increase of the gear friction

Figure 5.7 shows how the residual and CUSUM plots is affected by the fault. Residuals are presented on the left-hand side while the right-hand side has CUSUM plots.

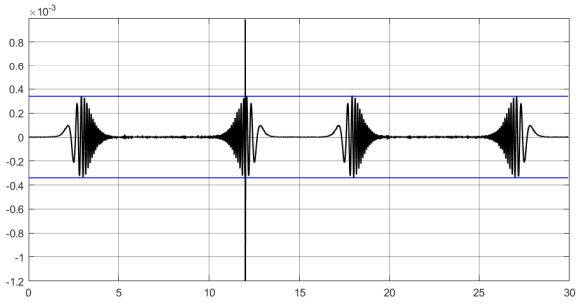

(a) R8

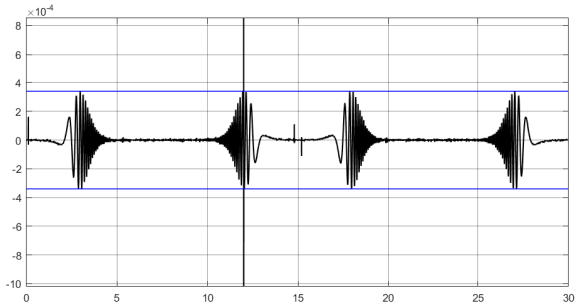

(b) R9

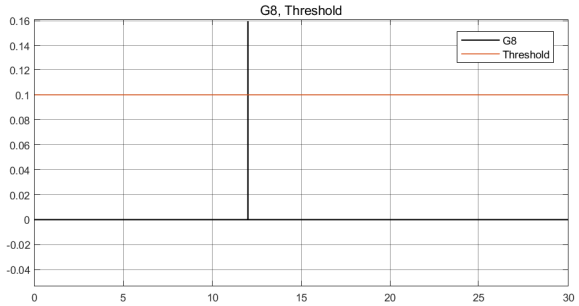

(c) G8

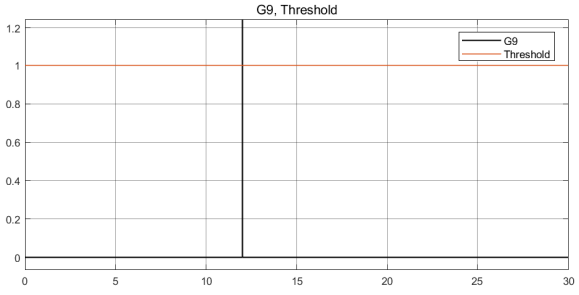

(d) G9

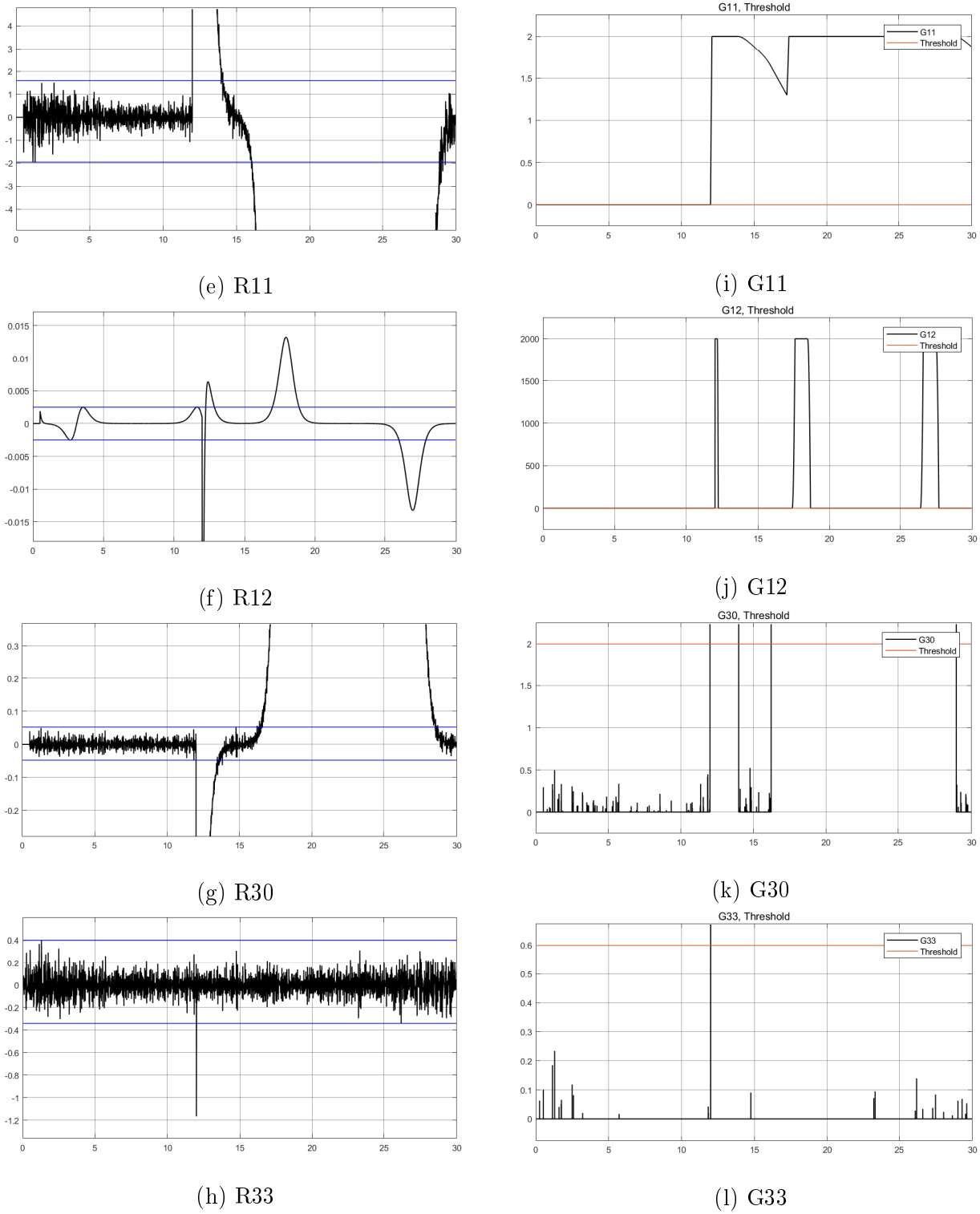

(e) R11

(i) G11

(f) R12

(j) G12

(g) R30

(k) G30

(h) R33

(l) G33

Figure 5.7: Residual plots (left-hand side) and CUSUM plots (right-hand side) with a fault occurring at $time = 12$ seconds. The blue lines in the residual plots indicates the maximum and minimum amplitude values for a flawless simulation.

Comparison with table 4.8 reveals that the indicators light combination is not unique. Meaning that the friction increase is unable to be isolated, as the same light combination will appear if

there is a fault in the gearbox stiffness.

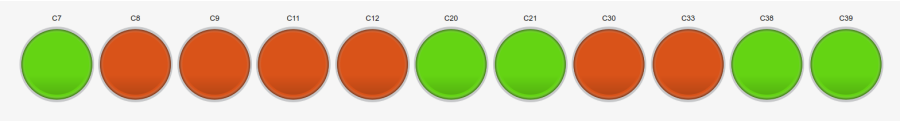

Figure 5.8: Indicators that corresponds to faults in both gearbox friction μ_{wh} and gearbox stiffness C_k according to table 4.8

5.5 Fault in Wire Cross Section

The third test is a decrease of the wire cross section A_w, which can happen due to normal wear and tear, that will affect the wire stiffness. Figure 5.9 shows implementing a 10% reduction of wire cross section , A_w, at $time = 23$ seconds.

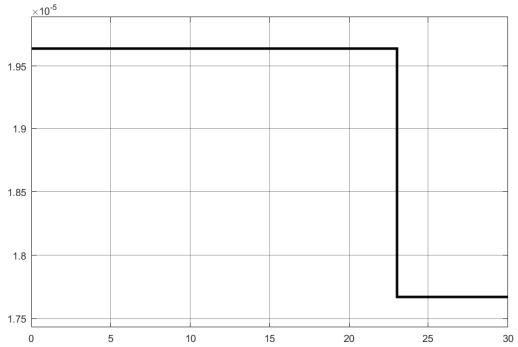

Figure 5.9: The step representing a reduction in the wire cross section

Figure 5.10 shows how the residual and CUSUM plots is affected by the fault. Residuals are presented on the left-hand side while the right-hand side has CUSUM plots.

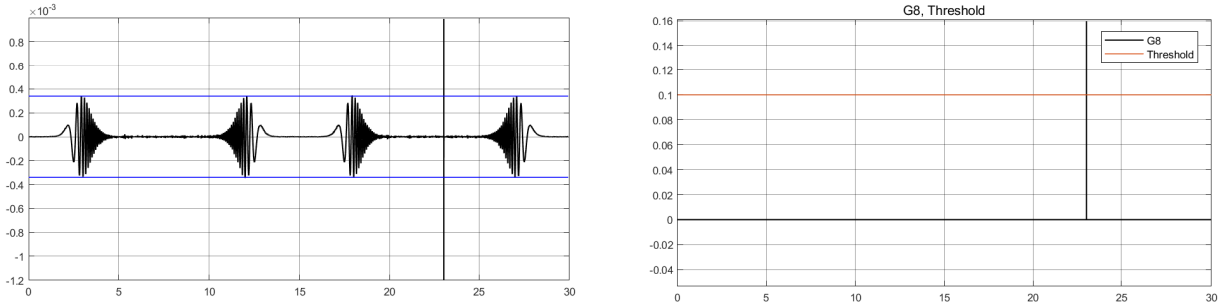

(a) R8

(b) G8

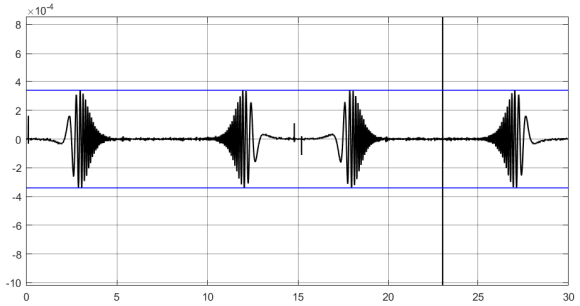

(c) R9

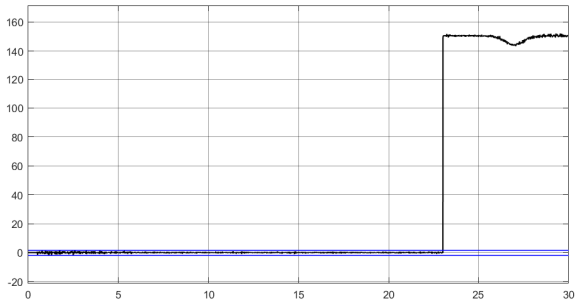

(d) R11

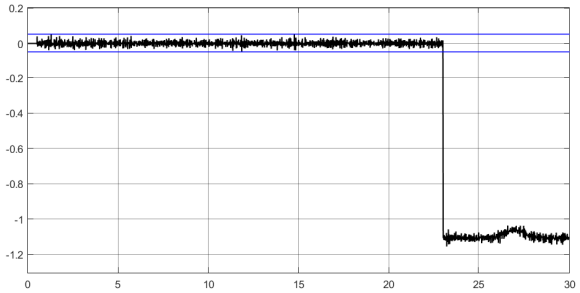

(e) R30

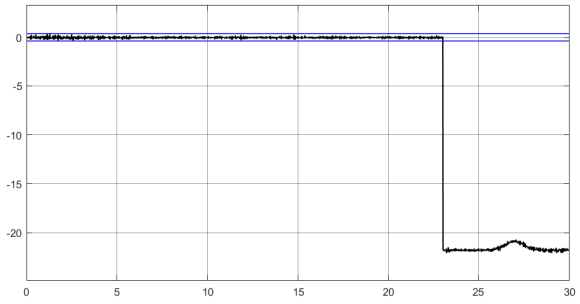

(f) R33

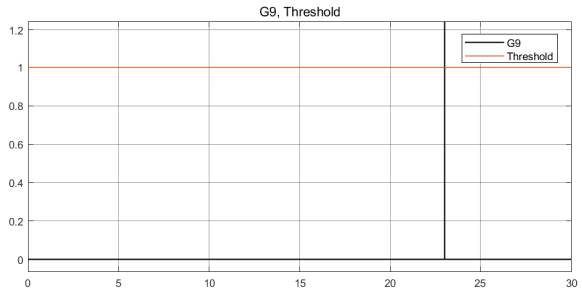

(g) G9

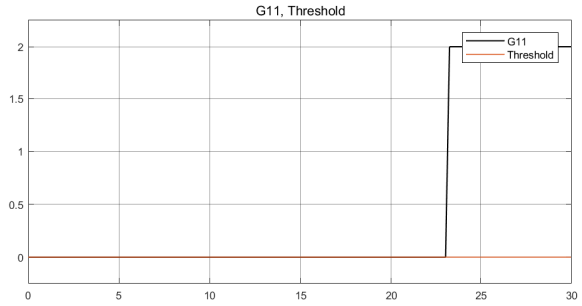

(h) G11

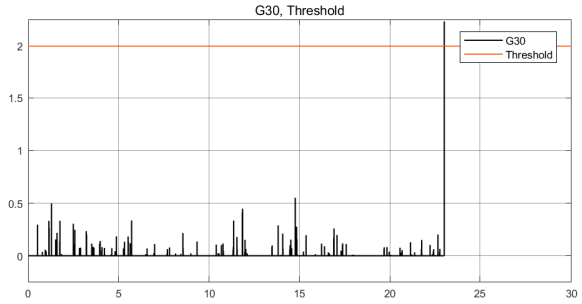

(i) G30

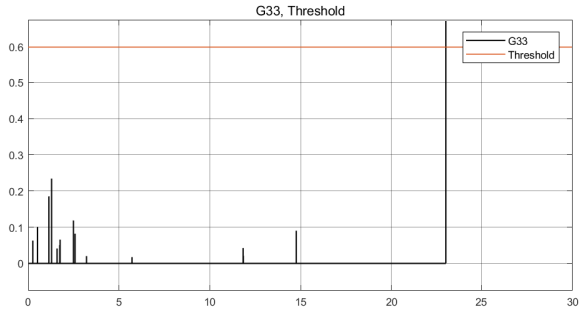

(j) G33

Figure 5.10: Residual plots (left-hand side) and CUSUM plots (right-hand side) with a fault occurring at $time = 23$ seconds. The blue lines in the residual plots indicates the maximum and minimum amplitude values for a flawless simulation.

Comparison of the light combination with table 4.8 shows that the fault is unique, and can be isolated to a fault in the wire.

Figure 5.11: Indicators that corresponds to a fault in the wire according to table 4.8

5.6 Fault in Outer Race Bearing

The fourth test is a deformation/dent in the outer race of a bearing. Figure 5.12 shows the step activating the fault, Db_{out}, at $time = 9$ seconds.

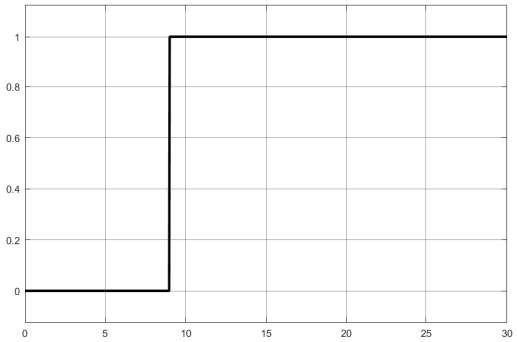

Figure 5.12: The step representing a damage in the outer race of the bearing.

Deformation in the outer race is simulated by a series of shocks that are occurring every time a ball passes over the deformation. Figure 5.13 illustrates these shocks which has a time period between them that varies with the rotational speed of the shaft supported by the bearing.

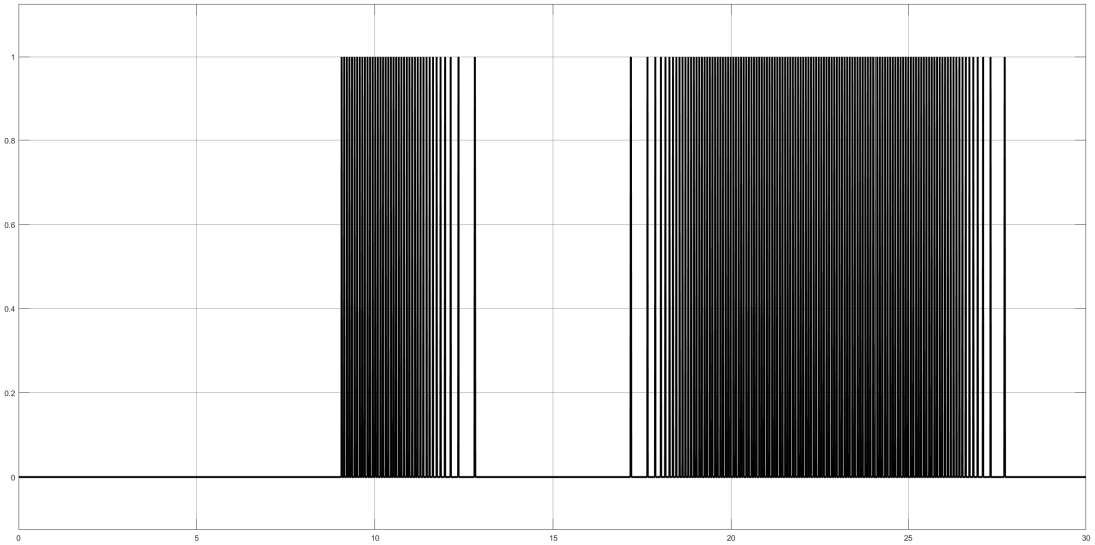

Figure 5.13: Each column in the plot represents a ball inside the bearing passing over the deformation in outer race

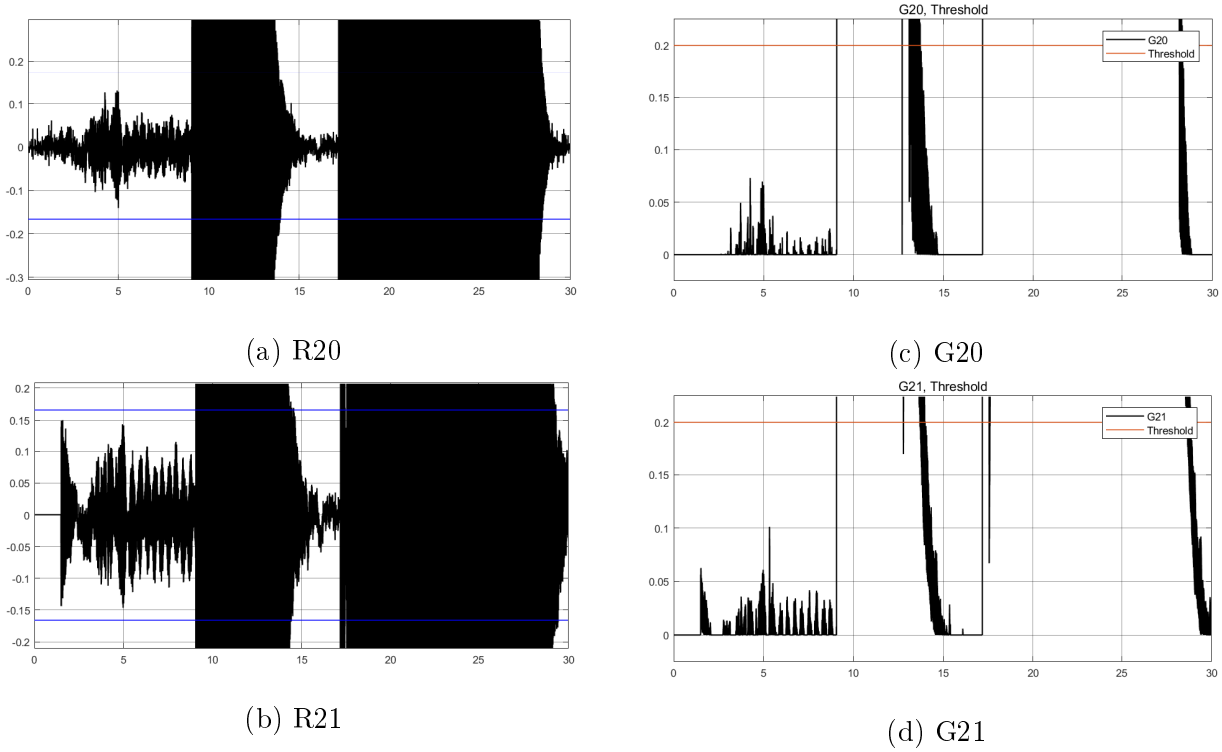

(a) R20

(c) G20

(b) R21

(d) G21

Figure 5.14: Residual plots (left-hand side) and CUSUM plots (right-hand side) with a fault occurring at $time = 9$ seconds. The blue lines in the residual plots indicates the maximum and minimum amplitude values for a flawless simulation.

Comparing the light combination with table 4.8 shows that the pattern, once more, is not unique. The combination is a group fault but is limited to bearing one.

Figure 5.15: Indicators that corresponds to a fault in bearing one according to table 4.8

5.7 Fault in Current Sensor

Last of the tests is a faulty current sensor. Figure 5.16a shows the step activating the fault at $time = 15$ seconds. The value is very small and is not visible in the sensor readings, illustrated in figure 5.16b.

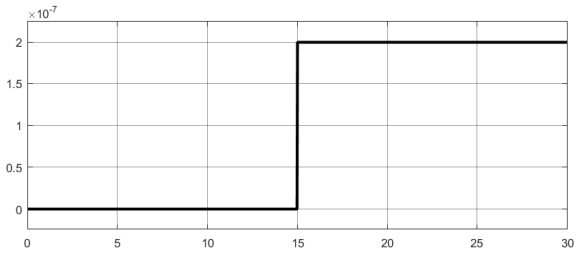

(a) The step representing a misreading from the current sensor.

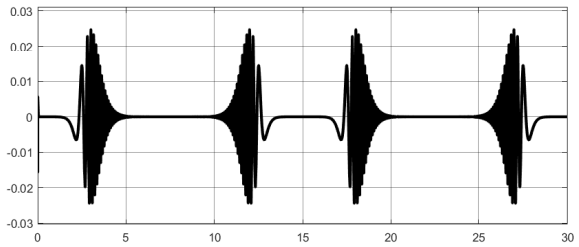

(b) Illustration of the unaffected current plot, i_{am}

Figure 5.16: An illustration of how the misreading error, occurring at $time = 15$ seconds, affects the sensor readings.

Figure 5.17 shows the small change in residual seven that is detected by CUSUM seven.

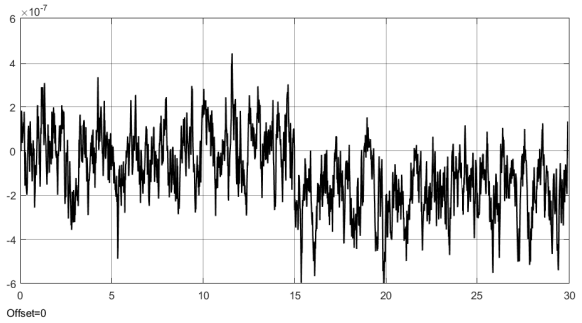

(a) R7

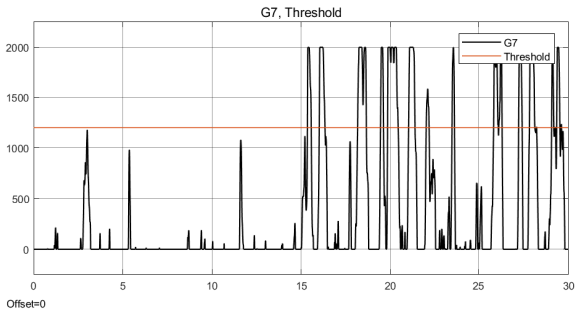

(b) G7

Figure 5.17: Residual plot (left-hand side) and CUSUM plot (rigth-hand side) with a fault occurring at $time = 15$ seconds

In this case, only one of the fault indicators are activated. Table 4.8 reveals that the constraint C7 is only affected by a fault in the current sensor. It is possible to isolate the fault even though only one indicator is activated.

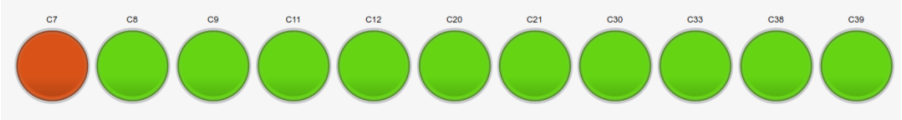

Figure 5.18: Indicators that corresponds to a fault in bearing one according to table 4.8

6 Discussion and Further Work

Several fault detection methods were considered during pre-studies of the subject. A common factor in the literature was that fault diagnosis were performed on isolated components, meaning that development of a method for more complex systems was needed. After evaluation of different methods, it was decided to base the diagnosis on structural analysis. This method requires a good mathematical model of the system to be monitored, introducing a profile of modelling and simulation to the thesis.

Parts of the mathematical model, primarily the PMSM dq-model, was handed out by our supervisor in the initial stages of the project. However, several adjustments were made during the process leading to completion. The project evolved to focus on model-based fault-detection prioritizing the opportunity to increase knowledge about developing mathematical models. The simulation model was made in Simulink, using visual programming and text-based function blocks, consisting of dynamic equations that are calculated for each time step in the simulation. The thesis did not have a dedicated winch available, but most of motor parameters were based on a PMSM motor installed at an electrical winch set-up located in the university's technical premises.

Some challenges were encountered, like the disadvantage of making a model without having a real system to extract test data from. Modelling of the mechanical system was done in line with subjects taught about this topic at the university utilizing both analytical skills and empirical assumptions. The steel wire in the system was modelled as a spring-damper, with a stiffness and mass dependent on the length of unrolled wire. In addition, a dynamic model of the drum radius and inertia could have been implemented but was ignored due to the payloads short range of motion during the simulations.

The mechanical models of bearings and the gearbox are mainly based on published articles and previous master theses. Several methods were analysed, where the best features were combined to achieve models that are simple, yet complex enough to inflict local faults. The gearbox was modelled as two stiff disks where the tooth contact was represented by a spring-damper in parallel. Initially, backlash was implemented along with varying teeth stiffness dependent on the rotational direction. Later, these features were neglected due to difficulties identifying correct parameter values.

Bearing dynamics were reduced to a two degree of freedom system. However, a five degree of freedom model was considered but it was desirable to keep the system simple. Bearings are modelled as mass-spring-damper systems, where stiffness between balls and bearing races were determined based on the Hertzian contact theory. Dynamic equations used to simulate a deformation in the outer race were implemented in the bearing model, emitting a pulse every time a ball passes the defect.

Residuals are generated by calculating the difference between estimated and measured values. The estimator bases on the concepts of state-observers, estimating the system dynamics based on calculations executed in parallel with the simulation model. Ideally, the difference between

estimated and measured values should be zero. However, the simulation model complexity increased during the project and introduction of random generated sensor bias made it difficult to achieve zero deviation in the generated residuals. Introduction of sensor bias, seen in section 5.1 , made it difficult to detect minor faults, leading to implementation of the cumulative sum technique.

Comparing the test results where faults are introduced during simulation, presented in sections 5.3 - 5.7, shows that some faults were easier to detect than others. A total of fifteen faults were implemented, but only five are presented in the report. The variety of fault conditions required several simulations runs alternating the faults and iteratively tuning of threshold values in order to allow the detection algorithms to register all errors independently.

Simulation results of the faulty current sensor, seen in section 5.7, verifies that implementation of CUSUM was helpful. For this case, the induced fault is very small and not visible on the sensor readings. However, the fault can be seen in the residual plot as a minor change of the mean value and significant peaks in the CUSUM plot (figure 5.17). Discovering this fault required fine tuning of threshold values and resulted in a delicate system sensitive to false alarms.

Some of the challenges by using only structural analysis method on a complex system, are that some components lack dynamic interrelationship with the system. Induced faults in the bearings were registered at component level, but the developed structural analysis failed to isolate what the faults are related to. The challenges could be solved by running different algorithms based on diverse methods, like vibration and structural analysis, and combine the data through sensor fusion.

Simplifications in the developed simulations model may contribute to complicate fault isolation, as more detailed component models would be better at mirroring realistic behaviour. For instance, the detection method registers if there is a fault in the gearbox but has difficulties identifying what kind of fault. Future of electrical winch technology may involve more use of permanent magnet motors, able to actuate the drum without need for a gearbox. It can also be argued that the simulation model could be made without the gearbox, reducing system complexity, which could result in increased accuracy regarding isolation of faults.

7 Conclusion

The results achieved in this thesis corresponds well with the objectives given in the problem description. Failure mode and effect analysis has been carried out for an electrical winch and the associated components. A simulation model of the system was made with regard to induce faults in individual components. Several fault detection and identification techniques were reviewed before the structural analysis theory and implementation are explained in detail. Fault detection and identification were achieved in the simulation model.

Tests performed on the Simulink model show that the fault diagnosis algorithm was able to detect fictive faults. Final threshold values were able to identify the region of each individual fault with accuracy down to the specific component, where five fault scenarios (faults in R_s, μ_{wh}, A_w, Db_{out} and i_a) are shown in the result section.

The proposed diagnostic method could be tested using faults generated by Finite Element Analysis. It is also desirable to perform further diagnostics on a real winch set-up and this is recommended for further work. Parameters used in the Simulink model can be changed with respect to match extracted parameters from a real winch set-up. This thesis has revolved around an electrical winch, but fault diagnosis and predictive maintenance is a wide subject that is applicable to a variety of systems.

Bibliography

[1] I. Alsyouf, "Maintenance practices in Swedish industries: Survey results," *International Journal of Production Economics*, vol. 121, no. 1, pp. 212–223, 2009. [Online]. Available: http://dx.doi.org/10.1016/j.ijpe.2009.05.005

[2] A. K. Jardine, D. Lin, and D. Banjevic, "A review on machinery diagnostics and prognostics implementing condition-based maintenance," *Mechanical Systems and Signal Processing*, vol. 20, no. 7, pp. 1483–1510, oct 2006. [Online]. Available: https://www.sciencedirect.com/science/article/pii/S0888327005001512

[3] Y. Lei, J. Lin, M. J. Zuo, and Z. He, "Condition monitoring and fault diagnosis of planetary gearboxes: A review," *Measurement*, vol. 48, pp. 292–305, feb 2014. [Online]. Available: https://www.sciencedirect.com/science/article/pii/S0263224113005551

[4] C. Markou, G. Cros, and A. Sng, "Airline Maintenance," *Airline Maintenance Cost*, no. April, 2015.

[5] S. Roberts, "Lecture 7 - The Discrete Fourier Transform," *Oxford Robots Lecture*, pp. 82–96, 2003.

[6] S. Singh, A. Kumar, and N. Kumar, "Motor Current Signature Analysis for Bearing Fault Detection in Mechanical Systems," *Procedia Materials Science*, vol. 6, pp. 171–177, jan 2014. [Online]. Available: https://www.sciencedirect.com/science/article/pii/S2211812814003861

[7] R. B. Randall and J. Antoni, "Rolling element bearing diagnostics—A tutorial," *Mechanical Systems and Signal Processing*, vol. 25, no. 2, pp. 485–520, feb 2011. [Online]. Available: https://www.sciencedirect.com/science/article/pii/S0888327010002530

[8] P. A. Delgado-Arredondo, D. Morinigo-Sotelo, R. A. Osornio-Rios, J. G. Avina-Cervantes, H. Rostro-Gonzalez, and R. d. J. Romero-Troncoso, "Methodology for fault detection in induction motors via sound and vibration signals," *Mechanical Systems and Signal Processing*, vol. 83, pp. 568–589, 2017. [Online]. Available: http://dx.doi.org/10.1016/j.ymssp.2016.06.032

[9] S. Singh, A. Kumar, and N. Kumar, "Detection of bearing faults in mechanical systems using motor current signature and acoustic signatures," *21st International Congress on Sound and Vibration 2014, ICSV 2014*, vol. 5, pp. 4269–4276, 2014. [Online]. Available: http://www.scopus.com/inward/record.url?eid=2-s2.0-84922737990{&}partnerID=40{&}md5=557d81393684a028e7aa43fe2dc809da

[10] B. M. Ebrahimi, J. Faiz, and M. J. Roshtkhari, "Static-, dynamic-, and mixed-eccentricity fault diagnoses in permanent-magnet synchronous motors," *IEEE Transactions on Industrial Electronics*, vol. 56, no. 11, pp. 4727–4739, 2009.

[11] S. T. Kandukuri, J. S. L. Senanayaka, V. K. Huynh, H. R. Karimi, and K. G. Robbersmyr, "Current signature based fault diagnosis of field-oriented and direct torque-controlled induction motor drives," *Proceedings of the Institution of Mechanical Engineers. Part I: Journal of Systems and Control Engineering*, vol. 231, no. 10, pp. 849–866, 2017.

[12] F. Ruiming and M. Hongzhong, "Application of MCSA and SVM to induction machine rotor fault diagnosis," *Proceedings of the World Congress on Intelligent Control and Automation (WCICA)*, vol. 2, no. 2, pp. 5543–5547, 2006.

[13] W. Thomson and M. Fenger, "Case histories of current signature analysis to detect faults in induction motor drives," *IEEE International Electric Machines and Drives Conference, 2003. IEMDC'03.*, vol. 3, 2003.

[14] "Brief review of motor current signature analysis," no. 1.

[15] M. Blanke and J. S. Thomsen, "Electrical steering of vehicles - fault-tolerant analysis and design," *Microelectronics Reliability*, vol. 46, no. 9-11, pp. 1421–1432, 2006.

[16] J. L. M. S. M. Blanke, M. Kinnaert, *Diagnosis and Fault-Tolerant Control Second Edition*. Springer, 2006.

[17] J. Zhang and G. Rizzoni, "Structural Analysis for Diagnosability and Reconfigurability, with pplication to Electric Vehicle Drive System," *IFAC-PapersOnLine*, vol. 48, no. 21, pp. 1471–1478, jan 2015. [Online]. Available: https://www.sciencedirect.com/science/article/pii/S2405896315018613

[18] R. Isermann, "Model-based fault-detection and diagnosis – status and applications," *Annual Reviews in Control*, vol. 29, no. 1, pp. 71–85, jan 2005. [Online]. Available: https://www.sciencedirect.com/science/article/pii/S1367578805000052

[19] C. Svärd, *Residual Generation Methods for Fault Diagnosis with Automotive Applications*, 2009, no. 1406.

[20] S. Nandi, H. A. Toliyat, and X. Li, "Condition monitoring and fault diagnosis of electrical motors - A review," *IEEE Transactions on Energy Conversion*, vol. 20, no. 4, pp. 719–729, 2005.

[21] C. Spreafico, D. Russo, and C. Rizzi, "A state-of-the-art review of FMEA/FMECA including patents," *Computer Science Review*, vol. 25, pp. 19–28, aug 2017. [Online]. Available: https://www.sciencedirect.com/science/article/pii/S1574013716301435

[22] K. S. Chin, Y. M. Wang, G. K. K. Poon, and J. B. Yang, "Failure mode and effects analysis by data envelopment analysis," *Decision Support Systems*, vol. 48, no. 1, pp. 246–256, 2009. [Online]. Available: http://dx.doi.org/10.1016/j.dss.2009.08.005

[23] M. Braglia, "MAFMA: multi-attribute failure mode analysis," *International Journal of Quality & Reliability Management*, vol. 17, no. 9, pp. 1017–1033, 2000. [Online]. Available: http://www.emeraldinsight.com/doi/10.1108/02656710010353885

[24] Z. Feng and M. J. Zuo, "Vibration signal models for fault diagnosis of planetary gearboxes," *Journal of Sound and Vibration*, vol. 331, no. 22, pp. 4919–4939, oct 2012. [Online]. Available: https://www.sciencedirect.com/science/article/pii/S0022460X12004415

[25] F. Chaari, T. Fakhfakh, and M. Haddar, "Dynamic analysis of a planetary gear failure caused by tooth pitting and cracking," *Journal of Failure Analysis and Prevention*, vol. 6, no. 2, pp. 73–78, apr 2006. [Online]. Available: https://doi.org/10.1361/154770206X99343

[26] C. Moolwan and S. Netpu, "Failure Analysis of a Two High Gearbox Shaft," *Procedia - Social and Behavioral Sciences*, vol. 88, pp. 154–163, 2013. [Online]. Available: http://www.sciencedirect.com/science/article/pii/S1877042813026220

[27] K. Gurumoorthy and A. Ghosh, "Failure investigation of a taper roller bearing: A case study," *Case Studies in Engineering Failure Analysis*, vol. 1, no. 2, pp. 110–114, apr 2013. [Online]. Available: https://www.sciencedirect.com/science/article/pii/S2213290213000163

[28] R. Upadhyay, L. Kumaraswamidhas, and M. Azam, "Rolling element bearing failure analysis: A case study," *Case Studies in Engineering Failure Analysis*, vol. 1, no. 1, pp. 15–17, jan 2013. [Online]. Available: https://www.sciencedirect.com/science/article/pii/S2213290212000065

[29] M. Zarei, Jafar, Poshtan, "Bearing Fault Detection in Induction Motor Using Pattern Recognition Techniques," vol. 3, pp. 749–753, 2008.

[30] P. S. Bhowmik, S. Pradhan, and M. Prakash, "F AULT D IAGNOSTIC A ND M ONITORING M ETHODS OF I NDUCTION M OTOR : A R EVIEW," vol. 1, no. 1, pp. 1–18, 2013.

[31] M. Akar and I. Çankaya, "Diagnosis of static eccentricity fault in permanent magnet synchronous motor by on-line monitoring of motor current and voltage," *Istanbul University - Journal of Electrical and Electronics Engineering*, vol. 9, no. 2, pp. 959–967, 2009.

[32] M. AKAR, S. TAŞKIN, A. S. ŞEKER, and L. ÇANKAYA, "Detection of static eccentricity for permanent magnet synchronous motors using the coherence analysis," *Turkish Journal of Electrical Engineering & Computer Sciences*, vol. 18, no. 6, pp. 963–975, 2010. [Online]. Available: http://online.journals.tubitak.gov.tr/publishedManuscriptDetails.htm?id=11265

[33] L. Harnefors, M. Hinkkanen, and O. Wallmark, "Control of Voltage-Source Converters and Variable-Speed Drives."

[34] S. Shah, A. Rashid, and M. K. L. Bhatti, "Direct quadrate (d-q) modeling of 3-phase induction motor using matlab/simulink," *Canadian Journal on Electrical and Electronics Engineering*, vol. 3, no. 5, pp. 237–243, 2012.

[35] D. E. N. Ingenier, I. T. Doctoral, J. C. Garc, and H. R. Alonso, "Análisis y caracterización holista de un sistema rotativo complejo," 2009.

[36] T. A. Harris and W. J. Anderson, *Rolling Bearing Analysis*, 1967, vol. 89, no. 4. [Online]. Available: http://tribology.asmedigitalcollection.asme.org/article.aspx?articleid=1461288

[37] E. Sobhani-Tehrani and K. Khorasani, "Fault Diagnosis of Nonlinear Systems Using a Hybrid Approach," vol. 383, pp. 21–50, 2009. [Online]. Available: http://link.springer.com/10.1007/978-0-387-92907-1

[38] M. Blanke, "Frequently asked questions on filtered noise," pp. 0–9, 2005. [Online]. Available: http://orbit.dtu.dk/en/publications/frequently-asked-questions-on-filtered-noise(0b7fe770-69db-47dc-a996-1449b3e1f25a).html

[39] S. Khanam, J. K. Dutt, and N. Tandon, "Impact Force Based Model for Bearing Local Fault Identification," *Journal of Vibration and Acoustics*, vol. 137, no. 5, p. 051002, 2015. [Online]. Available: http://vibrationacoustics.asmedigitalcollection.asme.org/article.aspx?doi=10.1115/1.4029988

[40] D. Senftenberg, "On Observer Based Fault Detection," *IFAC Proceedings Volumes*, vol. 30, no. 18, pp. 115–123, 1997. [Online]. Available: http://dx.doi.org/10.1016/S1474-6670(17)42389-5

A | Appendix

A.1 MATLAB Script

Contents


```
clear all;
close all;
```

Electrical parameters of PMSM motor

```
p = 4;                                  %Number of Poles
n_p=2;                                  %Pole Pairs
K_t = 2.5;                              %Constant torque[Nm/A]
I_rated = 2.07;                         %Current rated [A]
T_rated=K_t * I_rated;                  %Torque rated [Nm]
n_rated=2100;                           %[rpm]
u_rated=400;                            %[V] Datasheet states 400-460V
rated_voltage = u_rated/sqrt(3);        %[V]
J = 0.0011;                             %Motor inertia[kg.m^2]
f=50;                                   %[Hz]
w=2*pi*f;                               %[rad/s]
R_s = 5.2;                              %[Ohm]
L_d = 63e-3;                            %[H]
L_q = 133e-3;                           %[H]
L_s = (L_d + L_q)/2;                    %[H]
```

Calculated parameters:

```
Psi_R= 3*T_rated/sqrt(2)/p/I_rated; %Flux density
Ampmax = 400*sqrt(2)/sqrt(3)*3/2;   %Maximum current
```

Transformation matrices:

```
T_32 = [1 -1/2 -1/2; 0 sqrt(3)/2 -sqrt(3)/2 ];
T_23 = [2/3 0; -1/3 1/sqrt(3); -1/3 -1/sqrt(3)];
```

Current Controller

```
t_r = 1e-3;                             %Rise time[s]
w_BW = log(9)/t_r;                      %Bandwidth velocity
E_hat = 1i*w*Psi_R;
```

```
L_s_hat = L_s;
R_s_hat = R_s;
R_a = w_BW*L_s_hat - R_s_hat;
ki = w_BW*(R_s_hat+R_a);            %Integral Gain
kp = w_BW*L_s_hat;                  %Proportional Gain
```

Speed controller

```
w_sc= w_BW/10;                      %w_sc 10 times less than w_Bw
Kp_sc = J*(w_sc);                   %Proportional Gain
Ki_sc = 0.1*Kp_sc/(w_sc);           %Integral Gain
Ka_sc = 3./Kp_sc;                   %Anti-windup Gain
```

Mechanical

```
E_w = 210e9;                        %E-modulus for steel
D_w = 5e-3;                         %Wire Diameter[mm]
A_w = (pi/4) * D_w^2;               %Wire Area[mm^2]
L_0 = 1;                            %Inital Wire Length[m]
m_pl = 20;                          %Mass of Payload[Kg]
g = 9.81;                           %Gravity[Kgm/s^2]
r_d = (101.6e-3)/2;                 %Drum Radius[mm]
J_d = 8328e-6;                      %Drum Inertia
x_pl_init = 5;                      %Initial position of payload [m]
Delta_0 = m_pl*g*L_0/E_w/A_w;       %Initial wire elongation [m]
```

Gearbox

```
Z1 = 19;                            %Teeth pinion [-]
Z2 = 127;                           %Teeth gear [-]
n = Z2/Z1;                          %Gear ratio 1 [-]
m = 2;                              %module [mm]
Dp_p = m*Z1;                        %Pitch Diameter pinion [mm]
rp = (Dp_p/2)*1e-3;
Dp_w = m * Z2;                      %Pitch Diameter gear [mm]
r_wh = (Dp_w/2)*1e-3;
C_k = 20000;                        %Stiffness of gears
mu = 0;                             %Friction coeff.

%Mass and inertia
lambda = 10;                                    %Width factor
b = lambda * m;                                 %Width of cogwheel
rho_steel = 7.85e-6;                            %Density steel [kg/mm^3]
Mass_p = (pi * (Dp_p^2)/4 * b)*rho_steel;       %Mass of pinion
Mass_w = (pi * (Dp_w^2)/4 * b)*rho_steel;       %Mass of pinion

Ip = 10*Mass_p * rp^2;
J_wh = 10*Mass_w * rp^2;                        %Wheel inertia [kgm^2]
```

Bearing parameters

```
D = 0.0158;                         %Damping coe[N.s/mm]
D_b = 8.40;                         %Ball diameter [mm]
mb= 10e-3;                          %Bearing mass[Kg]
r_b=D_b/2;                          %Bearing radius[mm]
```

```
r_i= 4.375;                          %Radii curvature[mm]
N_b=4;                               %Number of ball
D_out= 47;                           %Outer-race diameter
r_out= D_out/2;
D_inn= 20;                           %Inner-race diameter
r_inn=D_inn/2;
r_i= 4.375;                          %Radii curvature [mm]
D_c = 33.9;                          %Cage diameter[mm]

ms=5.0+0.0350;                       %Mass[Kg](motor + inner race)


%Inner race Stiffness constant
Sigma_f_i= (1/r_b)+(1/r_b)+(1/r_inn)+(1/-r_i);               %Curva._sum

Diff_f_i= (((1/r_b)-(1/r_b))+((1/r_inn)-(1/-r_i)))/Sigma_f_i;%Curva._diff

%From table 6.1 in Harris
d_f_t_u=0.93657;
delta_t_u= 0.6112;

d_f_t_n=0.95738;
delta_t_n= 0.5551;

delta_i= (Diff_f_i*delta_t_u)/d_f_t_u;
delta_i1= (Diff_f_i*delta_t_n)/d_f_t_n;
delta_star= (delta_i+delta_i1)/2;   %Delta* inner-race

delta_inner= 2.79e-4* delta_star*(Sigma_f_i^(1/3));
C_inn= (1/delta_inner)^1.5;          %Constant inner race-ball[N/mm^1.5]



%Outer race Stiffness constant

Sigma_f_o= (1/r_b)+(1/r_b)+(1/-r_out)+(1/-r_i);

Diff_f_o= (((1/r_b)-(1/r_b))+((1/-r_out)-(1/-r_i)))/Sigma_f_o;

d_f_t_u_o=0.87366;
delta_t_u_o= 0.7169;

d_f_t_n_o=0.90999;
delta_t_n_o= 0.6636;

delta_o= (Diff_f_o*delta_t_u_o)/d_f_t_u_o;
delta_o1= (Diff_f_o*delta_t_n_o)/d_f_t_n_o;
delta_o_star= (delta_o+delta_o1)/2; %Delta* outer-race


delta_outer= 2.79e-4* delta_o1*(Sigma_f_o^(1/3));
C_out= (1/delta_outer)^1.5;          %Constant outer race-ball[N/mm^1.5]


C_eq= ((C_inn)*(C_out))/(((C_inn)^(2/3)+(C_out)^(2/3)))^1.5;     %[N/mm^1.5]


% Damping coeficient (experimental):
D = 0.01582;                         %[Ns/mm]
```

Noisy measurement

```
beta = 10;                          %Real constant
%Noise in drum encoder
sigmaTheta_D= 1*1e-7;
betaTheta_D = 10;
noiseTheta_D = 1;

%Noise in rotor encoder
sigmaTheta_r= 1*1e-7;
betaTheta_r = 10;
noiseTheta_r = 1;

%Noise in depth sensor
sigmaZ_pl= 1*1e-9;
betaZ_pl = 10;
noiseZ_pl = 1;

%Noise in current sensor (i_a, i_b)
sigmai_a= 1*1e-7;
betai_a = 10;
noisei_a = 1;

sigmai_b= 1*1e-7;
betai_b = 10;
noisei_b = 1;

%Noise in bearing displacement sensor ROTOR
sigmaY_in= 1*1e-9;
betaY_in = 10;
noiseY_in = 1;

sigmaX_in= 1*1e-9;
betaX_in = 10;
noiseX_in = 1;

%Noise in bearing displacement sensor DRUM
sigmaY_inn2= 1*1e-9;
betaY_inn2 = 10;
noiseY_inn2 = 1;

sigmaX_inn2= 1*1e-9;
betaX_inn2 = 10;
noiseX_inn2 = 1;
```

Defect

```
%Turn off all noise - uncomment

% noiseTheta_D = 0;
% noiseTheta_r = 0;
% noiseZ_pl = 0;
% noisei_a = 0;
% noisei_b = 0;
% noiseY_in = 0;
% noiseX_in = 0;
% noiseY_inn2 = 0;
% noiseX_inn2 = 0;
```

```
%Activate of Sensor Fault
Faulti_am = 0;
FaultTheta_r_m = 0;
FaultZ_pl = 0;
FaultTheta_D = 0;
FaultXin = 0;
FaultYin2 = 0;



%PMSM Motor
FaultR_s = 0;
b_friction = 3;                     %Motor friction coeff.[Nms]
Faultb_friction = 0;

%Gear
FaultC_k = 0;
Wh_friction = 0.5;                  %Wheel-pinion friction coeff.[Nms]
FaultWh_friction = 0;

%Wire
FaultA_w = 0;

%Bearing
FaultF_u =0;
FaultF_u2 =0;
FaultDb_out=0;                      %defect outer race bearing 1
FaultDb_out2 = 0;                   %defect bearing 2


% Outer race defect
L_dout= 0.5;                        %Length of defect[mm]
D_dout= 0.5e-2;                     %Depth of defect [mm]
alpha_di_out= 45*pi/180;            %Initial angle of defect[rad]
alpha_df_out=((L_dout/r_out) + alpha_di_out);   %Angle of end-defect[rad]
CAS= cos(alpha_di_out);             %Cosine Angle Start
CAF= cos(alpha_df_out);             %Cosine Angle Finite



Theta_d= L_dout/r_b;                %Angle of the arc [rad]
delta_h= D_b/2*(1- cos(Theta_d/2)); %Center of ball displacement [mm]


% Disequilibrium force (radial). Cause more waviness.
Fu=100;                             % [N]
Fu2 =200;                           % [N]

% External Forces on the ball bearing in X&Y axes
Fex=0;                              % [N]
Fey=0;                              % [N]
```

Published with MATLAB® R2017b

A.2 Simulink Model

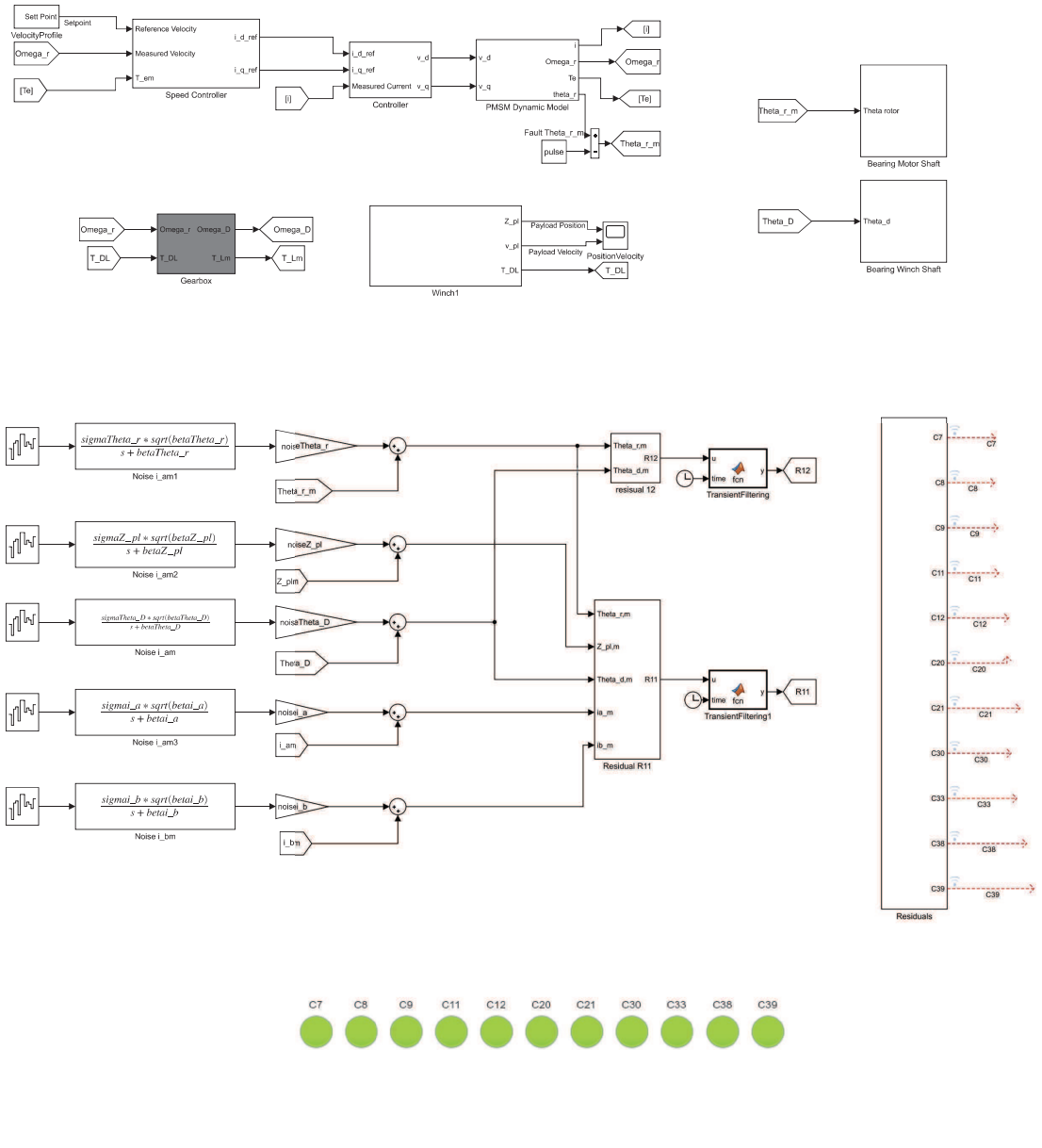

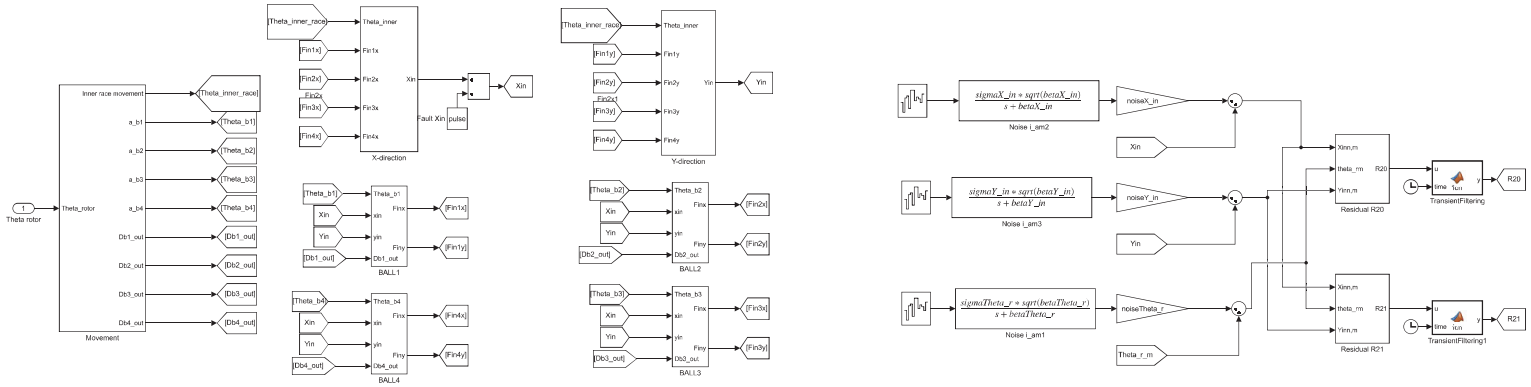
1
Theta rotor
Theta_rotor
Inner race movement
a_b1
a_b2
a_b3
a_b4
Db1_out
Db2_out
Db3_out
Db4_out
Movement
[Theta_inner_race]
[Theta_b1]
[Theta_b2]
[Theta_b3]
[Theta_b4]
[Db1_out]
[Db2_out]
[Db3_out]
[Db4_out]
Theta_inner
Fin1x
Fin2x
Fin3x
Fin4x
Xin
Fault Xin
pulse
X-direction
Fin1y
Fin2y
Fin3y
Fin4y
Yin
Y-direction
Theta_b1
Xin
Yin
Db1_out
Finx
Finy
BALL1
[Fin1x]
[Fin1y]
Theta_b2
Db2_out
BALL2
[Fin2x]
[Fin2y]
Theta_b3
Db3_out
BALL3
[Fin3x]
[Fin3y]
Theta_b4
Db4_out
BALL4
[Fin4x]
[Fin4y]

$\frac{sigmaX\_in * sqrt(betaX\_in)}{s + betaX\_in}$
Noise i_am2
noiseX_in
Xin
$\frac{sigmaY\_in * sqrt(betaY\_in)}{s + betaY\_in}$
Noise i_am3
noiseY_in
Yin
$\frac{sigmaTheta\_r * sqrt(betaTheta\_r)}{s + betaTheta\_r}$
Noise i_am1
noiseTheta_r
Theta_r_m
Xinn,m
theta_rm
Yinn,m
R20
Residual R20
TransientFiltering
R21
Residual R21
TransientFiltering1

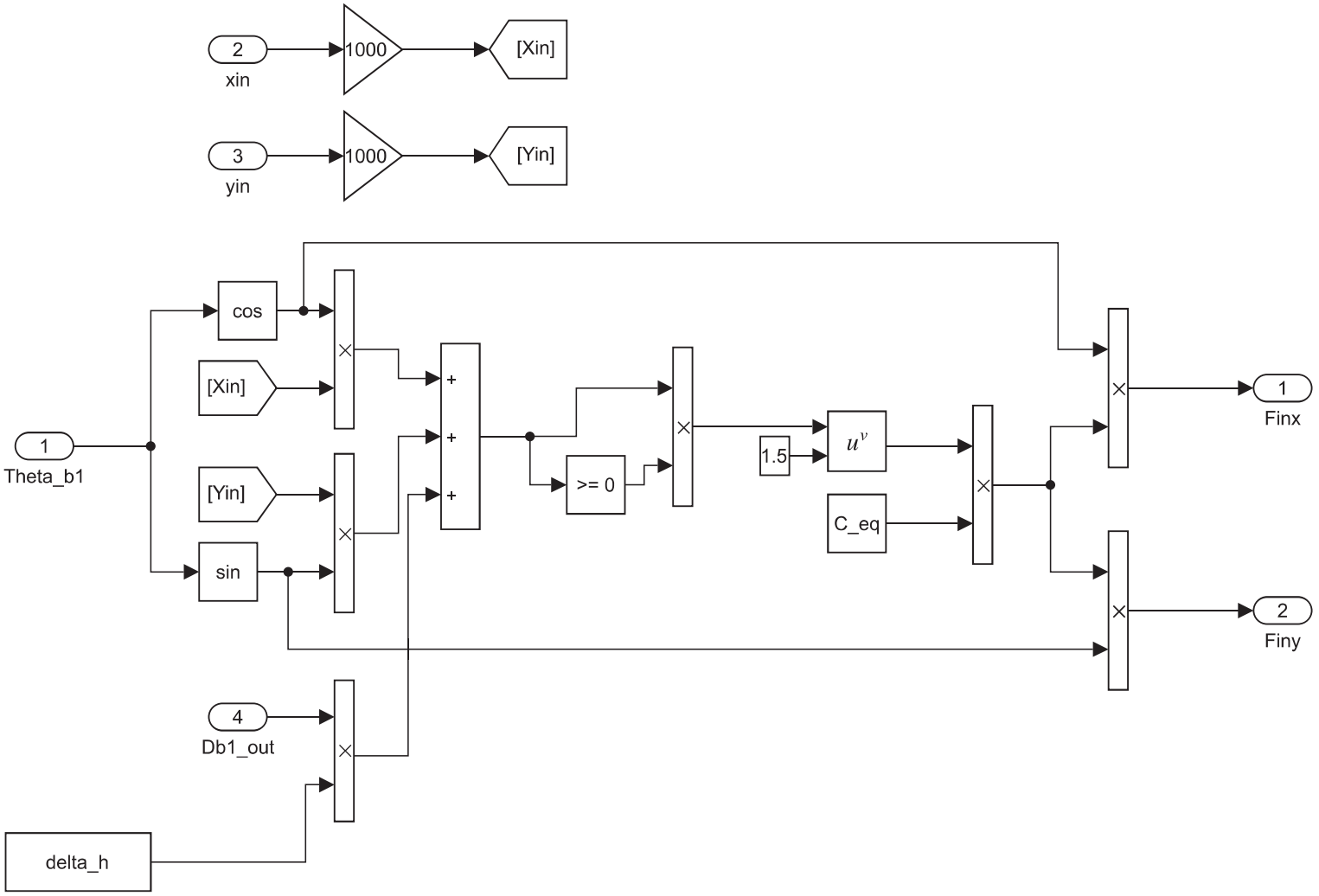
2
xin
1000
[Xin]
3
yin
1000
[Yin]
1
Theta_b1
cos
[Xin]
[Yin]
sin
4
Db1_out
delta_h
+
+
+
>= 0
1.5
u^v
C_eq
1
Finx
2
Finy

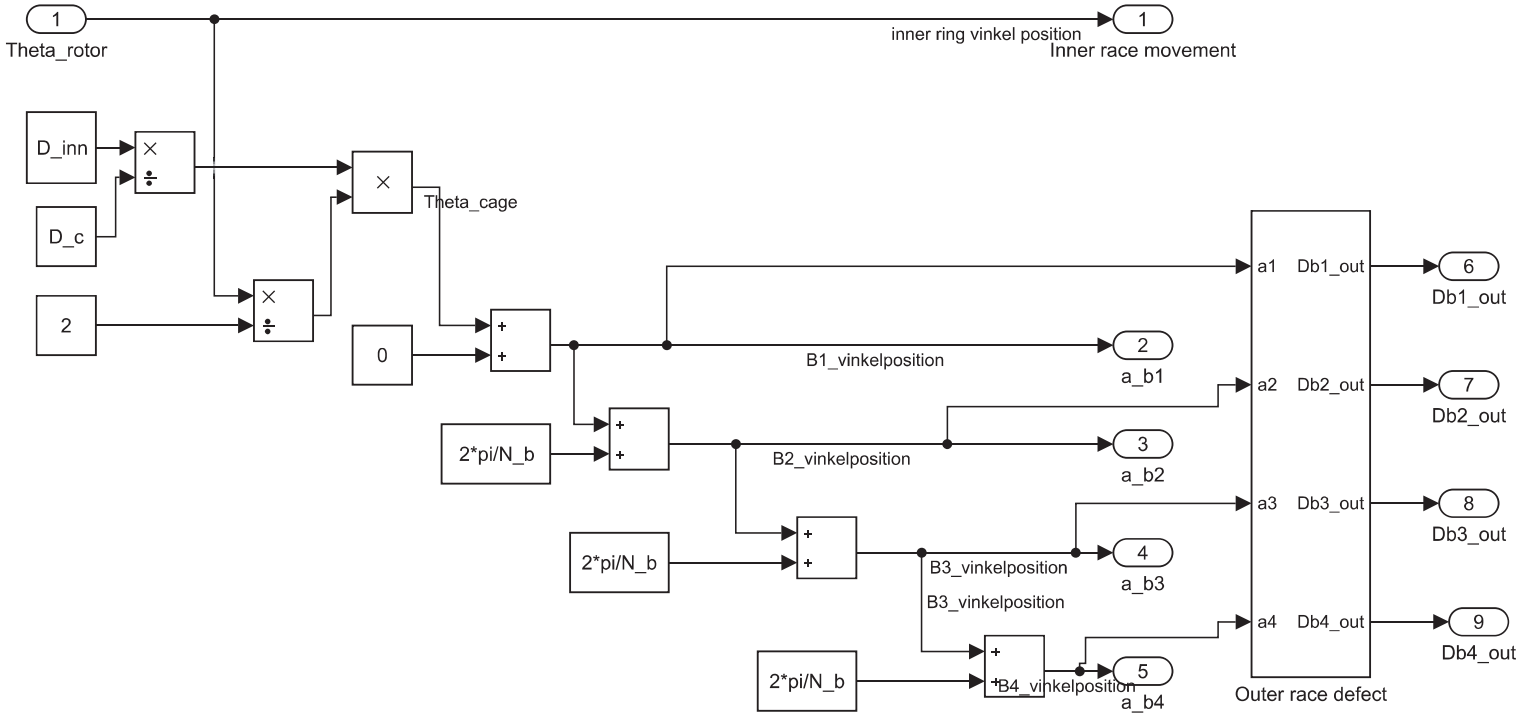
1
Theta_rotor
1
inner ring vinkel position
Inner race movement
D_inn
D_c
2
Theta_cage
0
2*pi/N_b
2*pi/N_b
2*pi/N_b
B1_vinkelposition
2
a_b1
B2_vinkelposition
3
a_b2
B3_vinkelposition
4
a_b3
B3_vinkelposition
B4_vinkelposition
5
a_b4
a1 Db1_out
a2 Db2_out
a3 Db3_out
a4 Db4_out
Outer race defect
6
Db1_out
7
Db2_out
8
Db3_out
9
Db4_out

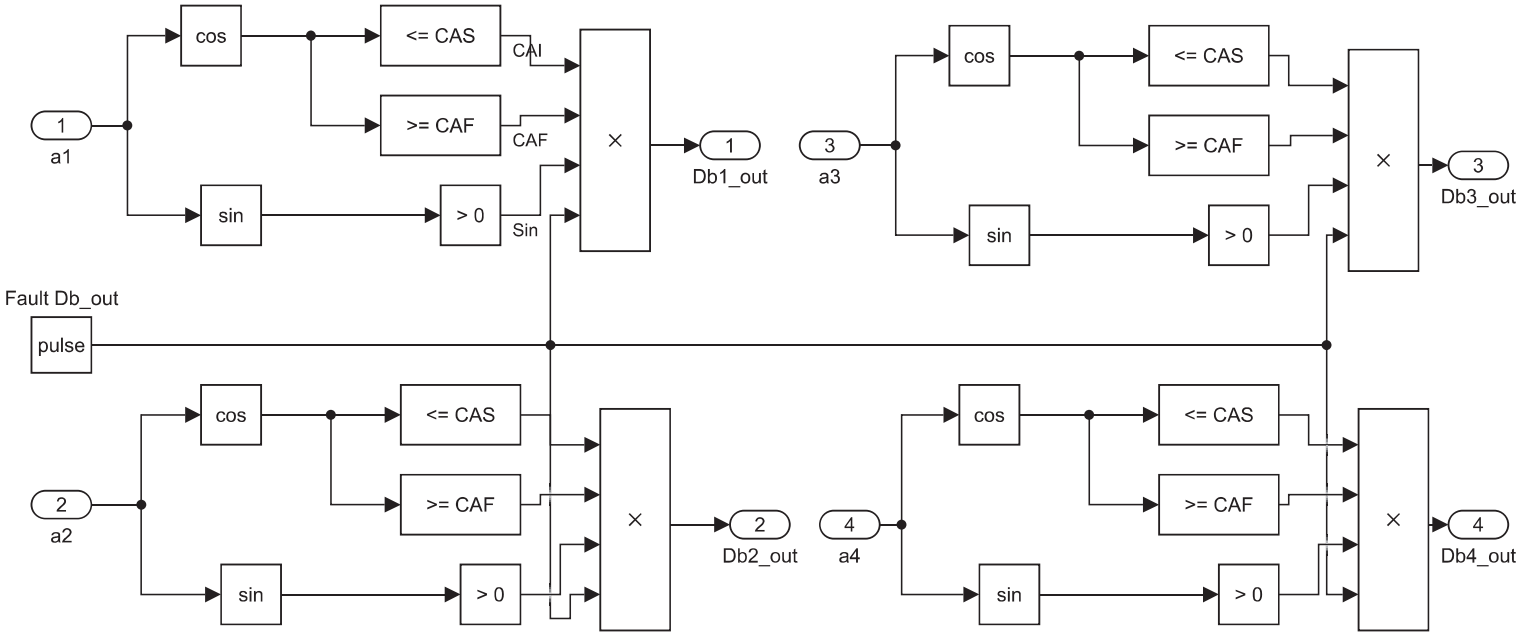
1
a1
cos
<= CAS
CAI
>= CAF
CAF
sin
> 0
Sin
×
1
Db1_out
3
a3
cos
<= CAS
>= CAF
sin
> 0
×
3
Db3_out
Fault Db_out
pulse
2
a2
cos
<= CAS
>= CAF
sin
> 0
×
2
Db2_out
4
a4
cos
<= CAS
>= CAF
sin
> 0
×
4
Db4_out

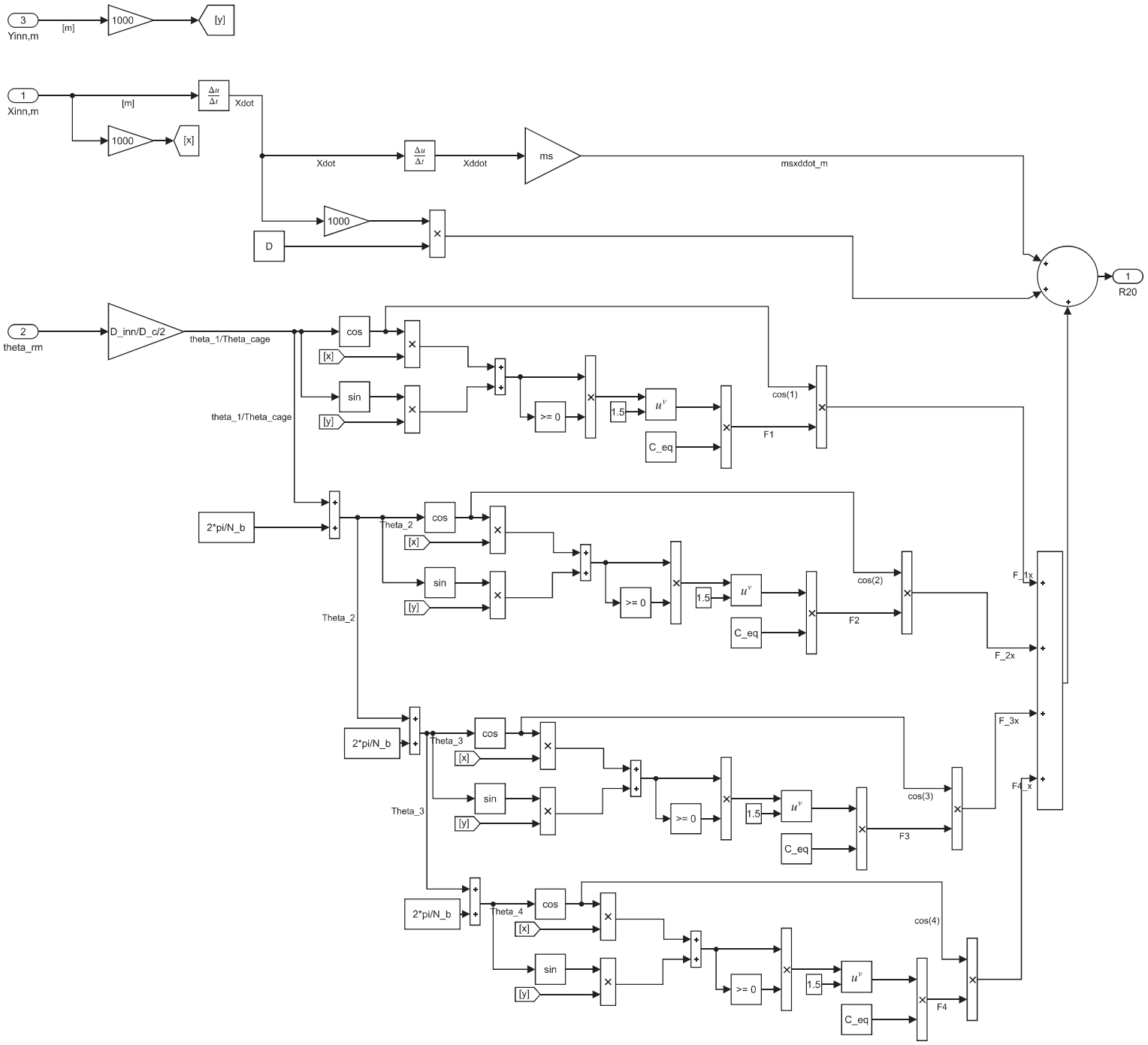
3
Yinn,m
[m]
1000
[y]
1
Xinn,m
[m]
Δu/Δt
Xdot
1000
[x]
Xdot
Δu/Δt
Xddot
ms
msxddot_m
1000
D
1
R20
2
theta_rm
D_inn/D_c/2
theta_1/Theta_cage
cos
[x]
sin
[y]
theta_1/Theta_cage
>= 0
1.5
u^v
C_eq
F1
cos(1)
2*pi/N_b
Theta_2
cos
[x]
sin
[y]
Theta_2
>= 0
1.5
u^v
C_eq
F2
cos(2)
F_1x
F_2x
2*pi/N_b
Theta_3
cos
[x]
sin
[y]
Theta_3
>= 0
1.5
u^v
C_eq
F3
cos(3)
F_3x
F4_x
2*pi/N_b
Theta_4
cos
[x]
sin
[y]
>= 0
1.5
u^v
C_eq
F4
cos(4)

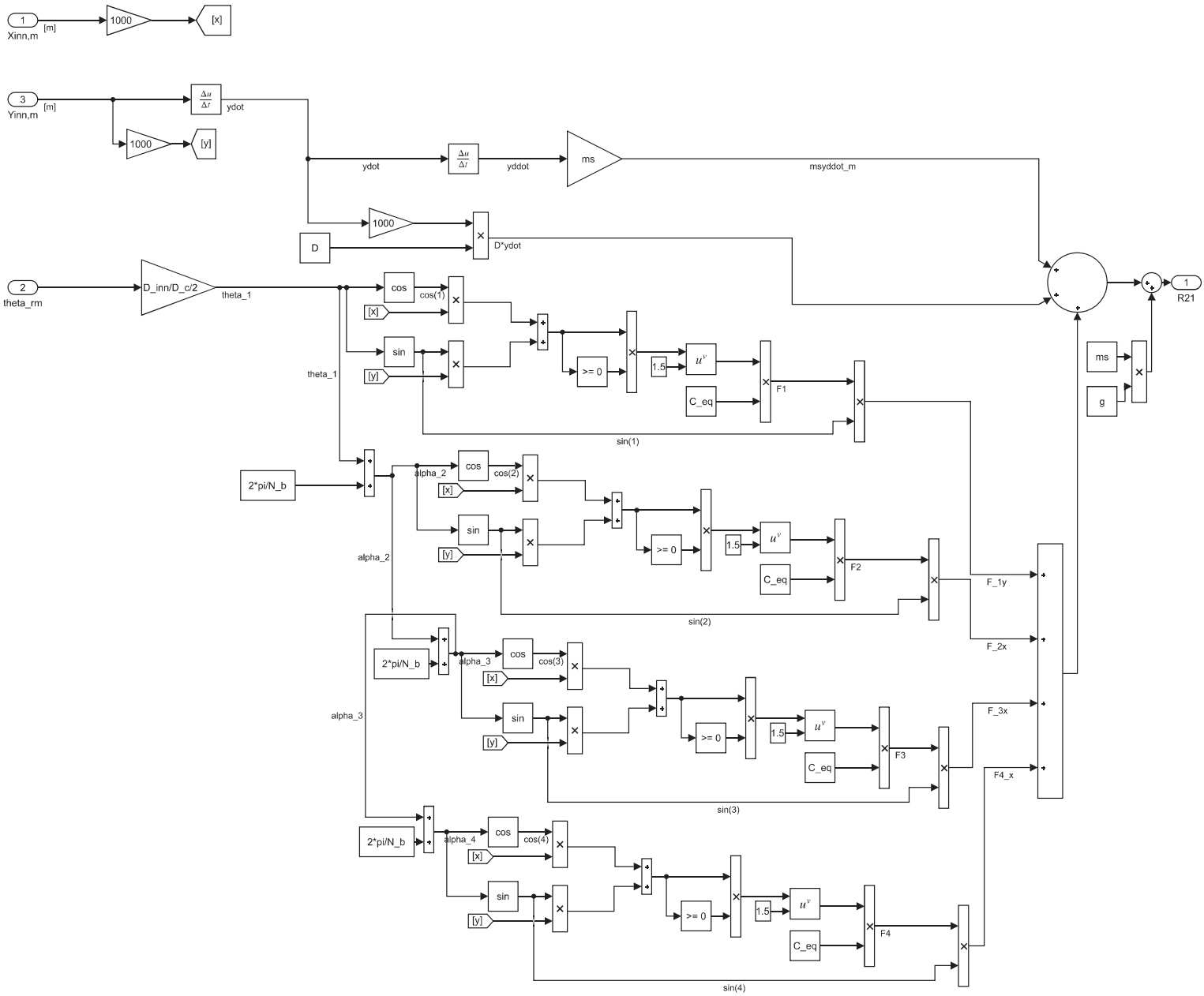
1
Xinn,m
[m]
1000
[x]
3
Yinn,m
[m]
1000
[y]
ydot
ydot
yddot
ms
msyddot_m
1000
D
D*ydot
2
theta_rm
D_inn/D_c/2
theta_1
cos
cos(1)
[x]
sin
[y]
theta_1
>= 0
1.5
C_eq
F1
sin(1)
ms
g
1
R21
2*pi/N_b
alpha_2
cos
cos(2)
[x]
sin
[y]
alpha_2
>= 0
1.5
C_eq
F2
sin(2)
F_1y
F_2x
2*pi/N_b
alpha_3
cos
cos(3)
[x]
sin
[y]
alpha_3
>= 0
1.5
C_eq
F3
sin(3)
F_3x
F4_x
2*pi/N_b
alpha_4
cos
cos(4)
[x]
sin
[y]
>= 0
1.5
C_eq
F4
sin(4)

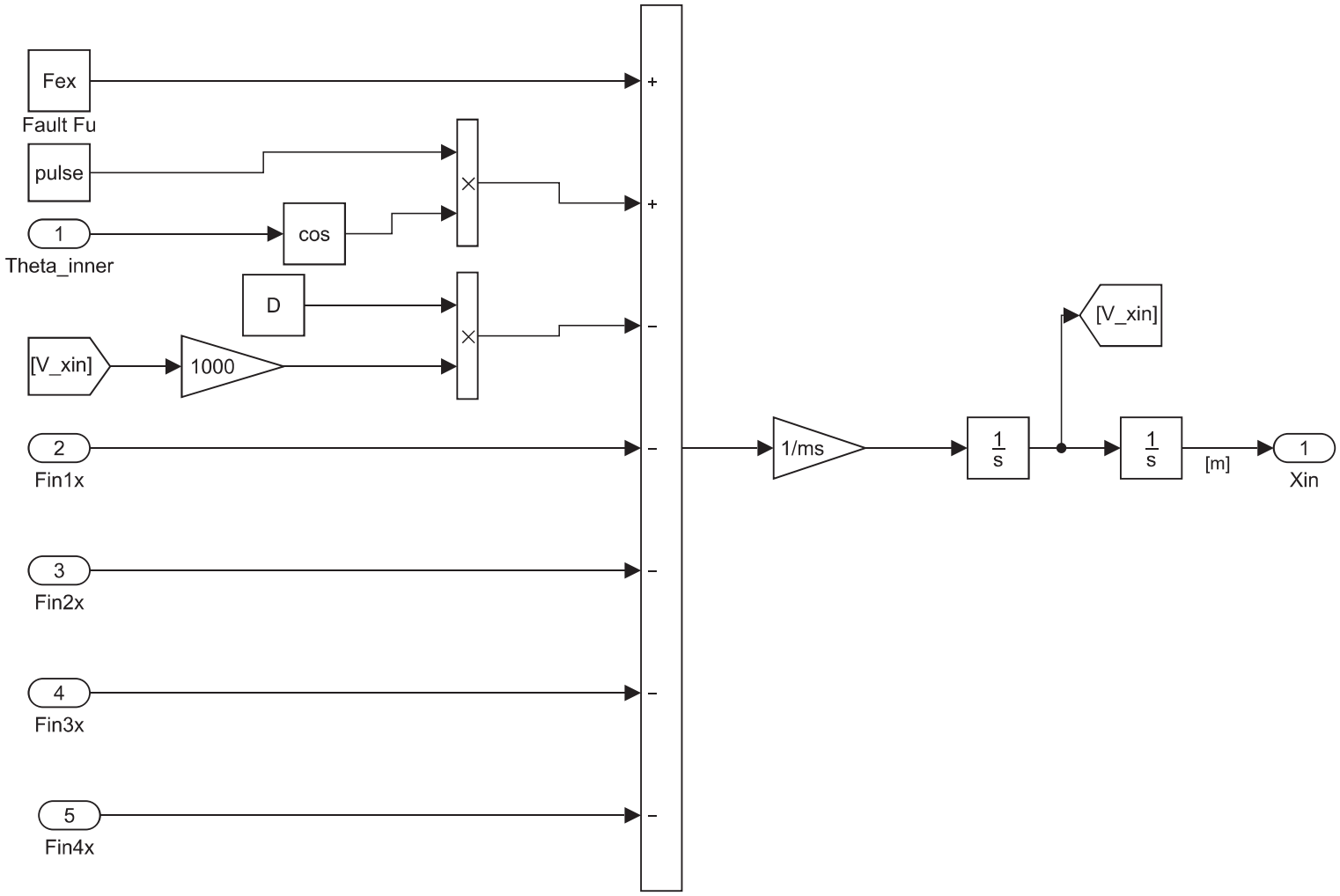
Fex
Fault Fu
pulse
1
Theta_inner
cos
D
[V_xin]
1000
2
Fin1x
3
Fin2x
4
Fin3x
5
Fin4x
+
+
-
-
-
-
-
1/ms
1
s
[V_xin]
1
s
[m]
1
Xin

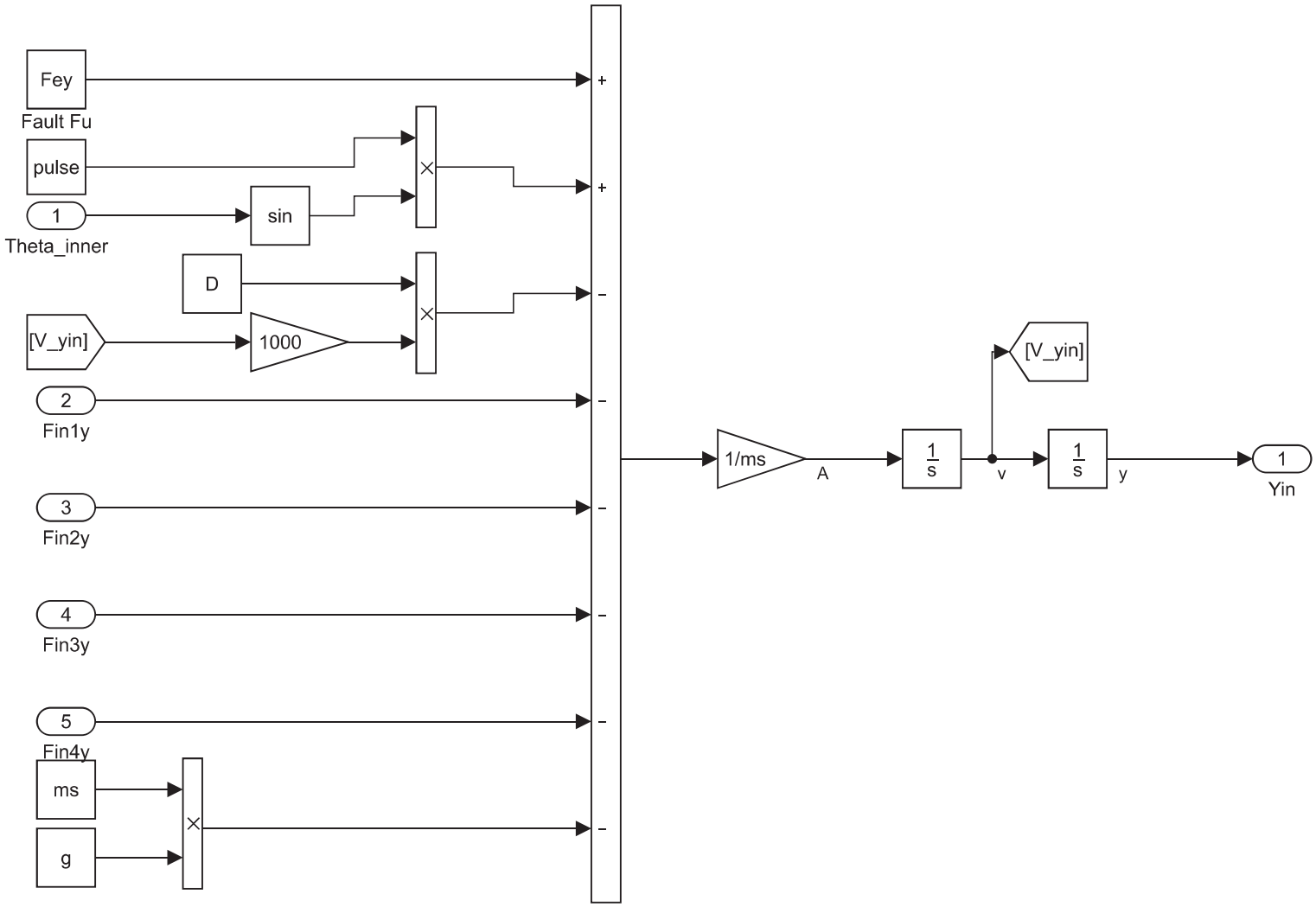
Fey
Fault Fu
pulse
1
Theta_inner
sin
D
[V_yin]
1000
2
Fin1y
3
Fin2y
4
Fin3y
5
Fin4y
ms
g
+
+
-
-
-
-
-
1/ms
A
1
s
v
[V_yin]
1
s
y
1
Yin

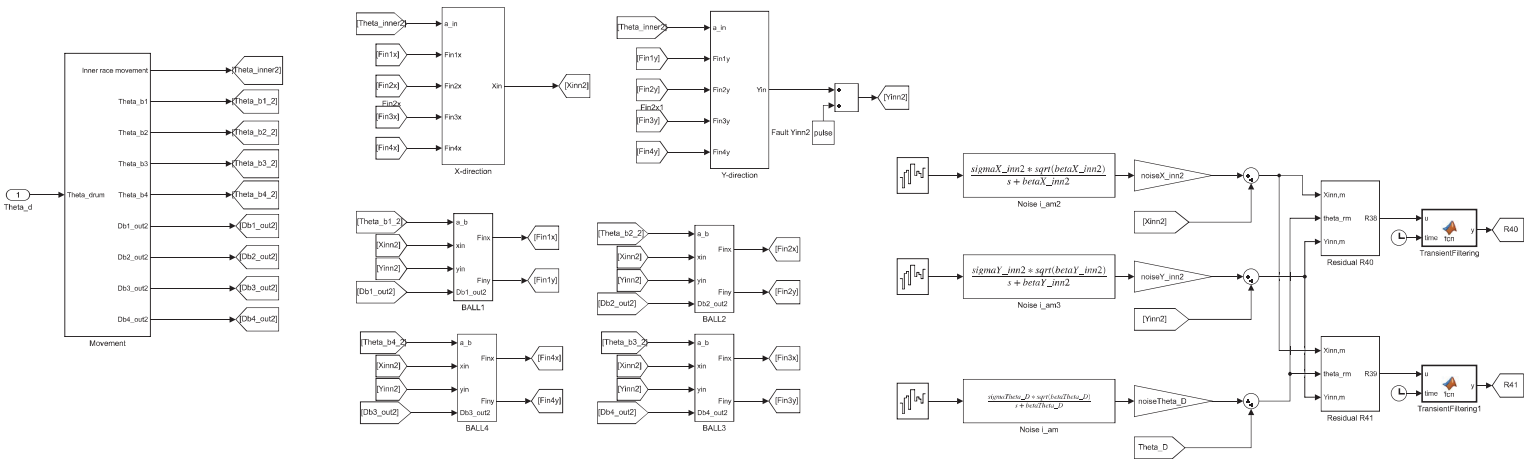
1
Theta_d
Inner race movement
Theta_b1
Theta_b2
Theta_b3
Theta_b4
Db1_out2
Db2_out2
Db3_out2
Db4_out2
Theta_drum
Movement
[Theta_inner2]
[Theta_b1_2]
[Theta_b2_2]
[Theta_b3_2]
[Theta_b4_2]
[Db1_out2]
[Db2_out2]
[Db3_out2]
[Db4_out2]
[Theta_inner2]
[Fin1x]
[Fin2x]
[Fin3x]
[Fin4x]
a_in
Fin1x
Fin2x
Fin3x
Fin4x
Xin
[Xinn2]
X-direction
[Theta_inner2]
[Fin1y]
[Fin2y]
[Fin3y]
[Fin4y]
a_in
Fin1y
Fin2y
Fin3y
Fin4y
Yin
Fault Yinn2
pulse
[Yinn2]
Y-direction
[Theta_b1_2]
[Xinn2]
[Yinn2]
[Db1_out2]
a_b
xin
yin
Finx
Finy
Db1_out2
[Fin1x]
[Fin1y]
BALL1
[Theta_b2_2]
[Xinn2]
[Yinn2]
[Db2_out2]
a_b
xin
yin
Finx
Finy
Db2_out2
[Fin2x]
[Fin2y]
BALL2
[Theta_b4_2]
[Xinn2]
[Yinn2]
[Db3_out2]
a_b
xin
yin
Finx
Finy
Db3_out2
[Fin4x]
[Fin4y]
BALL4
[Theta_b3_2]
[Xinn2]
[Yinn2]
[Db4_out2]
a_b
xin
yin
Finx
Finy
Db4_out2
[Fin3x]
[Fin3y]
BALL3
sigmaX_inn2 * sqrt(betaX_inn2) / s + betaX_inn2
Noise i_am2
noiseX_inn2
[Xinn2]
sigmaY_inn2 * sqrt(betaY_inn2) / s + betaY_inn2
Noise i_am3
noiseY_inn2
[Yinn2]
sigmaTheta_D * sqrt(betaTheta_D) / s + betaTheta_D
Noise i_am
noiseTheta_D
Theta_D
Xinn,m
theta_rm
Yinn,m
R38
Residual R40
u
time
fcn
y
TransientFiltering
R40
Xinn,m
theta_rm
Yinn,m
R39
Residual R41
u
time
fcn
y
TransientFiltering1
R41

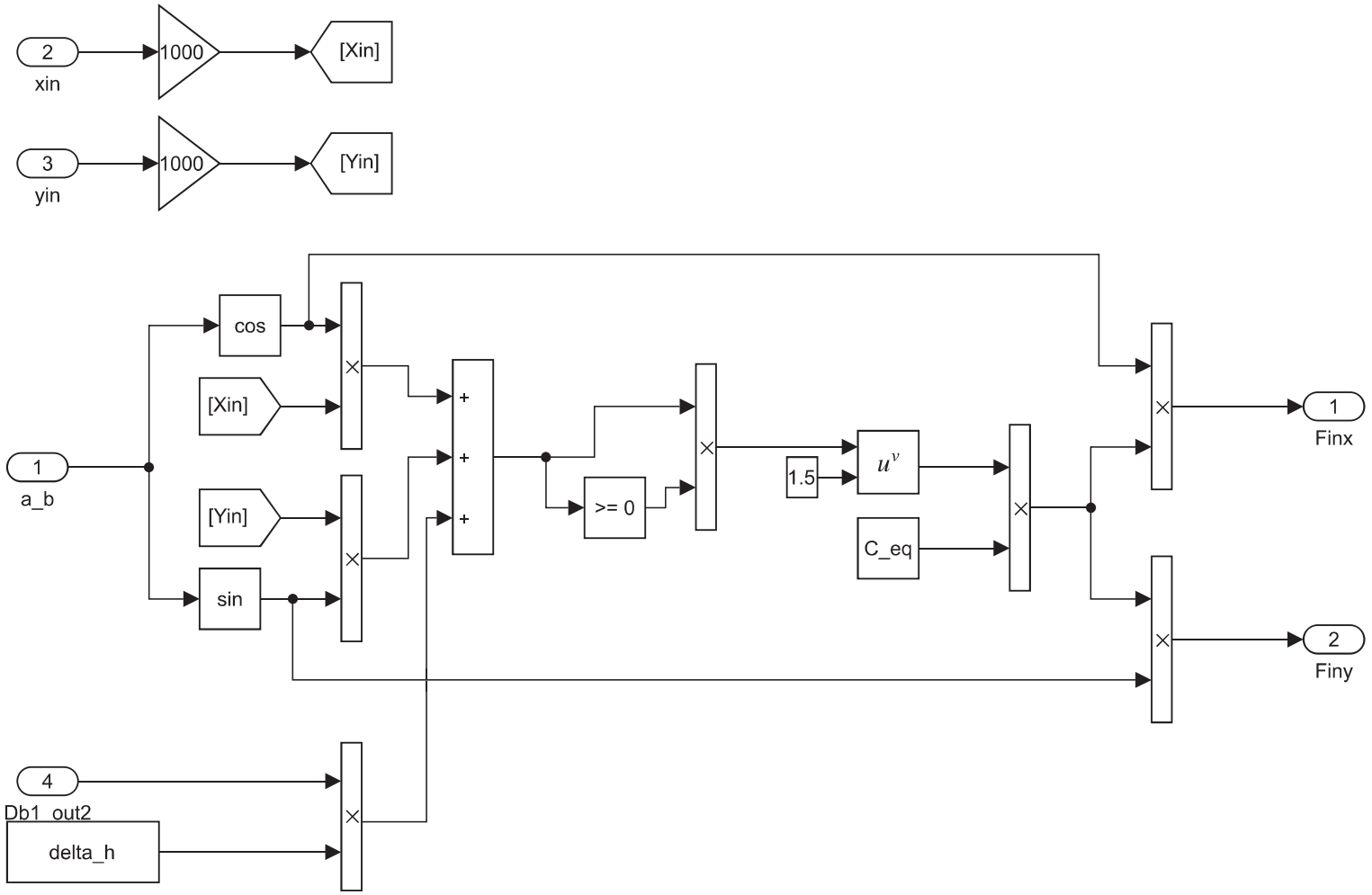
2
xin
1000
[Xin]
3
yin
1000
[Yin]
cos
[Xin]
1
a_b
[Yin]
sin
+
+
+
>= 0
1.5
u^v
C_eq
1
Finx
2
Finy
4
Db1_out2
delta_h

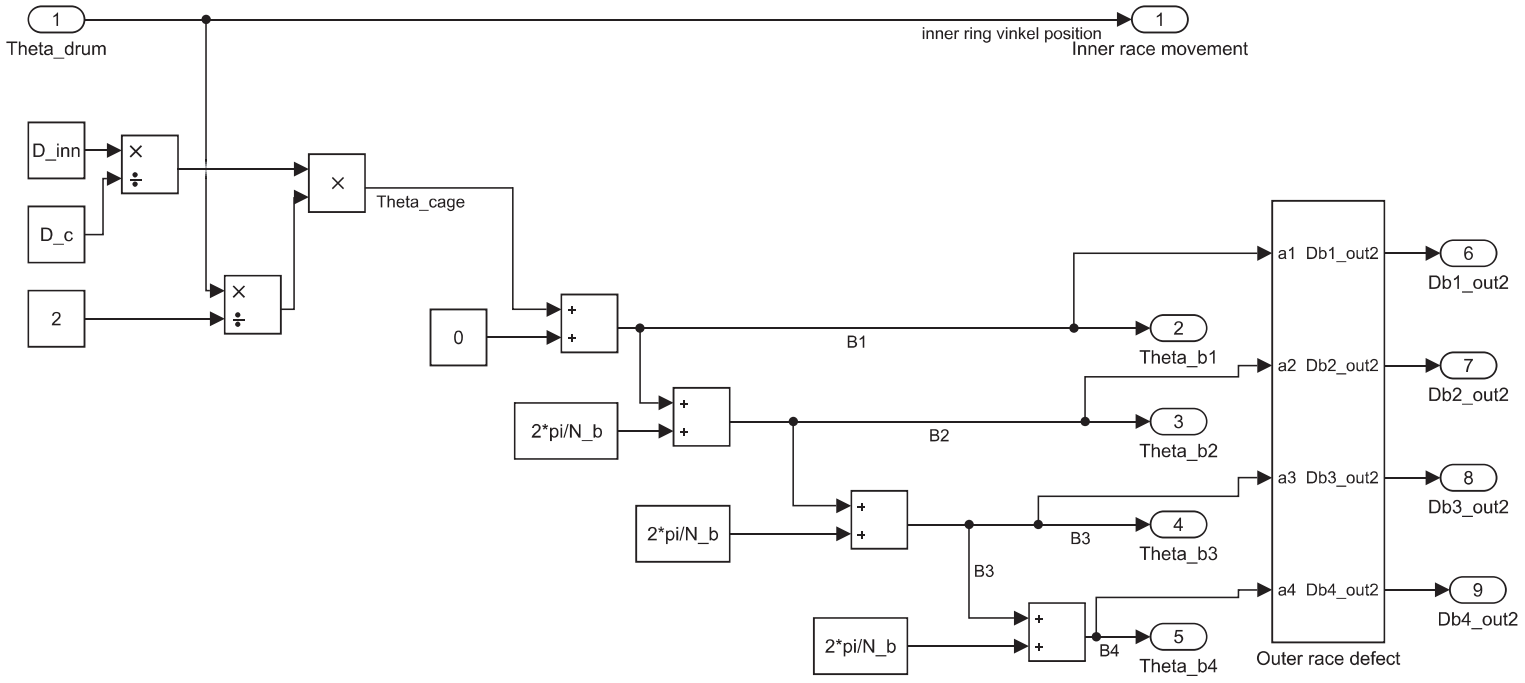
1
Theta_drum
1
inner ring vinkel position
Inner race movement
D_inn
D_c
2
Theta_cage
0
2*pi/N_b
2*pi/N_b
2*pi/N_b
B1
B2
B3
B3
B4
2
Theta_b1
3
Theta_b2
4
Theta_b3
5
Theta_b4
a1 Db1_out2
a2 Db2_out2
a3 Db3_out2
a4 Db4_out2
Outer race defect
6
Db1_out2
7
Db2_out2
8
Db3_out2
9
Db4_out2

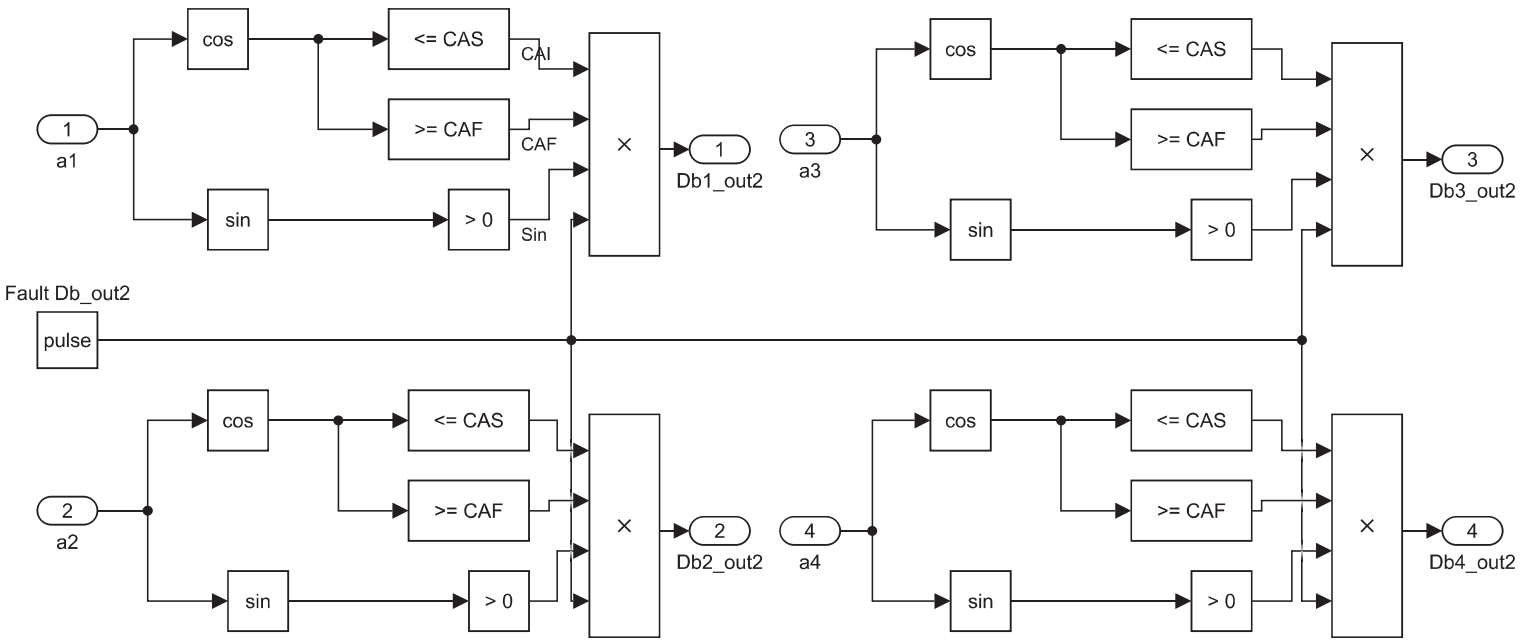
1
a1
cos
<= CAS
CAI
>= CAF
CAF
sin
> 0
Sin
×
1
Db1_out2
3
a3
cos
<= CAS
>= CAF
sin
> 0
×
3
Db3_out2
Fault Db_out2
pulse
2
a2
cos
<= CAS
>= CAF
sin
> 0
×
2
Db2_out2
4
a4
cos
<= CAS
>= CAF
sin
> 0
×
4
Db4_out2

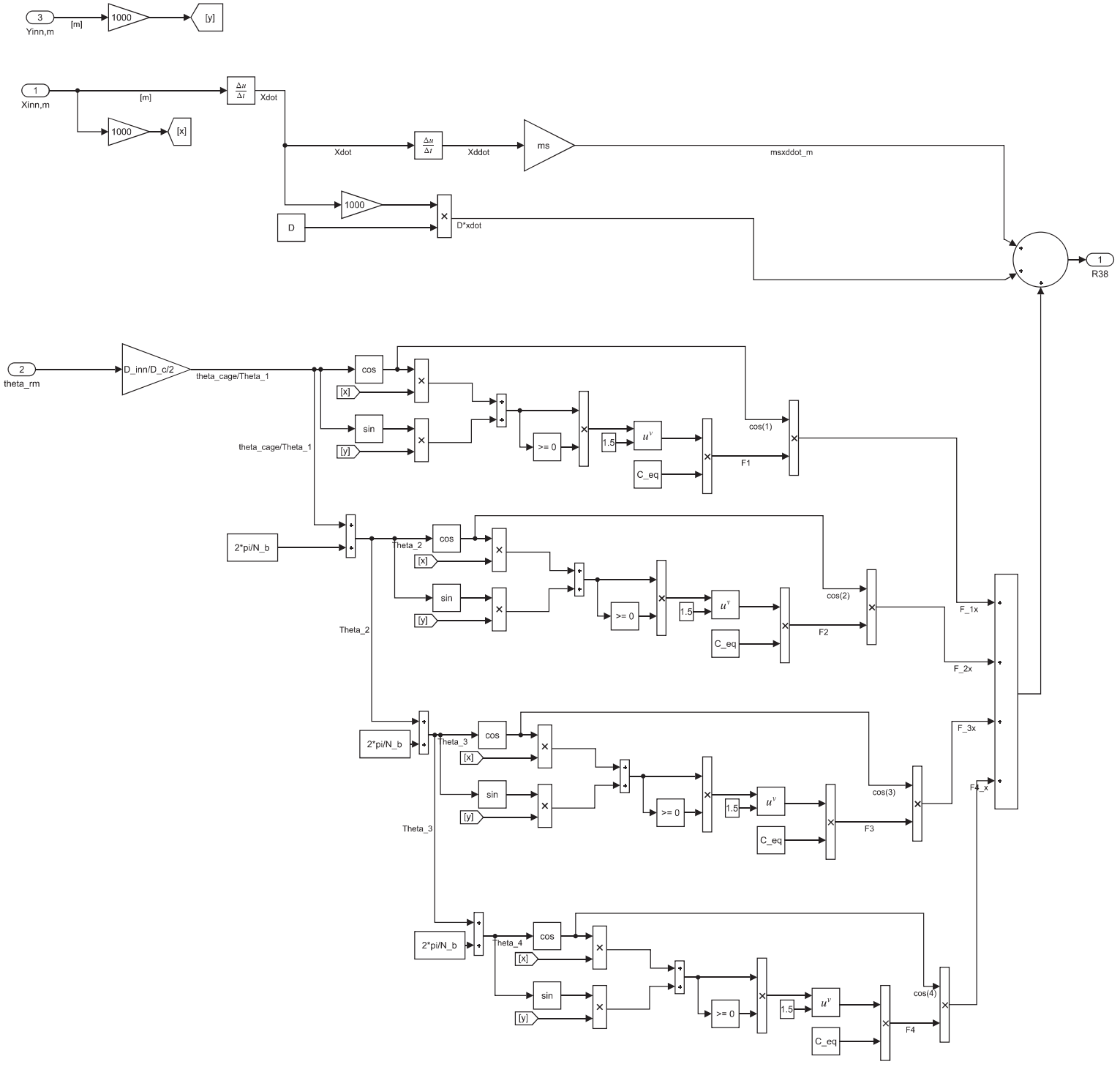
3
Yinn,m
[m]
1000
[y]
1
Xinn,m
[m]
Xdot
1000
[x]
Xdot
Xddot
ms
msxddot_m
1000
D
D*xdot
1
R38
2
theta_rm
D_inn/D_c/2
theta_cage/Theta_1
cos
sin
[x]
[y]
theta_cage/Theta_1
>= 0
1.5
C_eq
F1
cos(1)
2*pi/N_b
Theta_2
cos(2)
F2
F_1x
F_2x
2*pi/N_b
Theta_3
F_3x
cos(3)
F3
F_4x
Theta_3
2*pi/N_b
Theta_4
cos(4)
F4

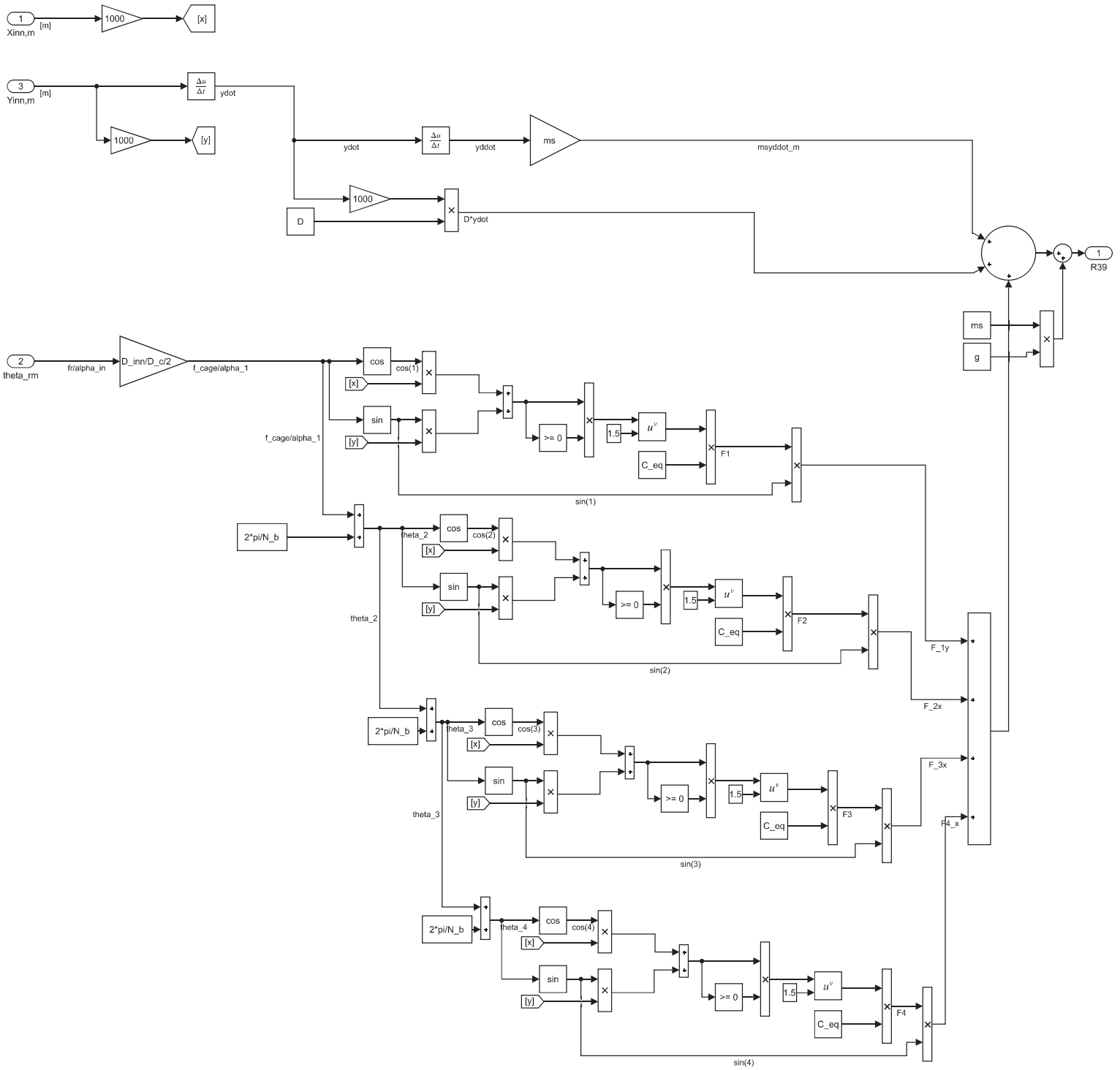
1
Xinn,m
[m]
1000
[x]
3
Yinn,m
[m]
1000
[y]
ydot
ydot
yddot
ms
msyddot_m
1000
D
D*ydot
1
R39
ms
g
2
theta_rm
fr/alpha_in
D_inn/D_c/2
f_cage/alpha_1
cos
cos(1)
[x]
sin
[y]
f_cage/alpha_1
>= 0
1.5
C_eq
F1
sin(1)
2*pi/N_b
theta_2
cos
cos(2)
[x]
sin
[y]
theta_2
>= 0
1.5
C_eq
F2
sin(2)
F_1y
F_2x
2*pi/N_b
theta_3
cos
cos(3)
[x]
sin
[y]
theta_3
>= 0
1.5
C_eq
F3
sin(3)
F_3x
F4_x
2*pi/N_b
theta_4
cos
cos(4)
[x]
sin
[y]
>= 0
1.5
C_eq
F4
sin(4)

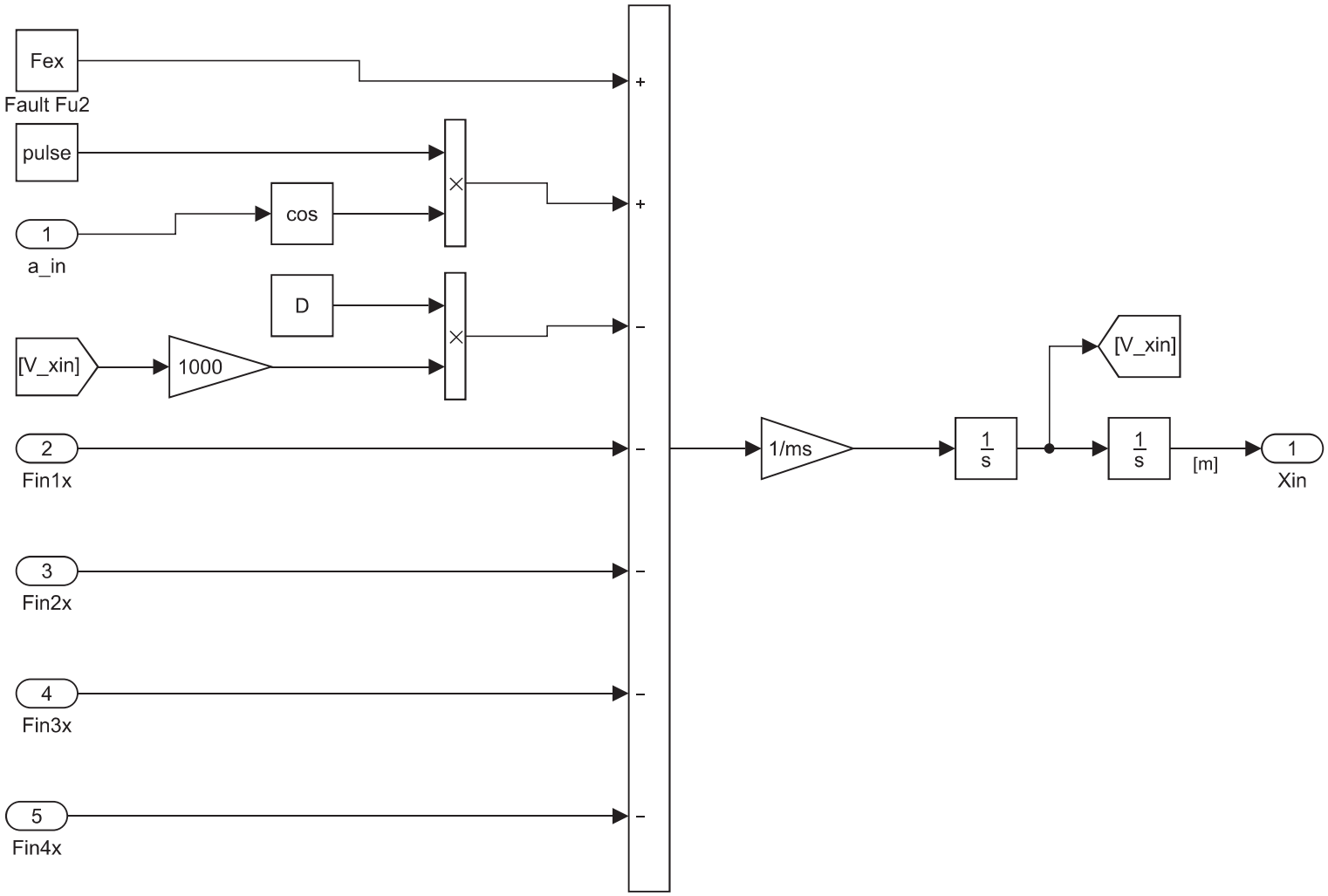
Fex
Fault Fu2
pulse
cos
1
a_in
D
[V_xin]
1000
2
Fin1x
3
Fin2x
4
Fin3x
5
Fin4x
+
+
-
-
-
-
-
1/ms
1
s
[V_xin]
1
s
[m]
1
Xin

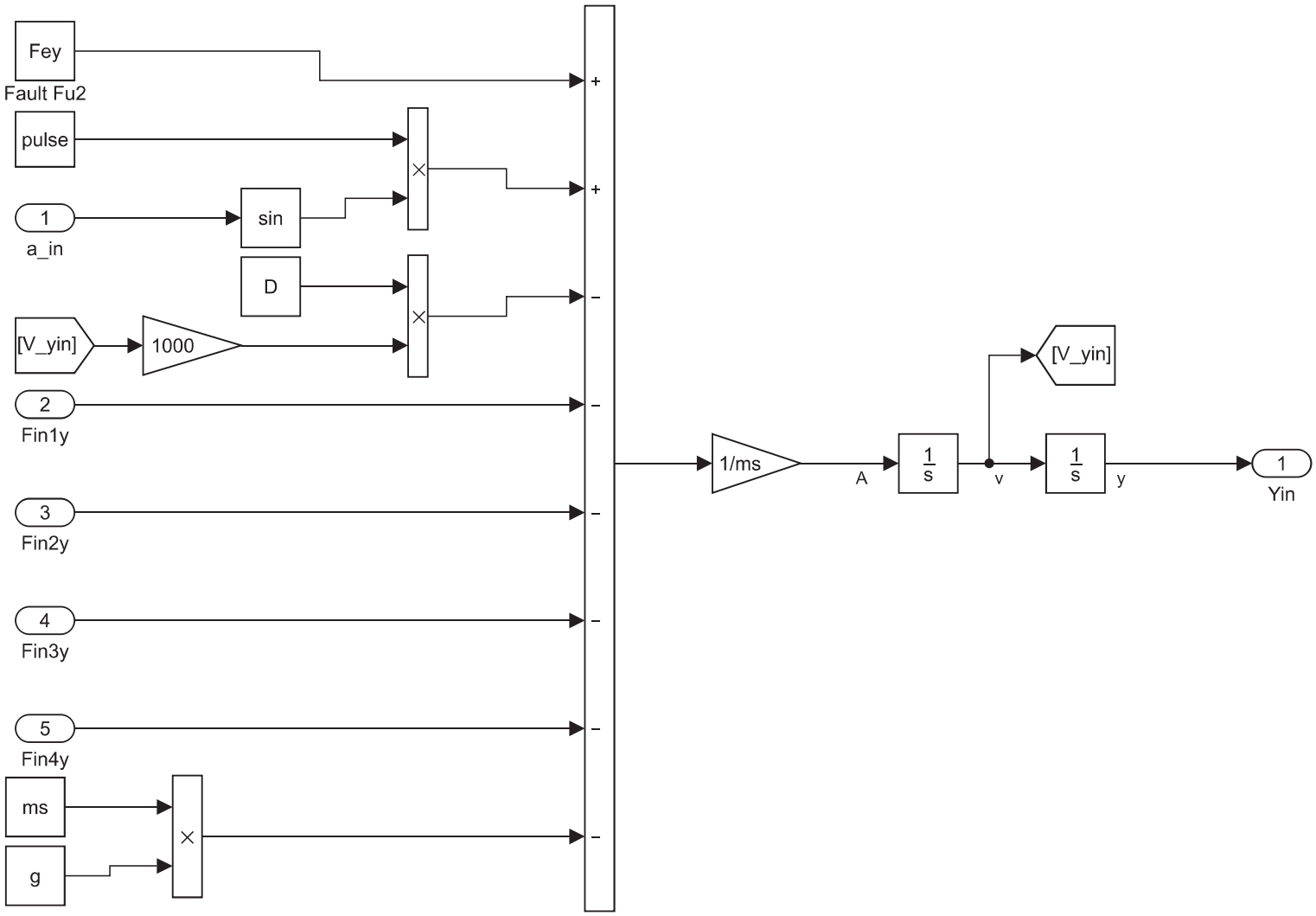
Fey
Fault Fu2
pulse
1
a_in
sin
D
[V_yin]
1000
2
Fin1y
3
Fin2y
4
Fin3y
5
Fin4y
ms
g
+
+
-
-
-
-
-
1/ms
A
1
s
v
[V_yin]
1
s
y
1
Yin

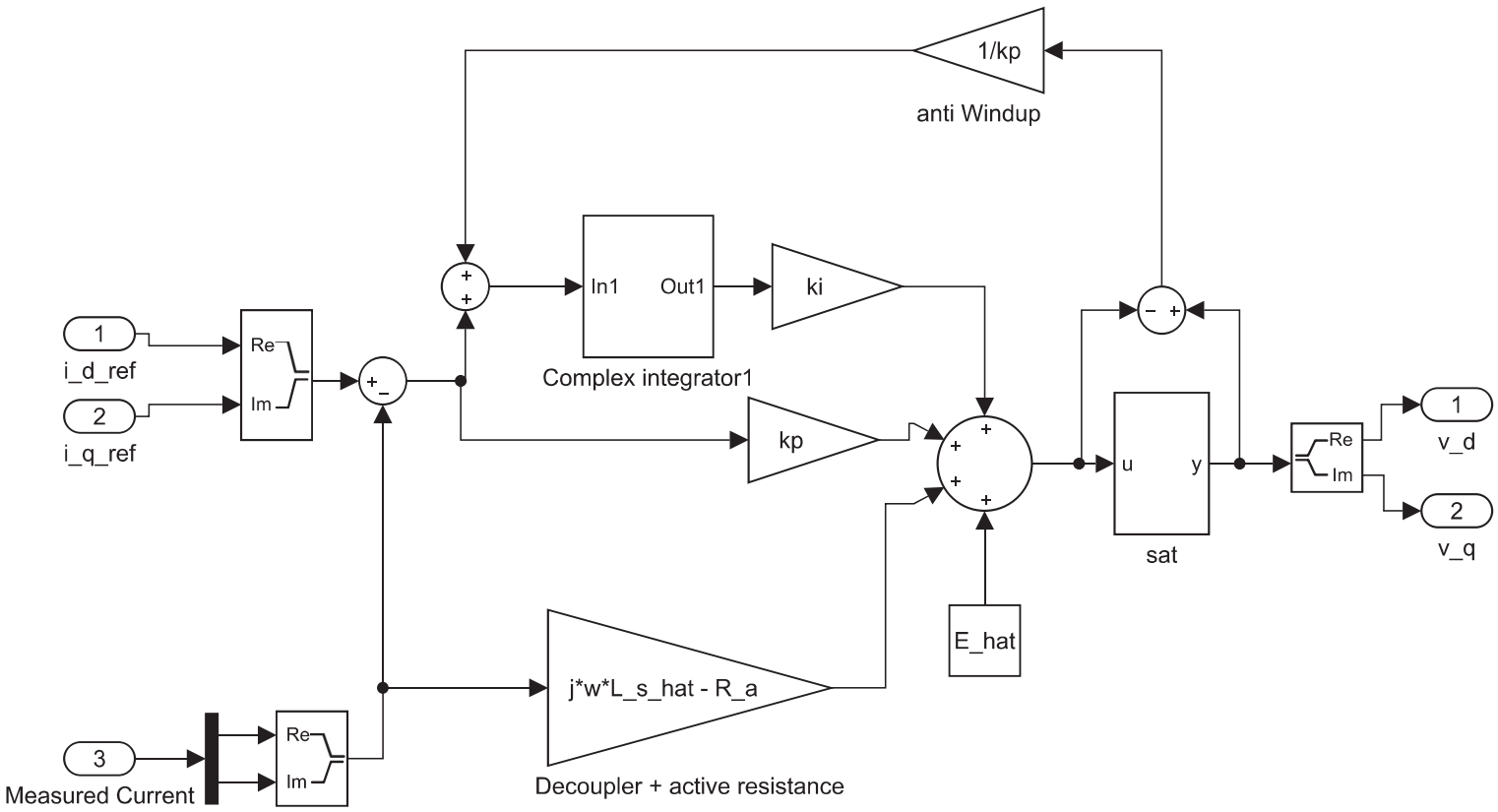
1/kp
anti Windup
In1
Out1
ki
Complex integrator1
1
i_d_ref
2
i_q_ref
Re
Im
kp
u
y
sat
Re
Im
1
v_d
2
v_q
E_hat
j*w*L_s_hat - R_a
Decoupler + active resistance
3
Measured Current
Re
Im

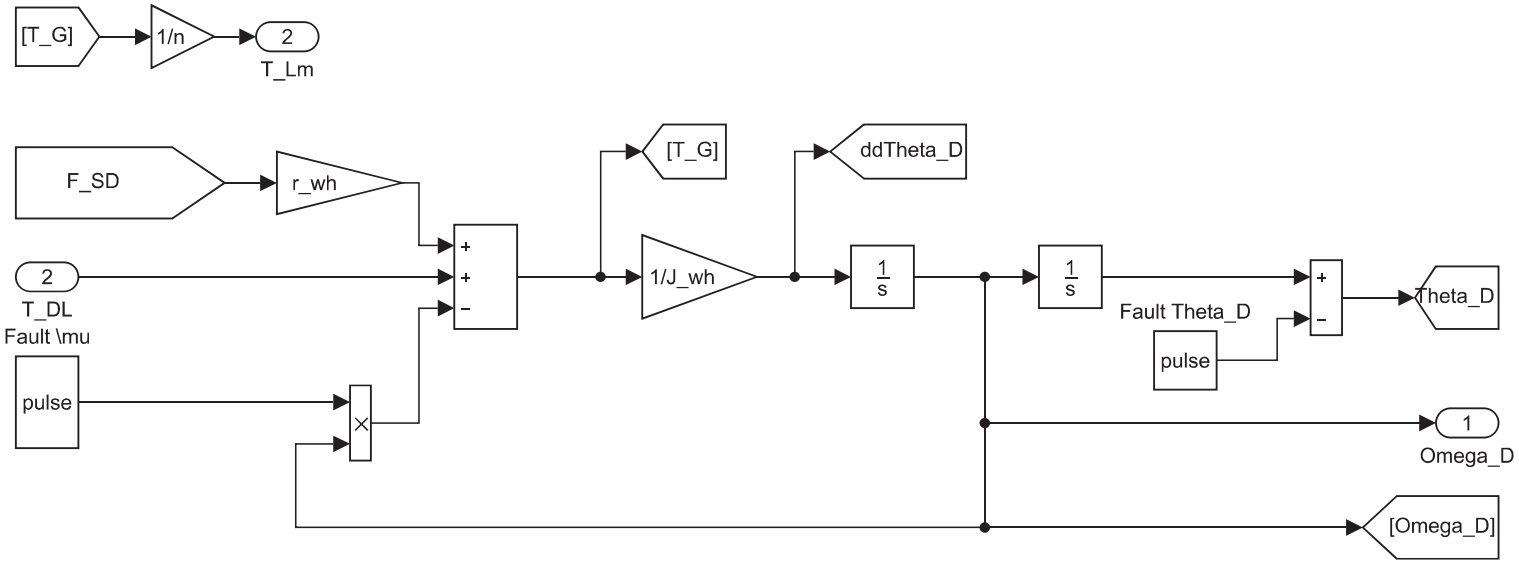
[T_G]
1/n
2
T_Lm
F_SD
r_wh
2
T_DL
Fault \mu
pulse
+
+
−
[T_G]
1/J_wh
ddTheta_D
1
s
1
s
Fault Theta_D
pulse
+
−
Theta_D
1
Omega_D
[Omega_D]

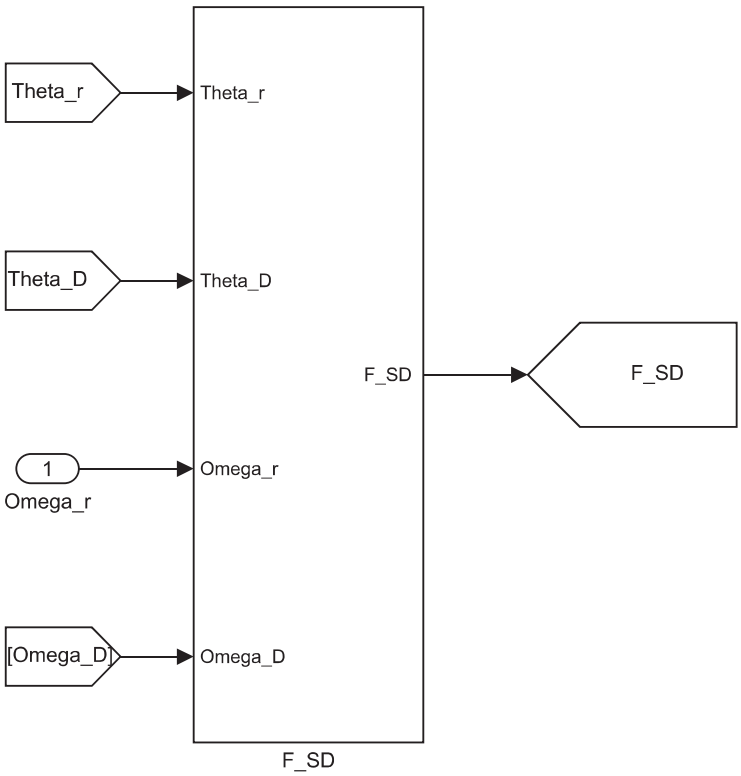
Theta_r
Theta_r
Theta_D
Theta_D
1
Omega_r
Omega_r
[Omega_D]
Omega_D
F_SD
F_SD
F_SD

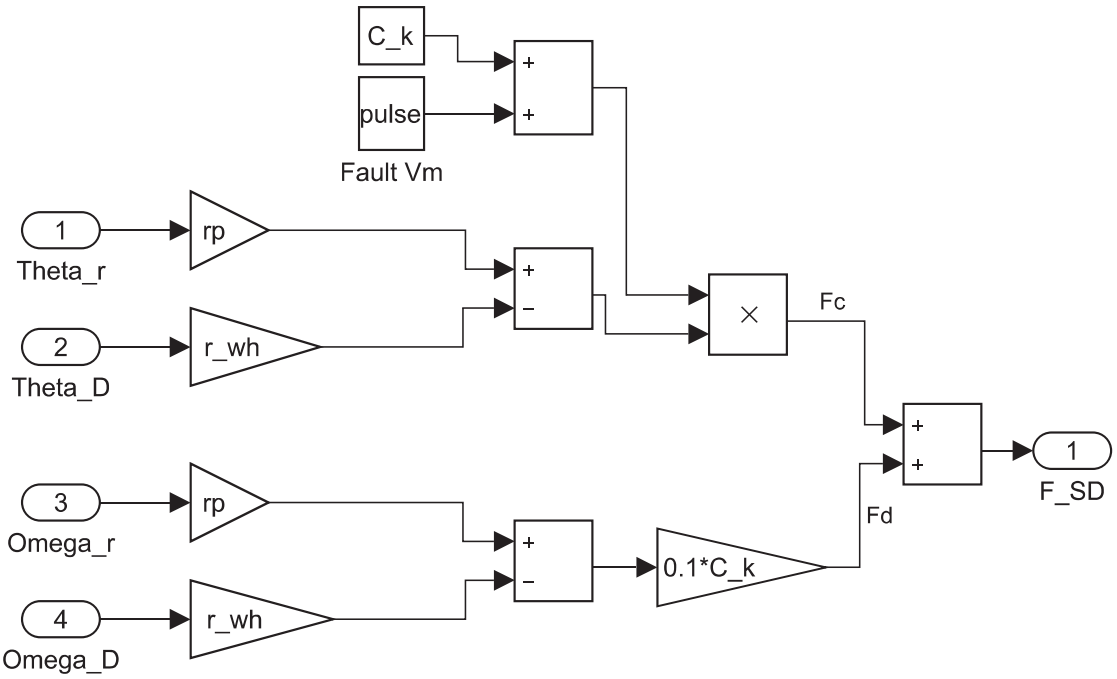
C_k
pulse
Fault Vm
1
Theta_r
rp
2
Theta_D
r_wh
3
Omega_r
rp
4
Omega_D
r_wh
Fc
Fd
0.1*C_k
1
F_SD

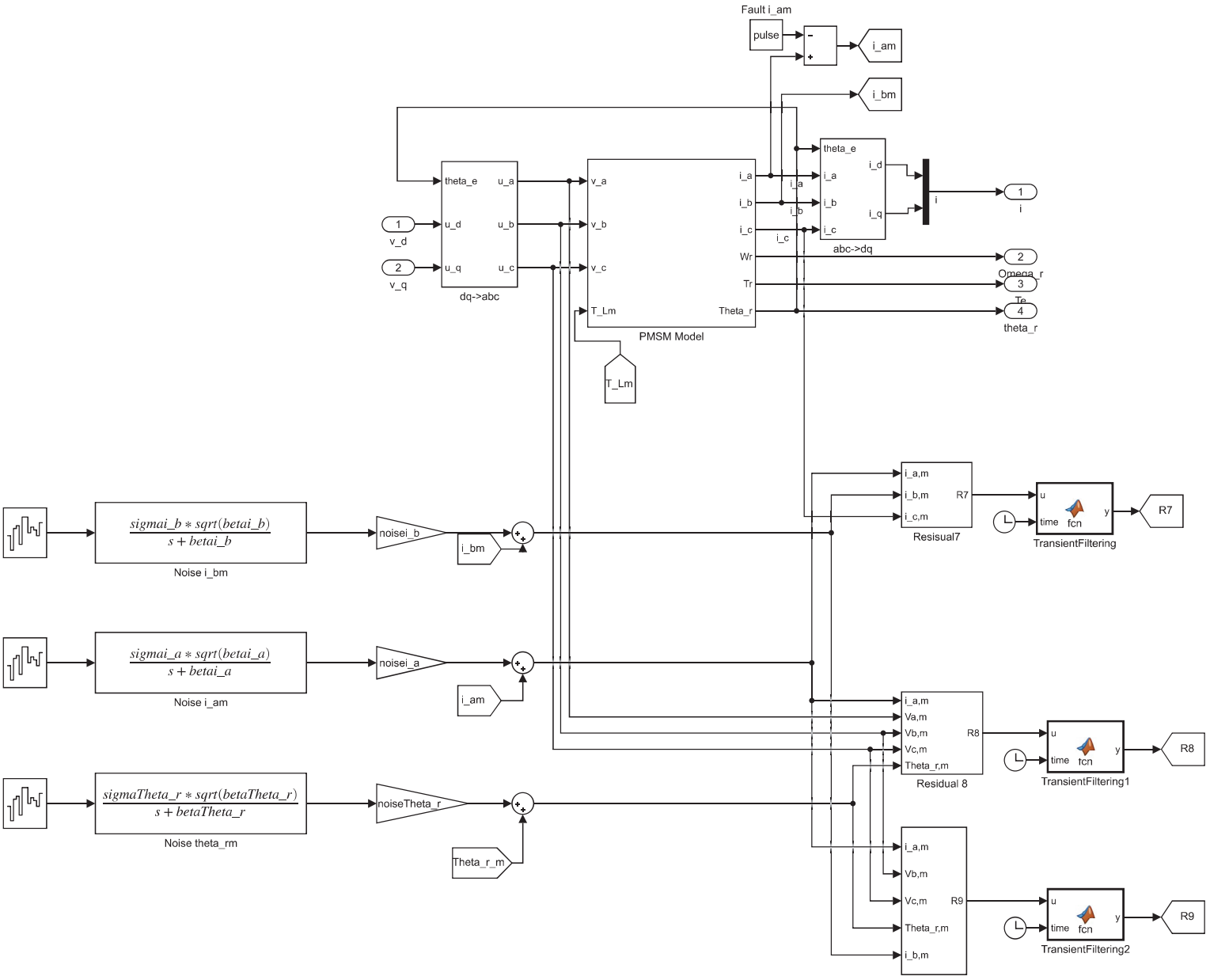
Fault i_am
pulse
i_am
i_bm
theta_e
u_a
u_d
u_b
u_q
u_c
dq->abc
1
v_d
2
v_q
v_a
v_b
v_c
T_Lm
i_a
i_b
i_c
Wr
Tr
Theta_r
PMSM Model
theta_e
i_d
i_a
i_b
i_q
i_c
abc->dq
i
1
i
2
Omega_r
3
Te
4
theta_r
T_Lm
sigmai_b * sqrt(betai_b)
s + betai_b
Noise i_bm
noisei_b
i_bm
sigmai_a * sqrt(betai_a)
s + betai_a
Noise i_am
noisei_a
i_am
sigmaTheta_r * sqrt(betaTheta_r)
s + betaTheta_r
Noise theta_rm
noiseTheta_r
Theta_r_m
i_a,m
i_b,m
i_c,m
R7
Resisual7
u
time
fcn
y
R7
TransientFiltering
i_a,m
Va,m
Vb,m
Vc,m
Theta_r,m
R8
Residual 8
R8
TransientFiltering1
i_a,m
Vb,m
Vc,m
Theta_r,m
i_b,m
R9
R9
TransientFiltering2

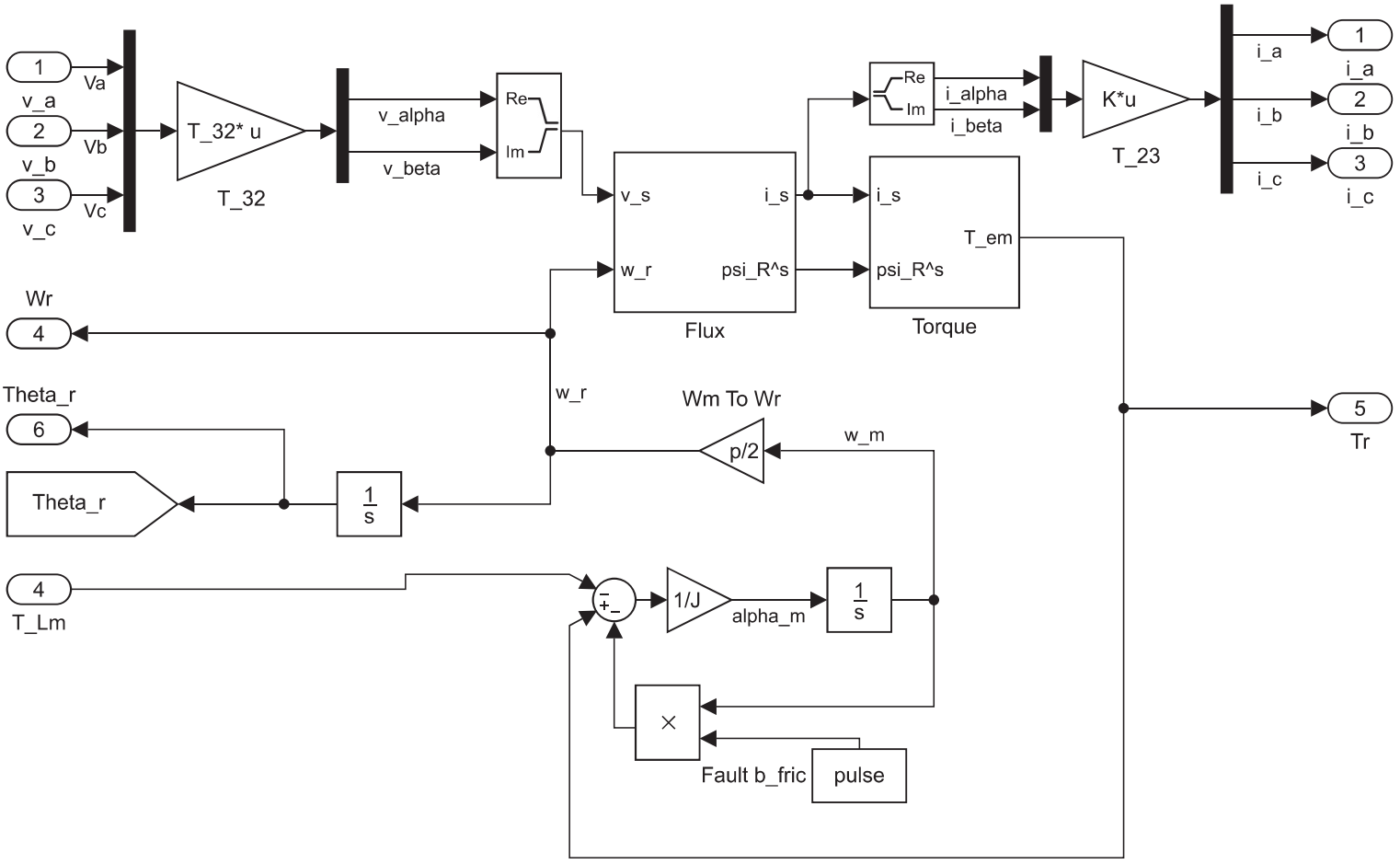
1
Va
v_a
2
Vb
v_b
3
Vc
v_c
T_32* u
T_32
v_alpha
v_beta
Re
Im
v_s
i_s
w_r
psi_R^s
Flux
Re
Im
i_alpha
i_beta
K*u
T_23
i_s
T_em
psi_R^s
Torque
1
i_a
i_a
2
i_b
i_b
3
i_c
i_c
Wr
4
Theta_r
6
Theta_r
1
s
w_r
Wm To Wr
p/2
w_m
5
Tr
4
T_Lm
1/J
alpha_m
1
s
Fault b_fric
pulse

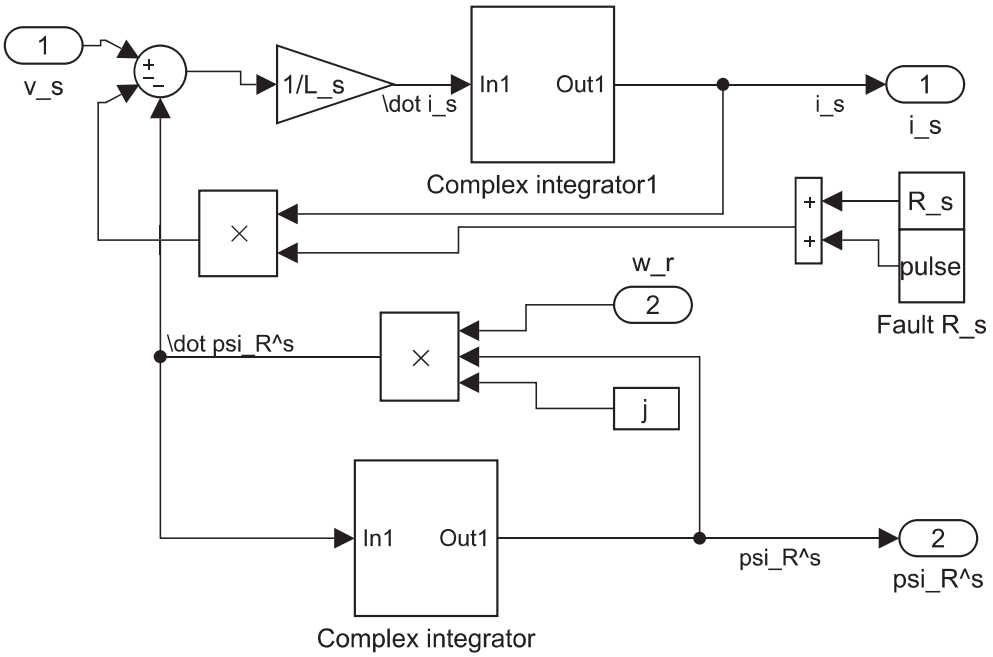
1
v_s
1/L_s
\dot i_s
In1
Out1
Complex integrator1
i_s
1
i_s
R_s
pulse
Fault R_s
w_r
2
\dot psi_R^s
j
In1
Out1
Complex integrator
psi_R^s
2
psi_R^s

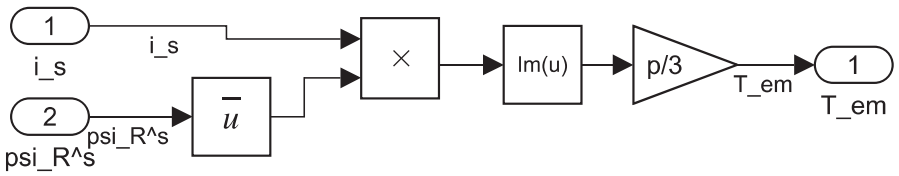
1
i_s
i_s
2
psi_R^s
psi_R^s
u
Im(u)
p/3
T_em
1
T_em

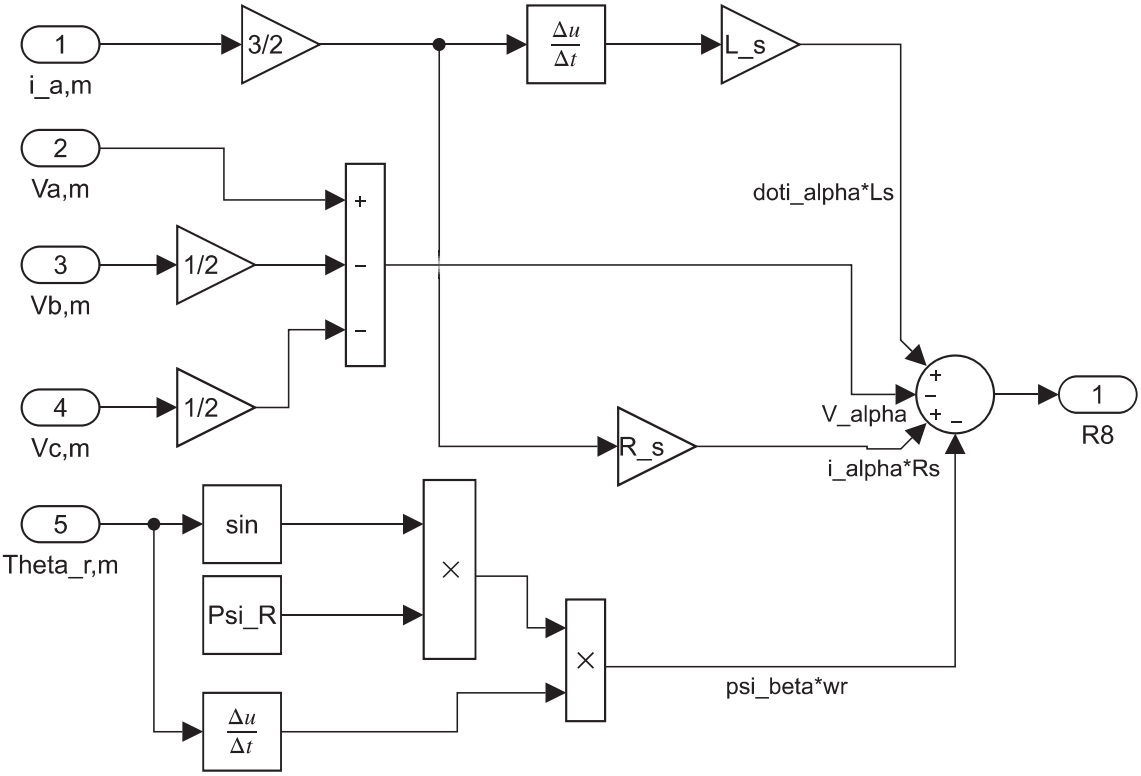
1
i_a,m
3/2
Δu/Δt
L_s
2
Va,m
doti_alpha*Ls
3
Vb,m
1/2
+
−
−
4
Vc,m
1/2
V_alpha
+
−
+ _
1
R8
R_s
i_alpha*Rs
5
Theta_r,m
sin
Psi_R
×
×
psi_beta*wr
Δu/Δt

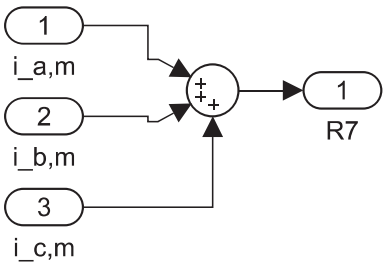
1
i_a,m
2
i_b,m
3
i_c,m
+
+
+
1
R7

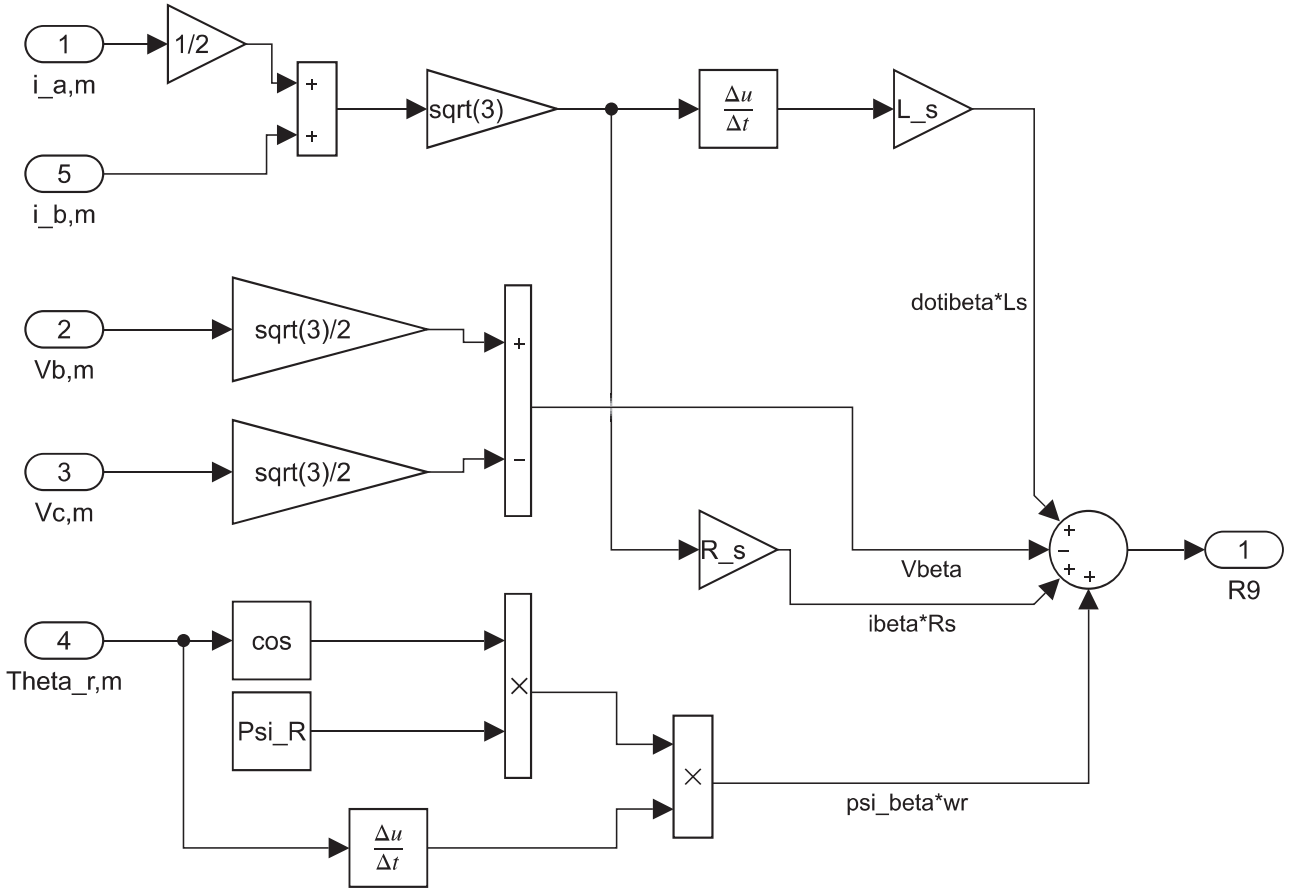
1
i_a,m
1/2
5
i_b,m
sqrt(3)
Δu/Δt
L_s
dotibeta*Ls
2
Vb,m
sqrt(3)/2
3
Vc,m
sqrt(3)/2
R_s
Vbeta
ibeta*Rs
1
R9
4
Theta_r,m
cos
Psi_R
psi_beta*wr
Δu/Δt

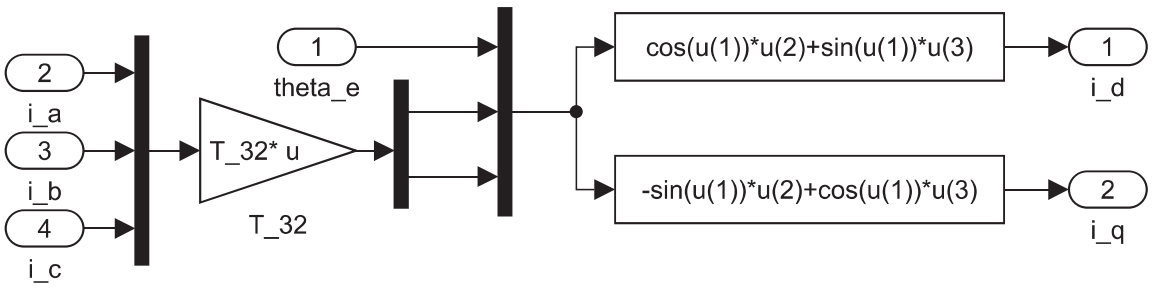
2
i_a
3
i_b
4
i_c
T_32* u
T_32
1
theta_e
cos(u(1))*u(2)+sin(u(1))*u(3)
-sin(u(1))*u(2)+cos(u(1))*u(3)
1
i_d
2
i_q

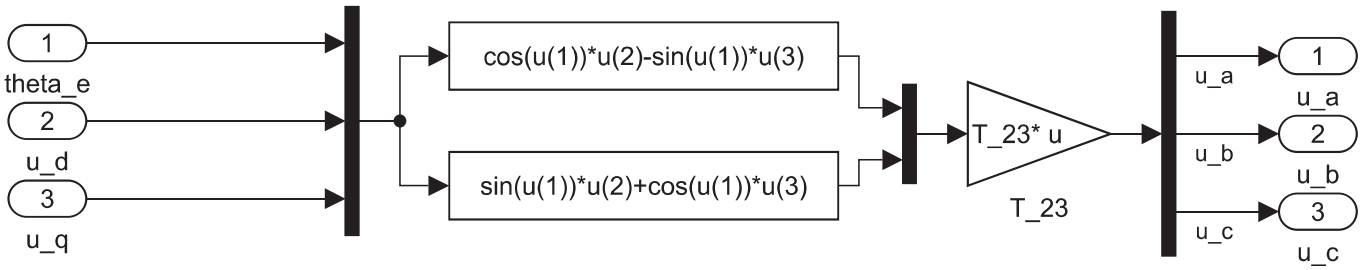
1
theta_e
2
u_d
3
u_q
cos(u(1))*u(2)-sin(u(1))*u(3)
sin(u(1))*u(2)+cos(u(1))*u(3)
T_23* u
T_23
u_a
u_b
u_c
1
u_a
2
u_b
3
u_c

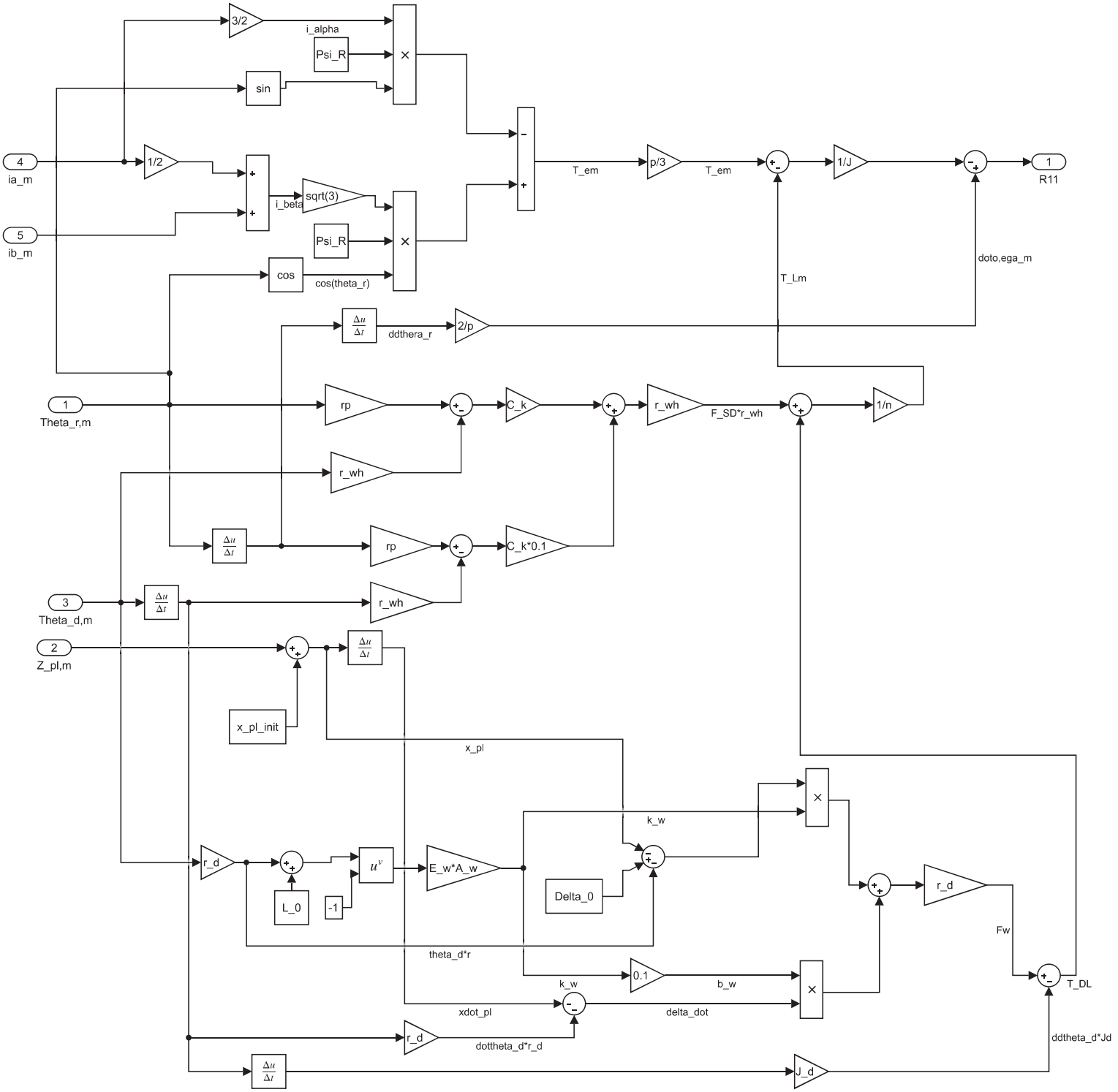
3/2
i_alpha
Psi_R
sin
4
ia_m
1/2
sqrt(3)
i_beta
5
ib_m
Psi_R
cos
cos(theta_r)
T_em
p/3
T_em
1/J
1
R11
T_Lm
doto,ega_m
ddthera_r
2/p
1
Theta_r,m
rp
C_k
r_wh
F_SD*r_wh
1/n
r_wh
rp
C_k*0.1
3
Theta_d,m
r_wh
2
Z_pl,m
x_pl_init
x_pl
k_w
r_d
L_0
-1
E_w*A_w
Delta_0
r_d
Fw
T_DL
theta_d*r
k_w
0.1
b_w
xdot_pl
delta_dot
r_d
dottheta_d*r_d
ddtheta_d*Jd
J_d

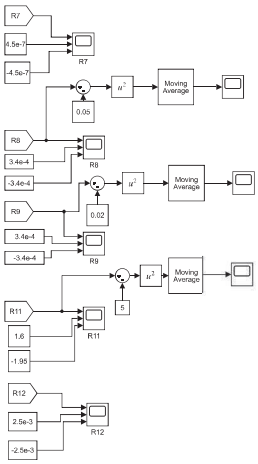
R7
4.5e-7
-4.5e-7
0.05
Moving Average
R8
3.4e-4
-3.4e-4
0.02
R9
3.4e-4
-3.4e-4
5
R11
1.6
-1.95
R12
2.5e-3
-2.5e-3

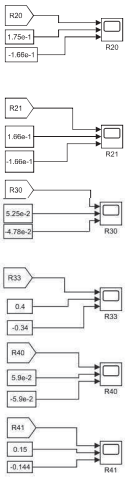
R20
1.75e-1
-1.66e-1
R21
1.66e-1
-1.66e-1
R30
5.25e-2
-4.78e-2
R33
0.4
-0.34
R40
5.9e-2
-5.9e-2
R41
0.15
-0.144

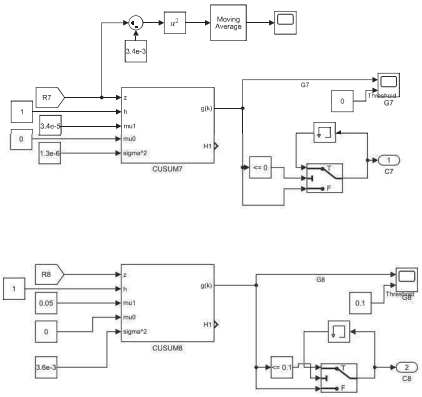
3.6e-3
Moving Average
R7
1
0
3.4e-5
1.3e-6
CUSUM7
G7
0
Threshold
C7
<= 0

R8
1
0.05
0
3.6e-3
CUSUM8
G8
0.1
Threshold
C8
<= 0.1

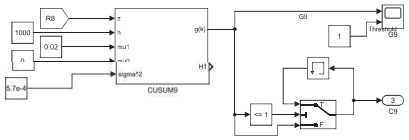
R8
1000
0.02
5.7e-5
CUSUM9
G9
1
Threshold
C9
<= 1

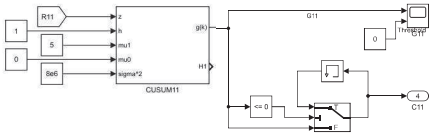
R11
1
5
0
8e6
CUSUM11
G11
0
Threshold
C11
<= 0

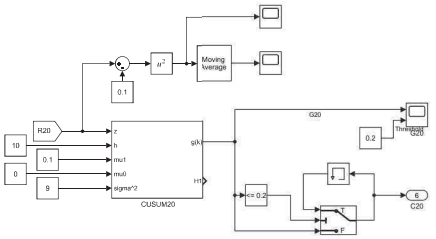
0.1
Moving Average
R20
10
0.1
0
9
CUSUM20
G20
0.2
Threshold
C20
<= 0.2

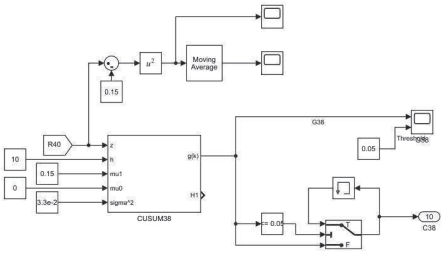
0.15
Moving Average
R40
10
0.15
0
3.3e-2
CUSUM38
G38
0.05
Threshold
C38
>= 0.05

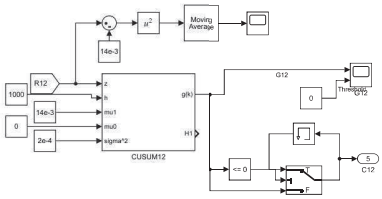
14e-3
Moving Average
R12
1000
14e-3
0
2e-4
CUSUM12
G12
0
Threshold
C12
<= 0

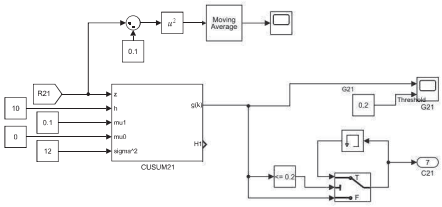
0.1
Moving Average
R21
10
0.1
0
12
CUSUM21
G21
0.2
Threshold
C21
<= 0.2

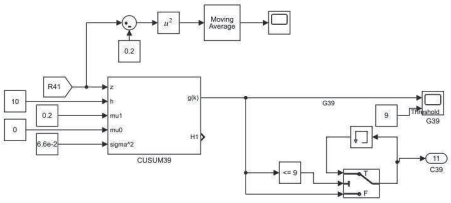
0.2
Moving Average
R41
10
0.2
0
6.6e-2
CUSUM39
G39
9
Threshold
C39
<= 9

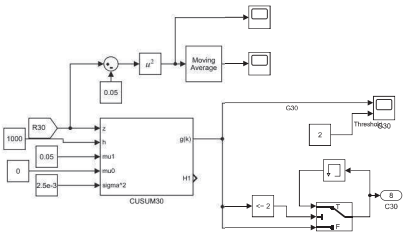
0.05
Moving Average
R30
1000
0.05
0
2.5e-3
CUSUM30
G30
2
Threshold
C30
<- 2

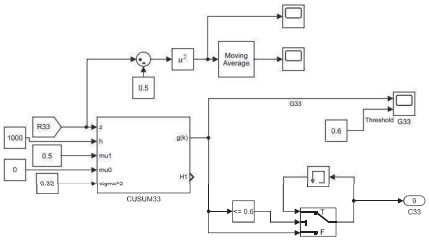
0.5
Moving Average
R33
1000
0.5
0
0.92
CUSUM33
G33
0.6
Threshold
C33
<= 0.6

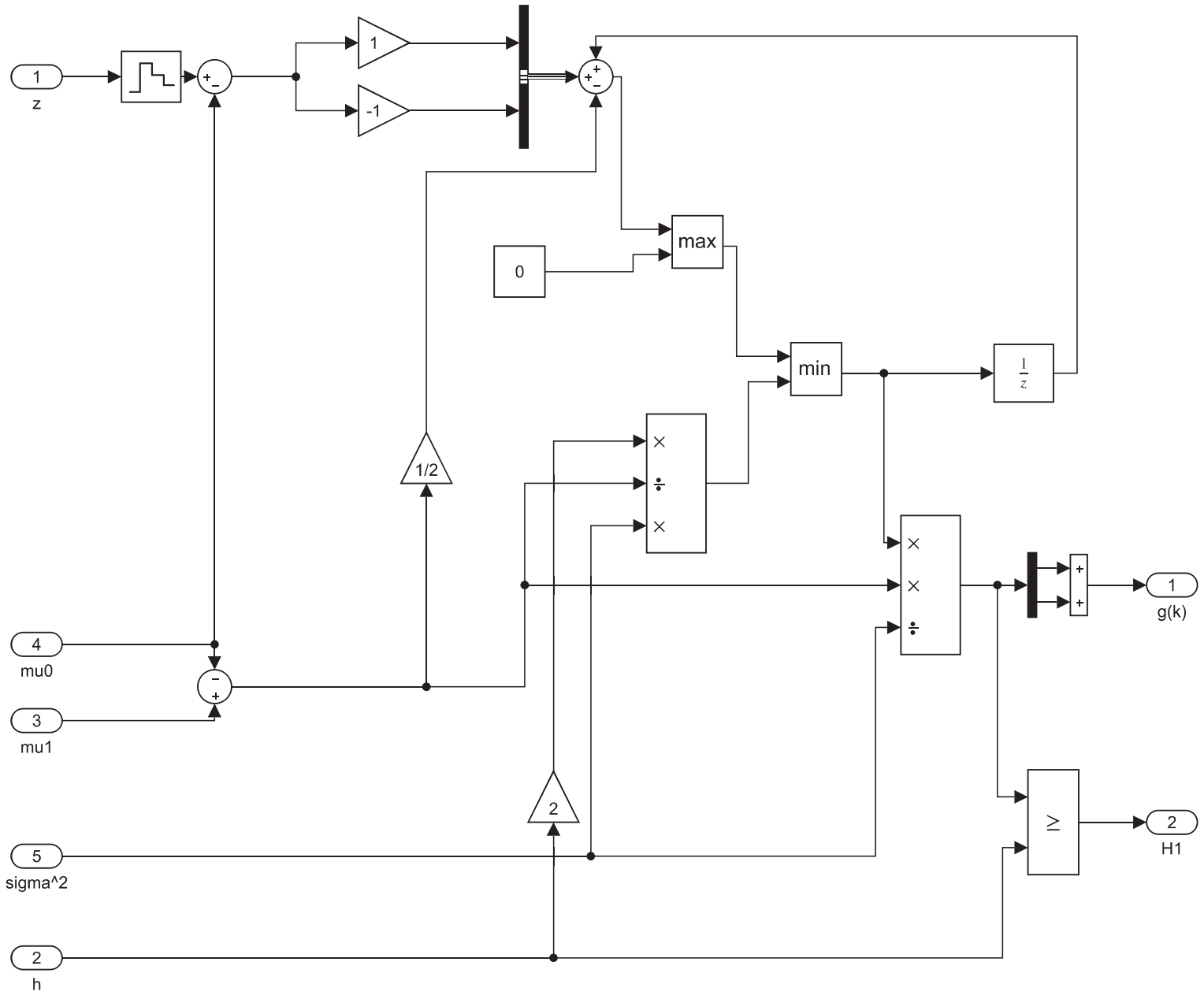
1
z
1
-1
max
0
min
1/2
4
mu0
3
mu1
2
5
sigma^2
2
h
1
g(k)
2
H1

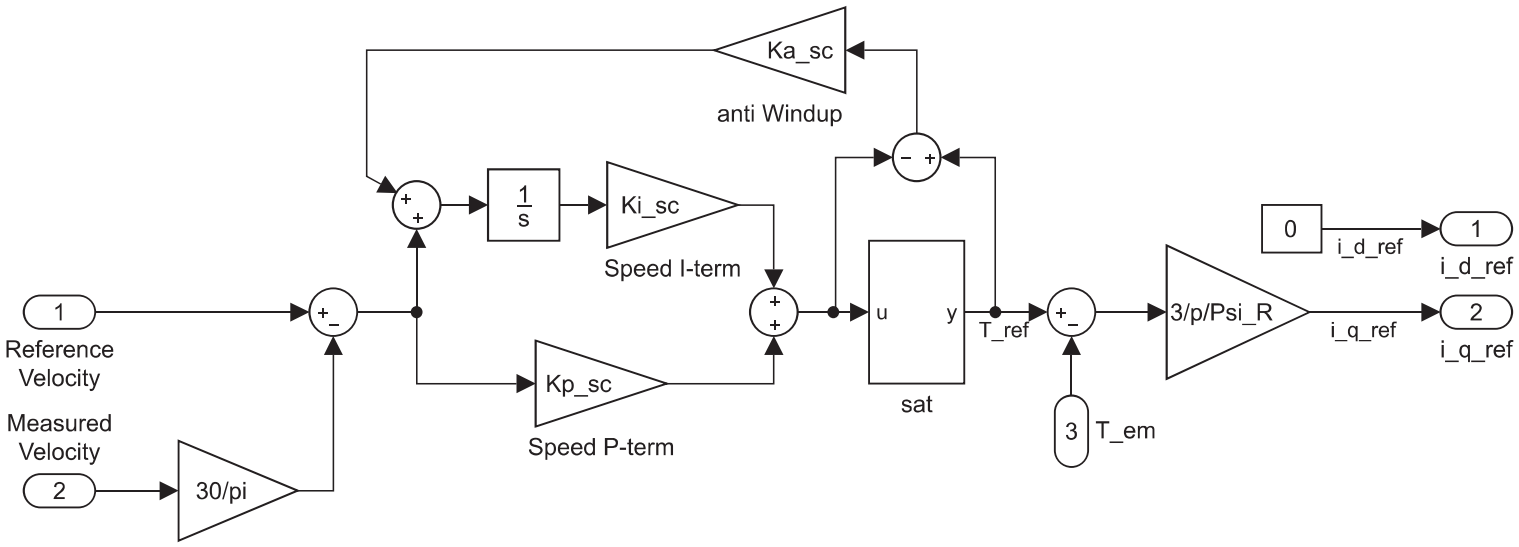
Ka_sc
anti Windup
1
s
Ki_sc
Speed I-term
1
Reference
Velocity
Measured
Velocity
2
30/pi
Kp_sc
Speed P-term
u
y
sat
T_ref
3
T_em
3/p/Psi_R
0
i_d_ref
1
i_d_ref
i_q_ref
2
i_q_ref

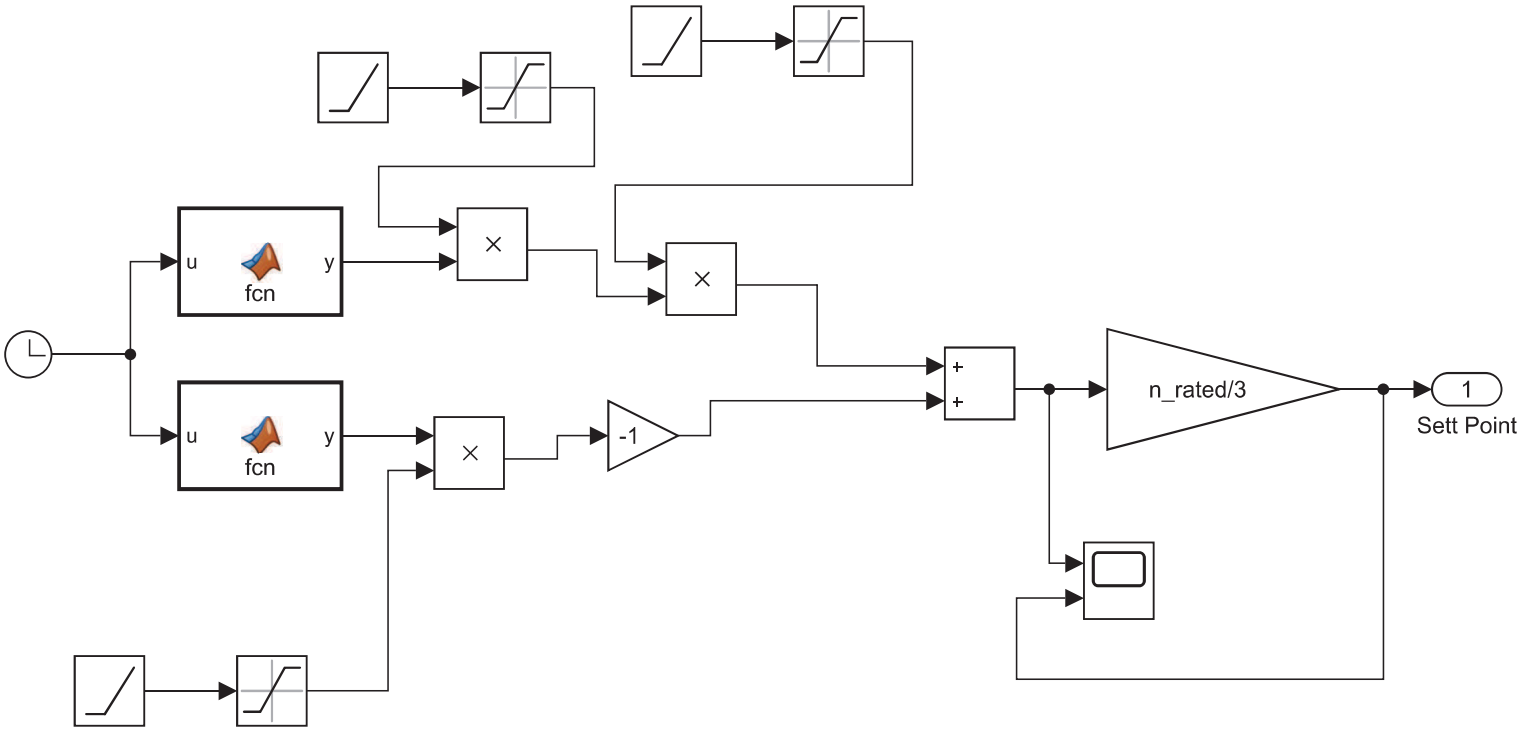
u
y
fcn
u
y
fcn
-1
+
+
n_rated/3
1
Sett Point

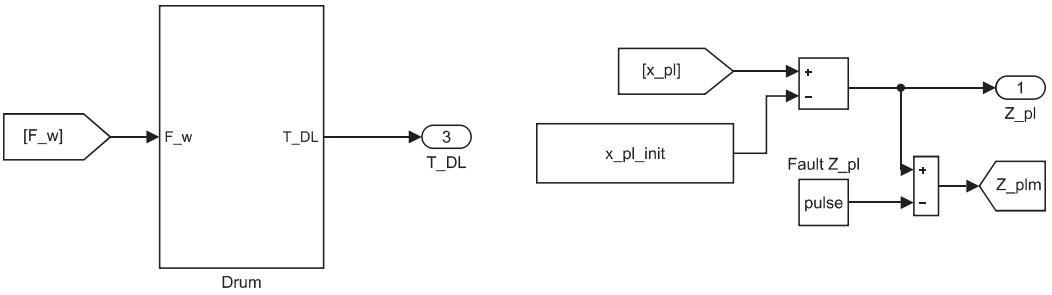
[F_w]
F_w
T_DL
3
T_DL
Drum
[x_pl]
x_pl_init
1
Z_pl
Fault Z_pl
pulse
Z_plm

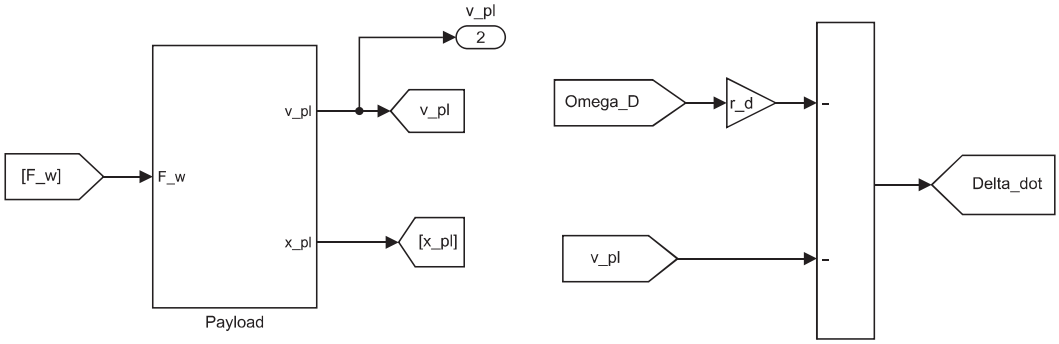
v_pl
2
[F_w]
F_w
v_pl
x_pl
v_pl
[x_pl]
Payload
Omega_D
r_d
v_pl
Delta_dot

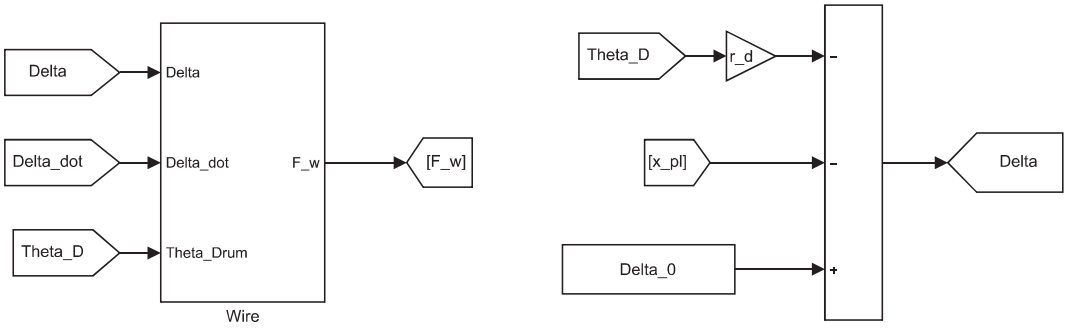
Delta
Delta_dot
Theta_D
Delta
Delta_dot
Theta_Drum
F_w
[F_w]
Wire
Theta_D
r_d
[x_pl]
Delta_0
Delta

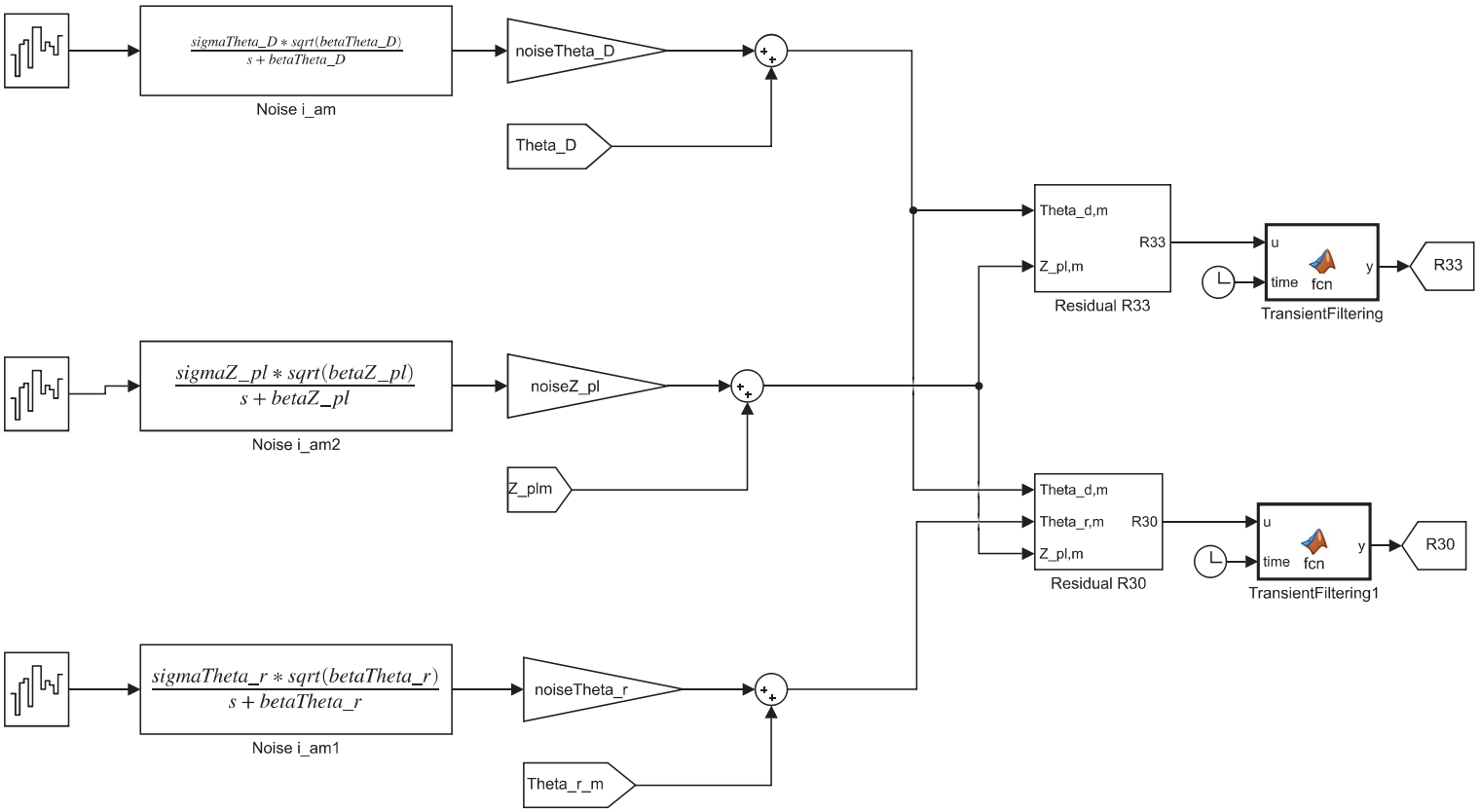
sigmaTheta_D * sqrt(betaTheta_D)
s + betaTheta_D
Noise i_am
noiseTheta_D
Theta_D
Theta_d,m
Z_pl,m
R33
Residual R33
u
time
fcn
y
R33
TransientFiltering
sigmaZ_pl * sqrt(betaZ_pl)
s + betaZ_pl
Noise i_am2
noiseZ_pl
Z_plm
Theta_d,m
Theta_r,m
Z_pl,m
R30
Residual R30
R30
TransientFiltering1
sigmaTheta_r * sqrt(betaTheta_r)
s + betaTheta_r
Noise i_am1
noiseTheta_r
Theta_r_m

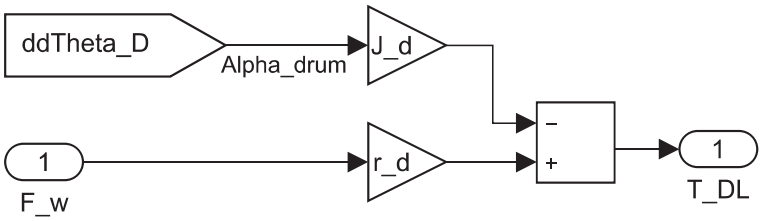
ddTheta_D
Alpha_drum
J_d
1
F_w
r_d
-
+
1
T_DL

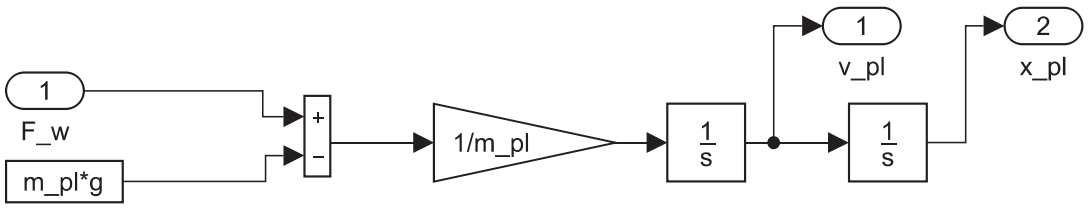
1
F_w
m_pl*g
+
−
1/m_pl
1
s
1
s
1
v_pl
2
x_pl

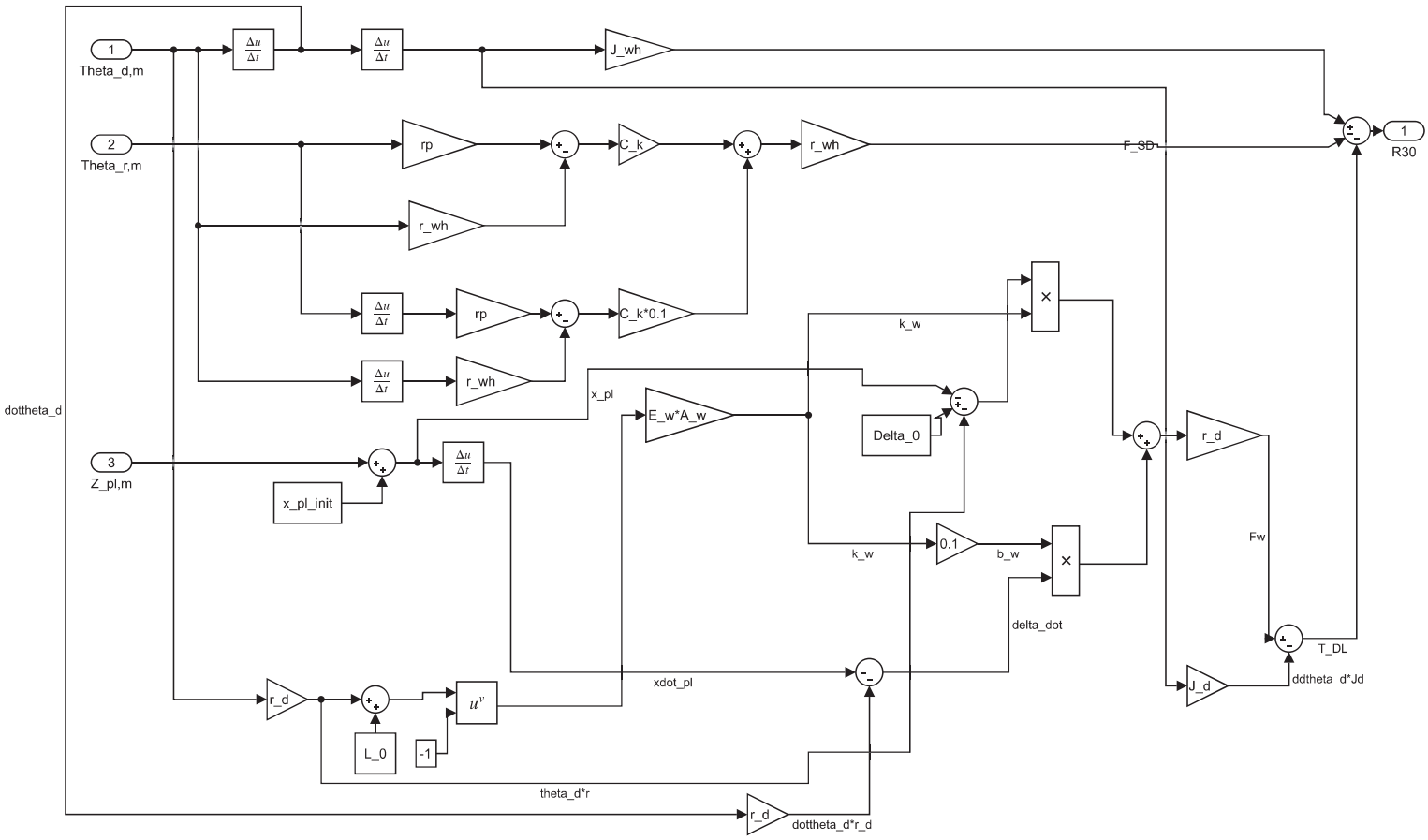
1
Theta_d,m
2
Theta_r,m
3
Z_pl,m
dottheta_d
J_wh
rp
C_k
r_wh
F_SD
1
R30
C_k*0.1
k_w
x_pl
E_w*A_w
Delta_0
r_d
x_pl_init
0.1
b_w
Fw
delta_dot
T_DL
xdot_pl
J_d
ddtheta_d*Jd
L_0
-1
theta_d*r
dottheta_d*r_d

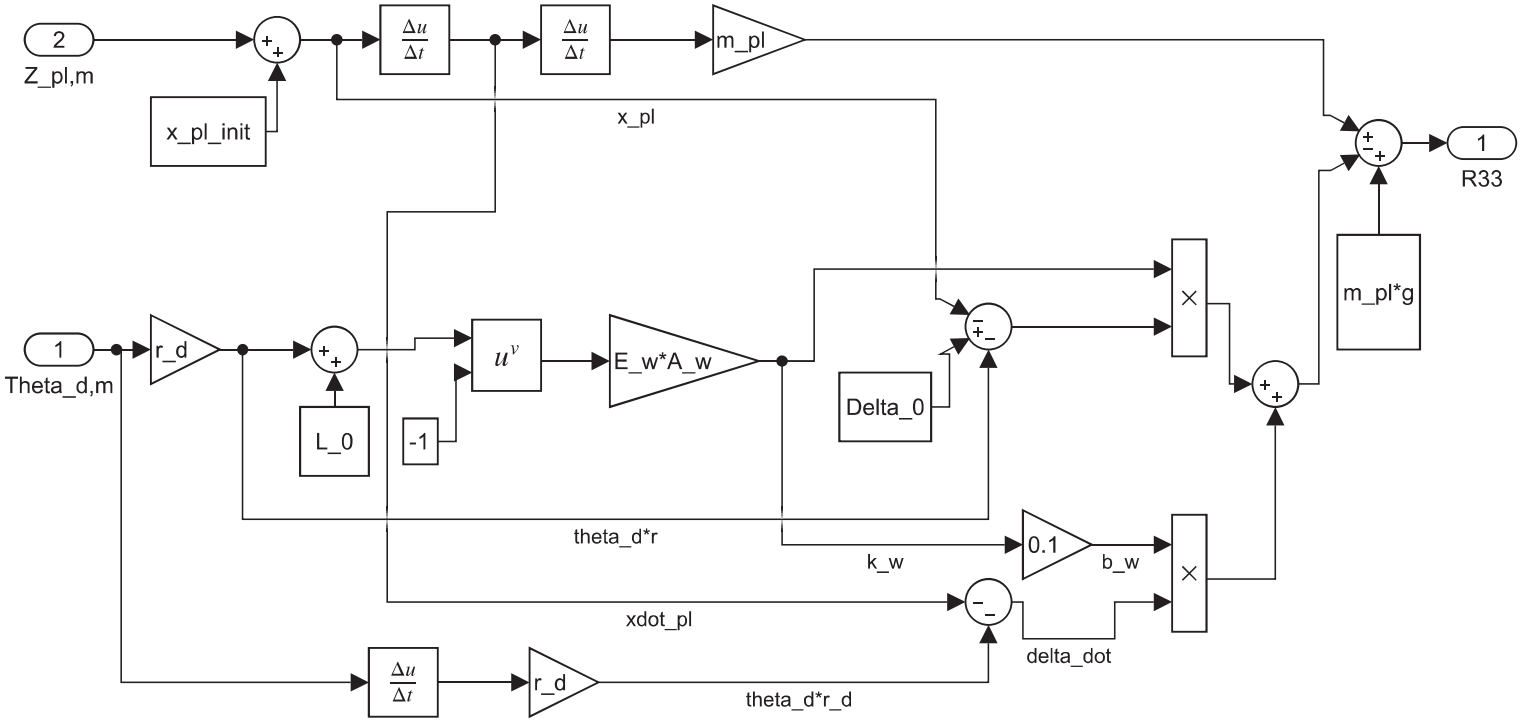
2
Z_pl,m
x_pl_init
Δu/Δt
Δu/Δt
m_pl
x_pl
1
R33
m_pl*g
1
Theta_d,m
r_d
L_0
-1
u^v
E_w*A_w
Delta_0
theta_d*r
k_w
0.1
b_w
xdot_pl
delta_dot
Δu/Δt
r_d
theta_d*r_d

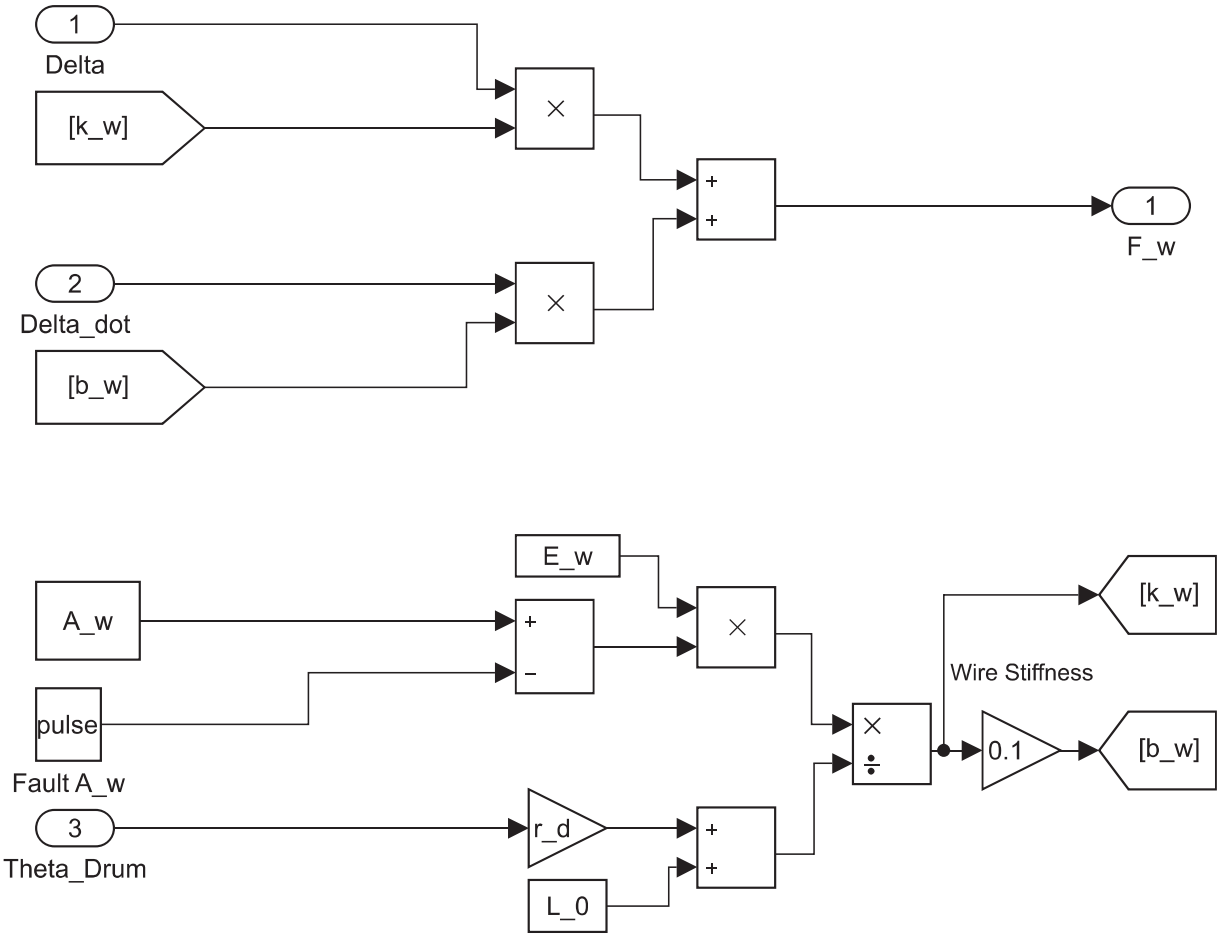
1
Delta
[k_w]
2
Delta_dot
[b_w]
1
F_w
E_w
A_w
pulse
Fault A_w
3
Theta_Drum
r_d
L_0
Wire Stiffness
[k_w]
0.1
[b_w]

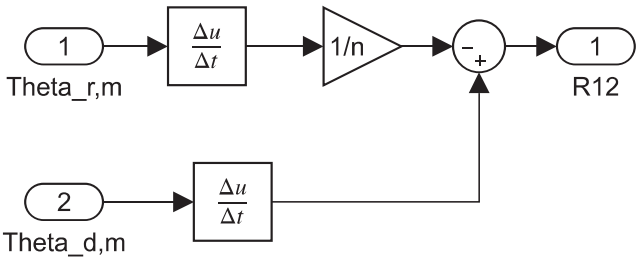
1
Theta_r,m
Δu/Δt
1/n
1
R12
2
Theta_d,m
Δu/Δt

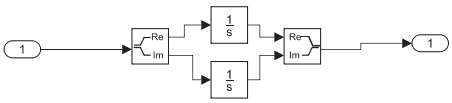
1
Re
Im
1
s
1
s
Re
Im
1

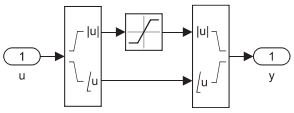
1
u
|u|
u
|u|
1
y

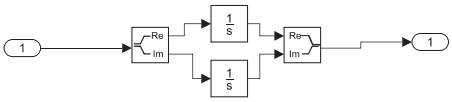
1
Re
Im
1
s
1
s
Re
Im
1

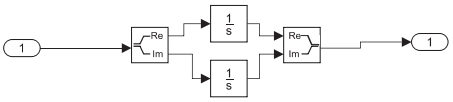
1
Re
Im
1
s
1
s
Re
Im
1